

UNIVERSITY OF BELGRADE

SCHOOL OF ELECTRICAL ENGINEERING

Stefan M. Dimitrijević

**CHARACTERISATION OF SPECIFIC NOISE SOURCES  
IN AN URBAN ENVIRONMENT AND PROTECTION  
METHODS**

Doctoral Dissertation

Belgrade, 2021

UNIVERZITET U BEOGRADU

ELEKTROTEHNIČKI FAKULTET

Stefan M. Dimitrijević

**KARAKTERIZACIJA SPECIFIČNIH IZVORA BUKE U  
URBANOJ SREDINI I METODE ZAŠTITE**

Doktorska disertacija

Beograd, 2021

I would like to acknowledge the financial support provided by  
**DENORMS** (Designs for Noise Reducing Materials and Structures)  
COST Action – CA 15125.



I would also like to acknowledge the support of **Structor Akustik AB**, Stockholm, Sweden for making available the necessary test equipment.



Finally, I would like to acknowledge the support of **Ports of Stockholm**, Stockholm, Sweden, for making the measurement data available for publishing.



## Acknowledgment

*I would like to express my gratitude to my supervisor Prof. Miomir Mijić who has guided me from the very beginning of my research career and, with his passion and devotion, made me fall in love with acoustics. I am thankful for all the advice, ideas, and often exhaustive discussions. He has taught me that, to engage in research, I must become a child again and consider, question, and investigate all possible facts and directions. Furthermore, he would always motivate me with the famous quote “If we knew what it was we were doing, it would not be called research, would it?” (Albert Einstein). Additionally, I would like to thank Prof. Dragana Šumarac Pavlović, who has often joined our discussions and contributed to their further development. I believe and hope that this dissertation is just an initial step of something bigger for all of us.*

*I owe immense gratitude to Kristoffer Fristedt, CEO of Structor Akustik, Stockholm, Sweden, who has been actively involved in my academic education and who has always been supportive and willing to contribute with his vast experience. I hope to have the opportunity to apply the knowledge gained in my research career to industry, and thus pay back his investment.*

*I would also like to express gratitude to Dr. Jean–Philippe Groby for inviting me to take part in the COST Action “DENORMS” and for supporting me in different project activities. Furthermore, I would also like to thank Prof. José Sánchez–Dehesa for his selflessness and will to share his expertise as well as for giving me opportunity to investigate a state–of–the–art sonic crystal he had personally designed. It is also indispensable to mention contribution of Dr. Víctor Manuel García Chocano, who has helped me with practical implementation of my ideas and to understand phenomena I have never faced before.*

*Next, I would like to express my sincere gratitude to Dr. Miloš Bjelić, Dr. Draško Mašović and many others who have helped me with implementation of demanding measurements as well as expert suggestions and discussions.*

*I would also like to thank Dr. Marco Miniaci and Francesco Morandi for making data from their research available for purposes of comparison.*

*Finally, I would like to mention unconditional support from my family, primarily from my beloved wife Marija Dimitrijević. Her patience and sacrifice have motivated me to persevere in my goals. I am looking forward to completely focusing on being a better husband and father, which is from now on my life goal.*

*Stefan Dimitrijević*

**Dissertation Title:** Characterisation of Specific Noise Sources in an Urban Environment and Protection Methods

**Abstract:** The first goal of this dissertation is the characterisation of outdoor noise emission of specific low–frequency noise sources: floating river clubs and moored ships. Their specificity is reflected in the fact that they are characterised by large dimensions, but also that they are not easily approachable. Most available measurement methods for determination of sound power levels define a large number of measurement positions around the sound source. Nevertheless, a relatively simple measurement method is preferred in practical applications, particularly if sound sources are located in such unfavourable environments. For this reason, the implementation of different existing measurement methods has been investigated in this dissertation in order to identify the most optimal one under the given circumstances. Additionally, indoor sound level spectra for different types of entertainment premises, including floating river clubs, have been investigated and a modified spectrum adaptation term for a single–number rating of sound insulation against the low–frequency entertainment noise has been proposed.

The second goal of this dissertation is the investigation of capabilities and limitations of *in situ* test methods for measuring acoustic properties of noise barriers. For this purpose, a dedicated measurement system consisting of a microphone array, signal processing device and signal generator, has been designed and applied to two types of noise barriers: a conventional sound absorbing barrier and a prototype of sound absorbing sonic crystal. While the application of the *in situ* methods to conventional noise barriers has been thoroughly investigated in the literature, there has been very limited data about their application to periodic structures, such as sonic crystals.

**Key words:** *in situ* characterisation, sound power level, entertainment noise, sound level spectra, ships, noise barriers, *sonic crystals*

**Scientific subfield:** Technical Sciences, Electrical Engineering

**Scientific subfield:** Acoustics

**UDK number:** 621.3

**Naslov doktorske disertacije:** Karakterizacija Specifičnih Izvora Buke u Urbanoj Sredini i Metode Zaštite

**Sažetak:** Prvi cilj ove disertacije je karakterizacija spoljne buke emitovane od strane specifičnih izvora niskofrekventne buke: plutajućih rečnih splavova i usidrenih brodova. Njihova specifičnost se ogleda u činjenici da se karakterišu velikim dimenzijama, ali i da im nije lako pristupiti. Većina dostupnih mernih metoda za određivanje zvučnih snaga definišu veliki broj mernih pozicija oko zvučnog izvora. Ipak, u praktičnim aplikacijama je poželjna relativno jednostavna merna metoda, posebno ukoliko se izvori buke nalaze u tako nepovoljnim okruženjima. Iz tog razloga, u disertaciji je istražena primena različitih postojećih mernih metoda kako bi se identifikovala najoptimalnija u datim okolnostima. Dodatno, istraženi su spektri zvučnih nivoa u zatvorenom za različite tipove objekata zabave, uključujući i rečne splavove, i predložen je modifikovani korekcionni faktor za merodavnu ocenu zvučne izolacije u slučaju niskofrekventne buke zabave.

Drugi cilj ove disertacije je istraživanje mogućnosti i ograničenja *in situ* metoda za merenje akustičkih svojstava zvučnih barijera. U tu svrhu, dizajniran je namenski merni sistem koji se sastoji od mikrofonskog niza, uređaja za obradu signala i signal generatora, i primenjen na dva tipa zvučnih barijera: konvencionalnu apsorbujuću zvučnu barijeru i prototip apsorbujućeg zvučnog soničnog kristala (eng. *sonic crystals*). Iako je primena *in situ* metoda na konvencionalnim barijerama detaljno istražena u literaturi, postoji vrlo ograničen broj podataka o njihovoj primeni na periodičnim strukturama, kao što su sonični kristali.

**Ključne reči:** *in situ* karakterizacija, nivo zvučne snage, buka objekata zabave, zvučni spektri, brodovi, zvučne barijere, *sonični kristali*

**Naučna oblast:** Tehničke nauke, Elektrotehnika

**Uža naučna oblast:** Akustika

**UDK broj:** 621.3

# Contents

<b>1</b>	<b>Introduction</b>	<b>1</b>
1.1	Low-frequency Noise	2
1.2	Protection methods	3
1.2.1	<i>Noise Barriers</i>	3
1.3	Objectives	4
<b>I</b>	<b>CHARACTERISATION OF SPECIFIC NOISE SOURCES</b>	<b>6</b>
<b>2</b>	<b>Outdoor Noise of Floating River Clubs</b>	<b>7</b>
2.1	Introductory Remarks	7
2.2	Measurement Methods for Determination of Sound Power Levels	7
2.2.1	<i>ISO 3744</i>	9
2.2.2	<i>Nordtest Method</i>	12
2.2.3	<i>ISO 9614–1</i>	17
2.3	Acoustic Scale Models	18
2.4	Experimental Setup	18
2.4.1	<i>Scale model experiment</i>	18
2.4.2	<i>Cottage with a Lightweight Façade</i>	20
2.4.3	<i>The Case of Floating River Clubs</i>	21
2.5	Experimental Result and Discussions	25
2.5.1	<i>A Scale Model Experiment</i>	25
2.5.2	<i>Cottage with a Lightweight Façade</i>	27
2.5.3	<i>Floating River Clubs</i>	30
<b>3</b>	<b>Indoor Noise of Entertainment Premises</b>	<b>37</b>
3.1	Introductory Remarks	37
3.2	Spectrum Adaptation Terms According to ISO 717–1	38
3.3	Experimental Setup	40
3.4	Experimental Results and Discussions	41
<b>4</b>	<b>Outdoor Noise of Moored Ships</b>	<b>45</b>
4.1	Introductory Remarks	45
4.2	Neptunes Measurement Procedure	45
4.2.1	<i>Characterisation of the Funnel Outlet in a Near-Field</i>	46
4.2.2	<i>Measurements in a Far-Field</i>	47
4.3	Emission Measurement Methods	48
4.4	Experimental Results and Discussions	49

<b>II PROTECTION METHODS</b>	<b>54</b>
<b>5 Acoustic Properties of Noise Barrier</b>	<b>55</b>
5.1 Introductory Remarks	55
5.2 Measurement Methods	57
5.2.1 <i>In Situ Measurement Methods</i>	57
5.2.2 <i>Laboratory Measurement Methods</i>	63
5.3 Experimental Setup	65
5.3.1 <i>Conventional Noise Barrier</i>	66
5.3.2 <i>Sonic Crystal</i>	68
5.4 Experimental Results and Discussions	69
5.4.1 <i>Conventional Noise Barrier</i>	69
5.4.2 <i>Sonic Crystal</i>	74
<b>6 Conclusions</b>	<b>82</b>
6.1 Scientific contributions	84
6.2 Future work	85
<b>References</b>	<b>86</b>
<b>Appendix A – Scale Model Experiment, Signal-to-Noise Ratio</b>	<b>94</b>
<b>Appendix B – Moored Ships, Sound Power Levels of Individual Noise Sources</b>	<b>95</b>
<b>Appendix C – Noise Barriers, Impulse Responses at Individual Microphones</b>	<b>96</b>
<b>Author’s Biography</b>	<b>103</b>
<b>SCI Publications</b>	<b>103</b>

# Chapter 1

## Introduction

*Environmental noise* is unwanted or harmful sound, often generated by human activities [1]. According to the relevant noise authorities, World Health Organization (WHO) and European Environment Agency (EEA), environmental noise is mostly caused by the operation of one of the following sources: road traffic, railways, aircraft, industry, wind turbines, and leisure [2,3]. The WHO marks environmental noise as “an important public health issue, featuring among the top environmental risks to health”. This is also supported by the EEA, which states that environmental noise is one of the major environmental health problems in Europe. Based on the EEA’s estimation, 113 million people in the EU are affected by harmful road traffic noise, 22 million people are affected by harmful railway noise, nearly 4 million people are affected by harmful aircraft noise and less than 1 million people are affected by harmful industrial noise. Prolonged exposure to high levels of environmental noise can lead to serious harmful health effects, such as hypertension and cardiovascular disease, sleep disturbance and annoyance. Hypertension and cardiovascular disease are important risk factors for premature mortality, which means that excessive environmental noise can indirectly reduce the lifespan of humans [4].

EEA’s report “Environmental Noise in Europe” [3] present an assessment of the population exposed to high levels of environmental noise in Europe and it is based on the “Environmental Noise Guidelines for the European Region” published by WHO [2]. Both documents define transport noise i.e., traffic, railways and aircraft, as relevant sources of environmental noise. In addition to these three sources of environmental noise, EEA also defines wind turbines and leisure, while WHO also defines industry as additional relevant sources of environmental noise. It is interesting to notice that WHO defines wind turbine noise and leisure among relevant sources of environmental noise, which has not been considered in the report published by EEA, which is due to the fact that there are variations in how environmental noise is defined as well as how the EEA defines environmental noise according to the Environmental Noise Directive (END) [5].

Although considered the most dominant source of environmental noise in Europe, road traffic noise is just one of many noise sources in urban environments. There are numerous other noise sources of concern to citizens and policymakers, some of which primarily generate low–frequency noise. Some examples would include entertainment premises i.e., noise from night clubs and discotheques, as well as moored ships, which are considered as *specific noise sources* in this dissertation. Calculating the impact of such noise on the environment differs from the case of road traffic noise, primarily regarding spectral content and directional characteristics.

Generally speaking, an analysis of influence of a noise source in an environment considers three basic elements: the source, the transmission path and the receiver. The first step in noise analysis is typically to describe the noise emission of a source by using appropriate acoustical parameters. This process is called *characterisation* of a noise source. The next step is usually to model noise propagation. In this step, a propagation medium must be described as accurately as possible, with all its characteristic parts such as obstacles, reflective and absorptive areas, and terrain data. Finally, results of noise calculations lead to values of sound pressure levels at endangered receivers.

The calculation of noise propagation in an urban environment can be carried out by applying one of many different prediction methods. Broadly speaking, the commonly utilised methods are ISO 9613–2, General Prediction Method, DAL 32, Cnossos–EU, etc. These methods are implemented in noise mapping software packages [6–8], which have been developed to facilitate the calculations as well as to provide a detailed analysis accompanied by graphical presentations. The basic input parameter in these methods is the *sound power level* of a source. The sound power level is a measure of the acoustic energy emitted from a source of noise, expressed in decibels. It is independent of the environment, distance, or direction. Sound power level can be determined experimentally through measurements of either sound pressure or sound intensity, by applying appropriate measurement methods. These different methods are

often defined by international ISO standards, e.g., [9,10], and differ in their accuracy, scope regarding sources and environments, representation of sound power levels, etc. [11]. Also, characterisation of noise sources is a frequency-dependant problem, so the choice of measurement method should be based on the spectral content of the analysed noise. Characterisation of low-frequency noise sources is usually different from characterisation of sources emitting middle-frequency and high-frequency noise, due to properties explained in the next section.

## 1.1 Low-frequency Noise

In the literature, *low-frequency noise* is typically defined as noise in the frequency range 10–100 Hz [12]. This definition includes *infrasound*, which is usually sound below 20 Hz. Also, some authors extend the upper limit of the low-frequency range up to 200 Hz [13,14]. Another example is The Public Health Agency of Sweden, which defines low-frequency noise guidelines in one-third octave bands 31.5–200 Hz [15].

Low-frequency noise is less tolerated and perceived as more annoying than middle-frequency and high-frequency noise [16,17], mostly due to two reasons. First, density of *equal-loudness contours* [18, Fig. 4–6] indicate that small changes of sound pressure level cause great changes in perceived loudness at low frequencies. At middle and high frequencies, the density of equal-loudness contours is lower and greater changes of sound pressure levels are thus needed in order to perceive changes in loudness. This means that the low-frequency components of noise cause greater *annoyance* than other frequency components when the noise varies in loudness. Second, low-frequency masking curves cover a wide frequency range causing masking effects even at higher frequencies. This is especially pronounced at higher sound pressure levels, meaning further noticeability of low-frequency components in broadband noise. Furthermore, it is often difficult to locate low-frequency noise sources even if annoyingly loud [17]. This occurs due to the fact that low-frequency noise annoyance occurs at levels only slightly higher than the hearing threshold. Sound localisation by ear also breaks down at frequencies below 100 Hz because of the relation between wavelength and the spacing of human ears. Being unable to locate the noise source increases the perceived annoyance of listeners. Finally, it is difficult to control this kind of noise. This originates from the fact that it is neither easy to perform a reliable measurement nor to efficiently apply simple protection methods. The former is due to large uncertainties when measuring low-frequency noise, while the latter occurs due to lesser attenuation of low-frequency sound by typical building materials. Because of aforementioned, low-frequency noise has become a growing concern in the urban environment.

Methods for the determination of sound power levels defined by the international ISO standards [9,10] are complex and rather impractical if the investigated noise source has limited accessibility. This is the case with many low-frequency noise sources. The requirement of a large number of measurement positions at different heights and at larger distances from the source, as well as the use of a reference sound source to determine the influence of surrounding reflecting objects are major practical disadvantages of these methods. Also, these methods are mainly intended for indoor (i.e., laboratory) noise measurements, while most low-frequency noise sources are located outdoors. Consequently, there is a growing need for alternative measurement methods that could be used for the characterisation of low-frequency noise sources in a more practical way, designed specifically to be suitable for outdoor implementations.

Based on the facts described above, this dissertation has focused on the implementation of different measurement methods and analyses of low-frequency noise sources located on the water, floating river clubs and moored ships. Their specificity is reflected in the spectral content of the generated noise as well as the fact that implementation of standardised measurement methods [9,10] is considerably difficult due to their limited accessibility i.e., the fact that they are located on the water. Precisely because of these specificities, this dissertation investigates possibilities of employing a simplified measurement method while, at the same time, maintaining sufficient accuracy when compared to the existing ISO measurement methods. Additionally, this dissertation investigates differences between sound power

levels determined by implementation of different measurement methods and measurements in a far-field.

## 1.2 Protection methods

After characterisation of noise sources and calculations of their noise in an environment, identifying an exceedance of noise levels requires introduction of appropriate protection methods. This can be done e.g., by using building elements with high values of sound insulation around noise sources as well as by placing noise barriers between noise sources and receivers. In the former case, rating of sound insulation of building elements is often performed by comparing their single-number quantities. These quantities are obtained by converting frequency-dependent descriptors of sound insulation. However, in the conversion process, the information about efficiency of building elements against different types of noise is lost. Therefore, spectrum adaptation terms are added to the single-number rating to include the characteristics of particular sound spectra. The procedure of this conversion has been described in the ISO 717-1 standard [19]. In the same standard, two different spectrum adaptation terms are defined:  $C$  for noise sources inside the building (A-weighted pink noise) and  $C_{tr}$  for traffic (A-weighted urban traffic noise). However, the spectral content of noise generated by entertainment premises is expected to be concentrated in the low-frequency range, due to existence of subwoofers. The existence of subwoofers requires introduction of a new sound spectrum and spectral adaptation term when rating the efficiency of sound insulation in this case. It is expected that the new sound spectrum will give a more realistic rating of the efficiency of building elements against the low-frequency entertainment noise. The latter case, which refers to noise barriers, is explained in the next section.

### 1.2.1 Noise Barriers

Changes in the propagation path present the most common way of dealing with environmental noise. Some typical examples would include noise barriers and urban planning. When noise sources operate in an existing environment, urban planning is no longer an option thereby rendering noise barriers as the most reasonable protection methods.

Noise barriers lower noise levels in the environment by changing the path of noise propagation. On the one hand, noise barriers should provide sufficient sound insulation so that sound transmitted through the barrier is not significant compared to the sound diffracted over the top. In order to design a noise barrier with adequate attenuation, some common rules of thumb have been developed [20,21]. On the other hand, noise barriers should provide adequate sound absorption in cases where reflections from barriers can increase sound levels at receivers. This can usually be improved using absorbent materials, redirection of specular reflections (e.g., by designing the shape of the barriers) and scattering of specular reflections [22].

A review of noise barriers has been summarized in [23], where a surface weight of at least  $10 \text{ kg/m}^2$  has been recommended in order to achieve attenuations of more than 20 dB for screen-type (i.e., conventional) barriers. The attenuation of 20 dB is stated sufficient so as not to affect the overall sound levels behind barriers caused by diffracted sound components. More recent findings on different noise barrier shapes have been provided in [24]. In addition to conventional noise barriers, the requirement for periodic structures as protection methods, the so-called *sonic crystals* (SCs), the geometry of which could optimise the barrier efficiency, has emerged in the literature during the last two decades [25]. Unlike conventional noise barriers employing the mass law, SCs utilise *multiple scattering* phenomena in order to provide attenuation. Compared to conventional noise barriers, SCs do not necessarily require foundations since they exhibit low resistance to wind. SCs are also lighter compared to traditional noise barriers providing greater aesthetic potential. A downside is that only narrow-band attenuation can be obtained if only multiple scattering phenomena is used, without help of absorbing and/or resonant structures. Therefore, additional mechanisms are usually used to improve the narrow-band attenuation properties of basic SCs. The recently developed concept of SCs as a noise protection method has recently drawn attention from the research community and as such has been investigated in this dissertation.

Some methods used to characterise the acoustic properties of noise barriers can be roughly divided into three groups: theoretical calculations, scale–model experiments and full–scale experiments. The first two groups often refer to oversimplified methods which provide indication rather than real data of noise barrier acoustic properties. The full–scale experiments yield more realistic data and indicate a potentially bad workmanship during the installation process. They can be implemented either in special laboratory facilities [26,27] or *in situ* [28,29]. Although widely used for certification purposes, laboratory measurements involve testing of sound barriers in a diffuse sound field, which is rarely the case with environmental noise. Therefore, *in situ* measurement methods have become increasingly accepted as standardised measurements in some countries (e.g., in Belgium).

It has been indicated in the literature [30] that the existing laboratory measurement methods [26,27] provide different results of acoustic properties of noise barriers compared to those obtained by the *in situ* [28,29] measurement methods. Furthermore, the *in situ* measurement methods have been widely applied to conventional noise barriers, but the applicability to SCs has not yet been sufficiently investigated. Both aspects have been covered in this dissertation.

### 1.3 Objectives

In this dissertation, two of three basic elements of noise propagation analysis have been investigated: the source and the transmission path, respectively. First, *in situ* characterisation of entertainment noise (both indoor and outdoor) and noise from moored ships have been investigated. Second, *in situ* characterisation of noise barriers has been investigated. Therefore, the dissertation has been divided into two parts. Each chapter contains a theoretical introduction followed by specific methods and experimental results. In that way, it is possible to read chapters independently from each other, although they are interrelated.

The goal of the first part of this dissertation is to investigate different existing *in situ* measurement methods and recommend the most optimal in case of floating river clubs, as a specific source of entertainment noise which can be found in Belgrade, Serbia. They are located on the water i.e., in an unfavourable environment, according to the implementing of the existing ISO standards [9,10]. For this reason, a simplified measurement method used in Nordic countries, the *Nordtest* method [31], has been introduced. A total of three pressure–based measurement methods have been considered: *ISO 3744* [9], the *Nordtest Sphere* method and the *Nordtest Box* method [31]. First, the methods have been applied to a scale model of a floating river club. Second, the methods have been applied to a cottage with a lightweight façade and compared to the *ISO 9614–1* [10] sound intensity–based measurement method. The cottage presents a simplified case of floating river clubs since it is located on the hard ground. Finally, two floating river clubs have been characterised by application of the *Nordtest Sphere* method, as the most optimal measurement method in this case. The results of the characterisation have been compared to those obtained by measurements in a far–field. Additionally, indoor sound level spectra for different types of entertainment premises have been investigated. Unlike two standardised sound spectra given by *ISO 717–1* [19], a modified spectrum for discotheques with pronounced low–frequency noise has been proposed by the author. These results have been published in [32]. At the end of the first part, analysis of the entertainment noise has been complemented with *in situ* measurements of moored ships, as another specific noise source emitting low–frequency noise. Both near–field and far–field measurements have been applied to four ships around Stockholm, Sweden. As in the case of floating river clubs, far–field measurements have been used to validate measurements of sound power levels closer to the ships.

The goal of the second part of this dissertation is to investigate capabilities and limitations of *in situ* test methods for measuring the airborne sound insulation and reflection properties of noise barriers, *EN 1793–6* [29] and *EN 1793–5* [28]. The methods have been applied to two different types of noise barriers. First, a conventional absorbing noise barrier installed along railway track in Knivsta, Sweden, has been investigated. Second, an absorbing SC barrier made of micro–perforated cylinders filled with rubber crumb installed in Valencia, Spain, has been investigated. The results in the latter case have

been compared to results from SC investigated by other authors [33]. These experimental results have been published so far in [34].

## Part I

# Characterisation of Specific Noise Sources

The first part of this dissertation starts with an overview of low-frequency noise of entertainment premises and more specifically, floating river clubs ([Section 2.1](#)), followed by a series of key characterisation standards and their principles ([Section 2.2](#)), and experimental results of their implementation ([Section 2.5](#)). Next, a rating of sound insulation with single-number quantities and spectrum adaptation terms ([Section 3.1–3.2](#)) has been introduced. Then, indoor sound level spectra of different types of entertainment premises, as a result of an extensive monitoring, has been presented ([Section 3.4](#)). Finally, measurement protocol for characterisation of moored ships, NEPTUNES, has been presented ([Section 4.2](#)) together with experimental results of its implementation ([Section 4.4](#)).

# Chapter 2

## Outdoor Noise of Floating River Clubs

### 2.1 Introductory Remarks

Amplified music from public entertainment premises has been increasingly causing annoyance in the urban environment [35,36]. Bars, pubs, clubs, and discotheques have become an inevitable part of urban areas, often incorporated as a part of residential buildings themselves. With powerful audio systems capable of producing significant sound levels, especially at low frequencies, these sources of noise present a challenge when suggesting an appropriate protection method.

Floating river clubs are typical representatives of specific entertainment noise sources in Belgrade, Serbia (see Figure 1). They are one of the major touristic attractions and a true symbol of Serbia's capital [37,38]. At the same time, floating river clubs are significant noise sources generating a large-scale ecological problem in the city. There are around 300 floating river clubs anchored on the banks of Sava and Danube rivers, many of which are nightclubs. Regardless of the time of the year, they are open long during night and often until early morning hours. Powerful audio systems for music reproduction are common for most of floating river clubs, usually producing indoor equivalent sound levels in the range 90–110 dBA. The high indoor sound levels are not sufficiently attenuated by their constructions which are, as a rule, made of lightweight partitions (wood, gypsum boards, aluminium, tarpaulin, and similar). Moreover, the average clubs' construction is also characterised by very large windows and often completely open segments, especially during summer. Consequently, sound generated inside the clubs causes annoyance in the environment. Low-frequency noise extends up to several kilometres away, affecting some of the residential areas of the city.

Noise from floating river clubs has been characterised mainly by measuring indoor sound levels, which is in accordance with the national regulations. Although this characterisation method has somehow contributed to the noise control in the environment, it does not provide information about the sound levels at receiver positions. In the recent years, a need to calculate the noise propagation from the clubs in different scenarios has emerged due to development of new residential areas in their vicinity. In that way, it is possible to predict noise levels at receiver positions as well as to suggest adequate noise protection methods. In fact, the prediction of sound levels caused by the floating river clubs could be done if their sound power levels were known. As mentioned earlier, sound power levels of a noise source are the most critical input parameter in software tools for noise prediction.

Due to their specific location on the water, floating river clubs are not easily approachable. This makes their outdoor characterisation more difficult and implies the use of vessels. Additional challenge is the fact that the noise from floating river clubs does not consist of steady-state noise components, which makes the characterisation with the actual music unreliable. Music usually varies between different genres and between reproduction and live performances, making the characterisation even more uncertain. Thus, a simple characterisation method is appreciated in order to characterise entertainment noise from floating river clubs. In the next section, the most common characterisation methods, ISO 3744 [9] and ISO 9614–1 [10], as well as Nordtest method [31] used in Nordic countries are described and their applicability in case of floating river clubs is discussed.

### 2.2 Measurement Methods for Determination of Sound Power Levels

Assessment of impact of noise sources on the environment usually implies measurement of sound pressure levels. However, sound pressure levels vary with measurement positions. In order to get an objective assessment of the impact, it is necessary to determine sound power levels, which are independent of the environment, distance or direction. Still, choosing a proper characterisation method



**Figure 1.** A cluster of floating river clubs along the Sava River in Belgrade, Serbia.

is not always an easy task. In general, several factors must be considered: type of noise, available equipment, testing environment, noise codes, etc. [11]. Given the fact that characterisation of noise sources is the first step in prediction of noise levels in the environment, its selection affects the accuracy of the calculations on a large scale.

There are two ways to determine sound power of a noise source: through the measurement of sound pressure [Pa] or sound intensity [ $\text{W}/\text{m}^2$ ]. On the one hand, determination of sound power through the measurement of sound pressure is usually done for the purpose of certification measurements, which are commonly done under specific environmental conditions (anechoic rooms or reverberation chambers). On the other hand, measurement of sound intensity can be applied in the presence of other noise sources since steady background noise does not influence the measured sound intensity. This kind of approach often implies limited frequency range, time demanding measurement methods and restrictions regarding the characteristics of the noise source.

In order to determine the sound power, the most common measurement methods are defined by ISO standards. They include both sound pressure [9] and sound intensity [10] measurements. Regardless of the chosen method, there are three different levels of accuracy:

- *Precision method* – The precision method gives the most accurate results. The measurements are performed in laboratory conditions with the most precise equipment available. While the method provides the lowest uncertainty, it requires the most effort in order to perform measurements.
- *Engineering method* – The engineering method is the most common characterisation method when it comes to noise analysis with the aim to suggest a protection method. It provides very accurate results and considers both the environment and the source type. The measurements can be performed *in situ*.
- *Survey method* – The survey method gives the least accurate results but does not require the most precise equipment. The results are used to compare characteristics of similar noise sources but have limited usage in noise prediction.

The abovementioned ISO standards have limited applicability in terms of environment in which measurements are implemented, type of noise they are intended for, the way in which the sound power is presented., etc. Still, main disadvantages are large number of measurement positions at different heights around the sound source and using a reference sound source in order to compensate for measurement

positions in the vicinity of reflective objects. Given the environment in which the floating river clubs are usually found, those two disadvantages limit the application of the ISO standards in their characterisation.

Unlike ISO standards, Nordtest method [31] used in Nordic countries prescribes simplified procedures for characterisation of noise sources. The method suggests less measurement positions as well as well-defined corrections in case when measurement positions are in the vicinity of reflecting objects. Although the method specifies a source strength which is the part of source sound power (not the sound power as in case of ISO standards), it is a part of the radiated noise which is relevant for the calculation of sound pressure levels in the environment. This is very practical in case of the floating river clubs, since they are usually located in the flat environment and the noise radiated upwards and under large angles is not of general interest.

In the next three sections, ISO 3744, Nordtest (Sphere and Box) and ISO 9614–1 characterisation methods are presented in more details. The methods have been presented regarding implementation in case of floating river clubs.

### 2.2.1 ISO 3744

The international ISO 3744 [9] standard specifies engineering methods (accuracy grade 2) for determination of the sound power level of noise sources from sound pressure levels, for an essentially free field over a reflecting plane. The method is suitable for all types of noise – steady, non-steady, fluctuating, isolated bursts of sound energy, etc. Also, the method can be applied to all types and sizes of noise sources. The sound pressure levels are measured on a surface enveloping the noise source (sphere, box, cylinder, or combination of two surfaces). The sound power level can be then calculated directly from measured sound pressure levels and areas of the surface. For general purposes, the frequency range containing octave bands centred at 125 Hz – 8 000 Hz is employed. However, the frequency range can be extended in case that the given noise source requires such modifications.

The first step in determining the sound power levels of noise sources is to define the *reference box*. The reference box is the smallest right parallelepiped imaginary surface that encloses the source under test. Here, parts protruding from the source, but not having an active role in noise emission, can be left outside the reference box. The dimensions of the measurement surface are determined from the *characteristic source dimension*  $d_0$ . The characteristic dimensions and reference boxes in cases when the noise source is located on one, two and three reflecting planes, are shown in Figure 2.

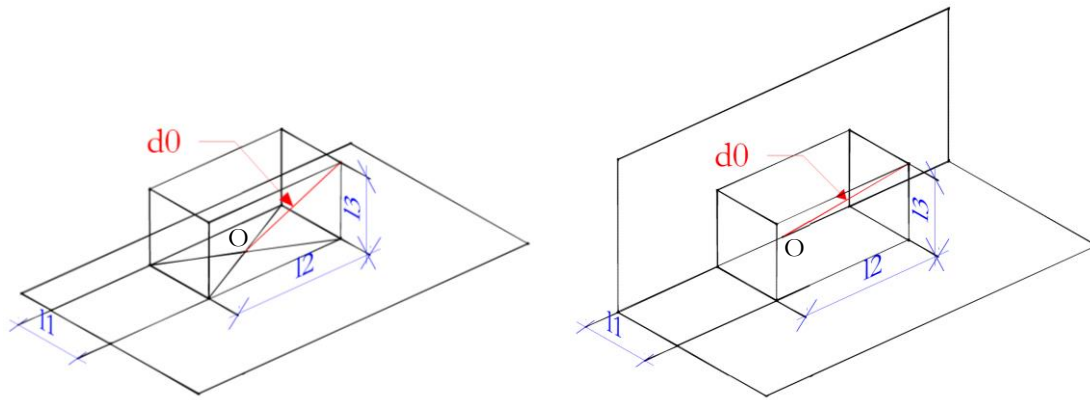
The second step in determining the sound power levels of noise sources is to choose an appropriate measurement surface. The type of measurement surface is selected based on the shape and size of the noise source. The general tendency is that all measurement positions are located at approximately same distance from the noise source. Accordingly, there are four possible measurement surfaces: the hemisphere (half-hemisphere, quarter-hemisphere), the right parallelepiped, the cylinder (half-cylinder, quarter-cylinder) and a combination of any two previous segments. In this dissertation, only ISO 3744 hemisphere measurement surface have been considered.

The hemisphere measurement surface has its origin at the position  $O$  and a measurement radius  $r$ , which is at least twice the characteristic dimension  $d_0$ . Distribution of microphone positions is shown in Figure 3. The microphone positions are located at positions listed in Table 1. The method is used when the purpose of the measurement is to determine the A-weighted sound power level directly from measurements of A-weighted sound levels on a hemisphere.

Finally, the sound power level,  $L_W$ , is calculated using equation:

$$L_W = \overline{L_p} + 10 \log \frac{S}{S_0} \text{ dB} \quad (1)$$

where  $S$  is the area of the measurement surface ( $\text{m}^2$ ),  $S_0$  is the reference area ( $1 \text{ m}^2$ ), and  $\overline{L_p}$  is the surface time-averaged sound pressure level defined as:

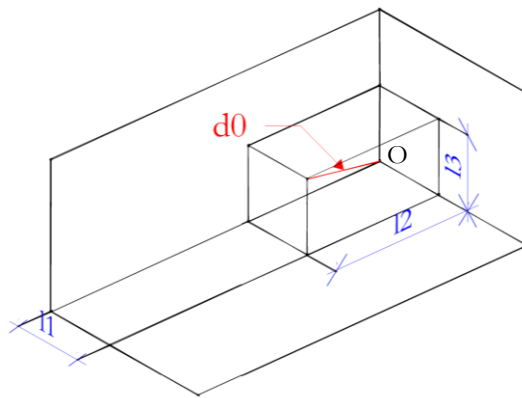


(a) Reference box on one reflecting plane,

$$d_0 = \sqrt{\left(\frac{l_1}{2}\right)^2 + \left(\frac{l_2}{2}\right)^2 + l_3^2}$$

(b) Reference box on two reflecting planes,

$$d_0 = \sqrt{l_1^2 + \left(\frac{l_2}{2}\right)^2 + l_3^2}$$



(c) Reference box on three reflecting planes,

$$d_0 = \sqrt{l_1^2 + l_2^2 + l_3^2}$$

**Figure 2.** Examples of characteristic dimensions ( $l_1$ ,  $l_2$  and  $l_3$ ) and reference boxes.

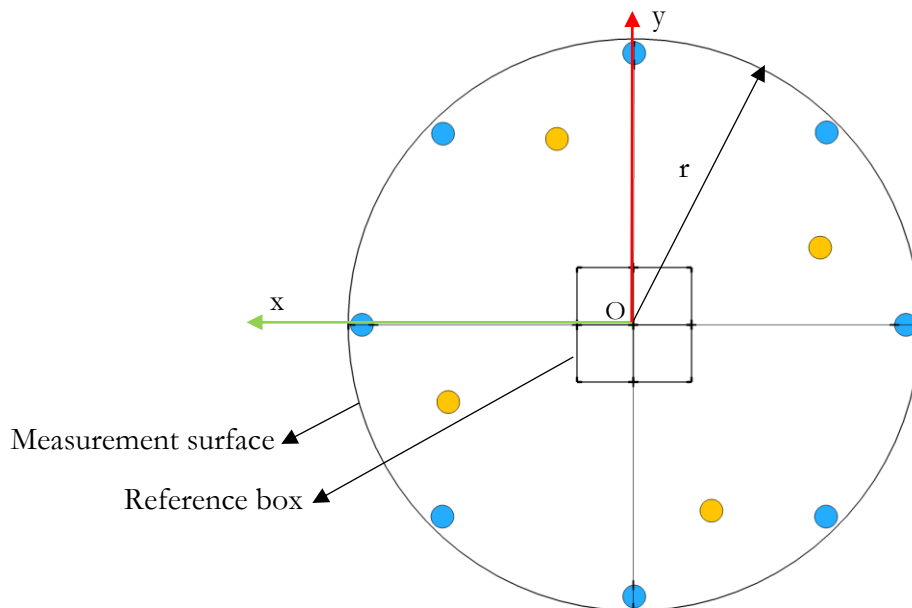


**Figure 3.** Distribution of measurement positions on a hemisphere measurement surface according to Annex F in ISO 3744 [9]. Blue and orange circles represent measurement positions at two different heights, see Table 1.

**Table 1.** Coordinates of microphone positions for hemisphere measurement surface.

Position number	$x/r^a$	$y/r^a$	$z/r$	$z$
1	$a$	0	–	1.5 m
2	$0.707a$	$-0.707a$	–	1.5 m
3	0	$-a$	–	1.5 m
4	$-0.707a$	$-0.707a$	–	1.5 m
5	$-a$	0	–	1.5 m
6	$-0.707a$	$0.707a$	–	1.5 m
7	0	$a$	–	1.5 m
8	$0.707a$	$0.707a$	–	1.5 m
9	0.65	–0.27	0.71	–
10	–0.27	–0.65	0.71	–
11	–0.65	0.27	0.71	–
12	0.27	0.65	0.71	–

<sup>a</sup> The constant  $a$  depends on the measurement radius defined in Table 2.

**Table 2.** Values of the constant,  $a$ .

$r$ [m]	$a$
4	0.927
6	0.968
8	0.982
10	0.989
12	0.992
14	0.994
16	0.996

$$\overline{L_p} = \overline{L'_{p(ST)}} - K_1 - K_2 \quad (2)$$

where  $\overline{L'_{p(ST)}}$  is the mean time-averaged sound pressure level defined in (3),  $K_1$  is the background noise correction defined in (4), and  $K_2$  is the environmental correction defined in (5).

The mean time-averaged sound pressure level is calculated according to:

$$\overline{L'_{p(ST)}} = 10 \log \left[ \frac{1}{N_M} \sum_{i=1}^{N_M} 10^{0.1L'_{pi(ST)}} \right] \text{ dB} \quad (3)$$

where  $L'_{pi(ST)}$  is the frequency-band or A-weighted time-averaged sound pressure level measured at the  $i^{\text{th}}$  microphone position or  $i^{\text{th}}$  microphone traverse with the noise source under test in operation, in decibels, and  $N_M$  is the number of microphone positions.

The background noise correction,  $K_1$ , is calculated according to:

$$K_1 = -10 \log(1 - 10^{-0.1\Delta L_p}) \text{ dB} \quad (4)$$

where  $\Delta L_p = \overline{L'_{p(ST)}} - \overline{L_{p(B)}}$  in which  $\overline{L'_{p(ST)}}$  is the mean frequency–band or A–weighted time–averaged sound pressure level from the array of microphone positions over the measurement surface, with the noise source under test in operation, in decibels, and  $\overline{L_{p(B)}}$  is the mean frequency–band or A–weighted time–averaged sound pressure level of the background noise from the array of microphone positions over the measurement surface, in decibels. Equation (5) is employed only if condition  $6 \text{ dB} \leq \Delta L_p \leq 15 \text{ dB}$  is fulfilled. If  $\Delta L_p > 15 \text{ dB}$ ,  $K_1$  is assumed to be zero. If  $\Delta L_p < 6 \text{ dB}$  in at least one one–third octave band, the accuracy is reduced and  $K_1$  to be applied is 1.3 dB.

The environmental correction,  $K_2$ , is given by:

$$K_2 = L_W^* - L_{W(RSS)} \quad (5)$$

where  $L_W^*$  is the environmentally uncorrected sound power level of the reference sound source, in decibels, and  $L_{W(RSS)}$  is the sound power level of the calibrated reference sound source under the meteorological conditions of the test, in decibels.

### 2.2.1.1 Measurement Uncertainty

According to ISO 3374 [9], upper bound values of the standard deviations for most of the applications are presented in Table 3. The values of the standard deviations are based on results obtained from round robin tests [39,40] and refer to engineering method, e.g., accuracy grade 2.

**Table 3.** Standard deviations of measured sound power levels according to ISO 3374.

Frequency bandwidth	One–third octave mid–band	Standard deviation of
	frequency	reproducibility
	Hz	dB
One–third octave	100–160	3
	200–315	2
	400–5000	1.5
	6300–10000	2.5
A–weighted per Annex E		1.5 <sup>a</sup>

<sup>a</sup> Applicable to noise sources which emit sound with a relatively “flat” spectrum in the frequency range 100–10000 Hz.

### 2.2.2 Nordtest Method

The Nordtest engineering method [31], part NT ACOU 080, defines procedures for measuring sound pressure levels at defined positions around sound sources and calculating the *source strength* based on the measured sound pressure levels. According to the method itself, the source strength is defined as part of the sound power level radiated between  $0^\circ$  and  $20^\circ$  above the horizontal plane, which is relevant for the calculation of sound pressure levels at certain distances from the source. The sound radiated vertically upwards is neglected. Measurements are performed *in situ* outdoors and data are primarily intended for use as input in prediction methods. However, care must be taken to define acoustic centre of the sound source, since it is regarded later as a point source in prediction models.

First, the reference box is determined from the size and the shape of the sound source, in a same manner as described in the previous section. The reference box is imaginary parallelepipedal surface enclosing all parts of the noise source under test that contribute to emission of sound energy. Afterwards, the *characteristic dimension*  $d_0$  defined as half the diagonal of the box enveloping the reference box is calculated (see Figure 2). Hereafter, one of the two measurement methods, Nordtest Sphere Method or Nordtest Box Method (explained in more details in next sections), is chosen and the total source strength,  $L_W$ , in each octave band is calculated according to:

$$L_w = \overline{L_p} + 10 \cdot \log \frac{S}{S_0} \text{ [dB]} \quad (6)$$

where  $S$  is the area of measurement surface,  $S_0$  is the reference area (1 m<sup>2</sup>), and  $\overline{L_p}$  is defined as:

$$\overline{L_p} = 10 \cdot \log \left( \frac{1}{N} \cdot \sum_{i=1}^N 10^{\frac{L_{pi} - K_i}{10}} \right) \quad (7)$$

where  $N$  is the number of microphone positions,  $L_{pi}$  is the sound pressure level measured at microphone position  $i$ , and  $K_i$  is the environmental correction to be applied at microphone position  $i$ .

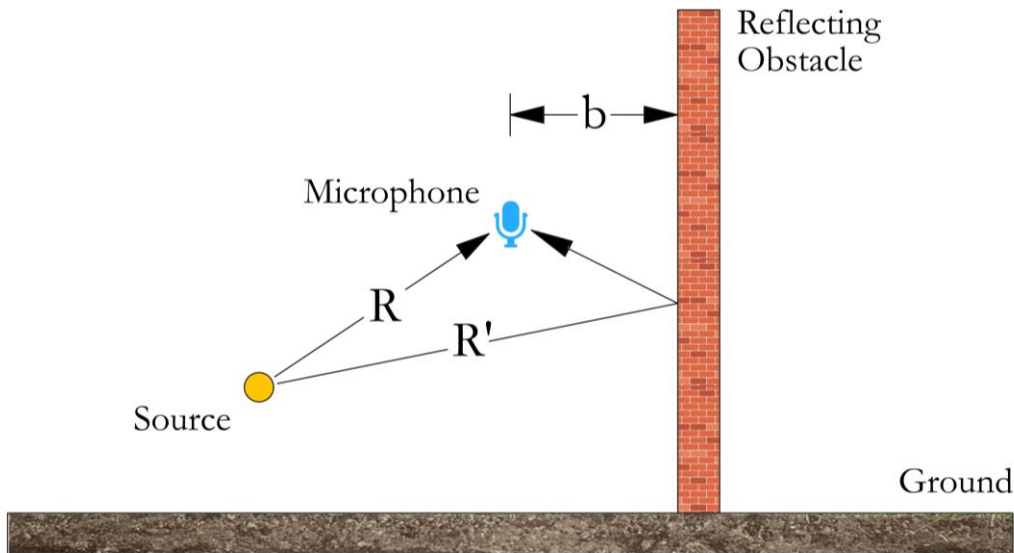
The source strength in (6) is calculated both as overall A-weighted value and octave band values within the frequency range 63–8000 Hz. Octave bands centred at 31.5 Hz and 16 kHz are optional and can be calculated in case when energy radiated by the source cannot be neglected in those bands. The environmental correction  $K$  in (7) is estimated based on theoretical and empirical considerations. Following rules are applied (see Figure 4 for specific distances):

- $K$  is approx. 6 dB when  $b < 0.1\lambda_c$ ;
- $K$  is approx. 3 dB when  $\lambda_c < b < R / 10$ ;
- $K$  is approx. 0 when  $R' > 2R$ ;
- When  $R / 10 < b$ ,  $b > \lambda_c$  and  $R' < 2R$ , the value of  $K$  is taken from Table 4.

**Table 4.** Environmental correction  $K$  due to a sound reflecting obstacle.

$b/R$ [-]	< 0.10	0.1 – 0.3	0.3 – 0.5	> 0.5
$K$ [dB]	3	2	1	0

Finally, the acoustic centre is determined, and data is used in prediction models. The acoustic centre in the horizontal plane is usually defined as geometrical centre of the reference box, while the acoustic centre in the vertical plane is defined either at a height of two thirds the height of the reference box or as the position of dominating sound source (if such exists).



### 2.2.2.1 Nordtest Sphere Method

The Nordtest Sphere Method defines microphone positions over part of a sphere which encloses the sound source under test. In order to get as precise data at low frequencies as possible, sphere radius must be quite large. Hence, the application of the sphere method is limited to favourable acoustic environment. The term “favourable” refers to cases where it is possible to implement measurements at distances from the source equal to at least twice the characteristic dimension of the source ( $R \geq 2 \cdot d_0$ ). The key and additional measurement positions are shown in Figure 5, depending on the number of reflecting planes the reference box terminates on. The centre of the measurement surface is the centre of the reference box.

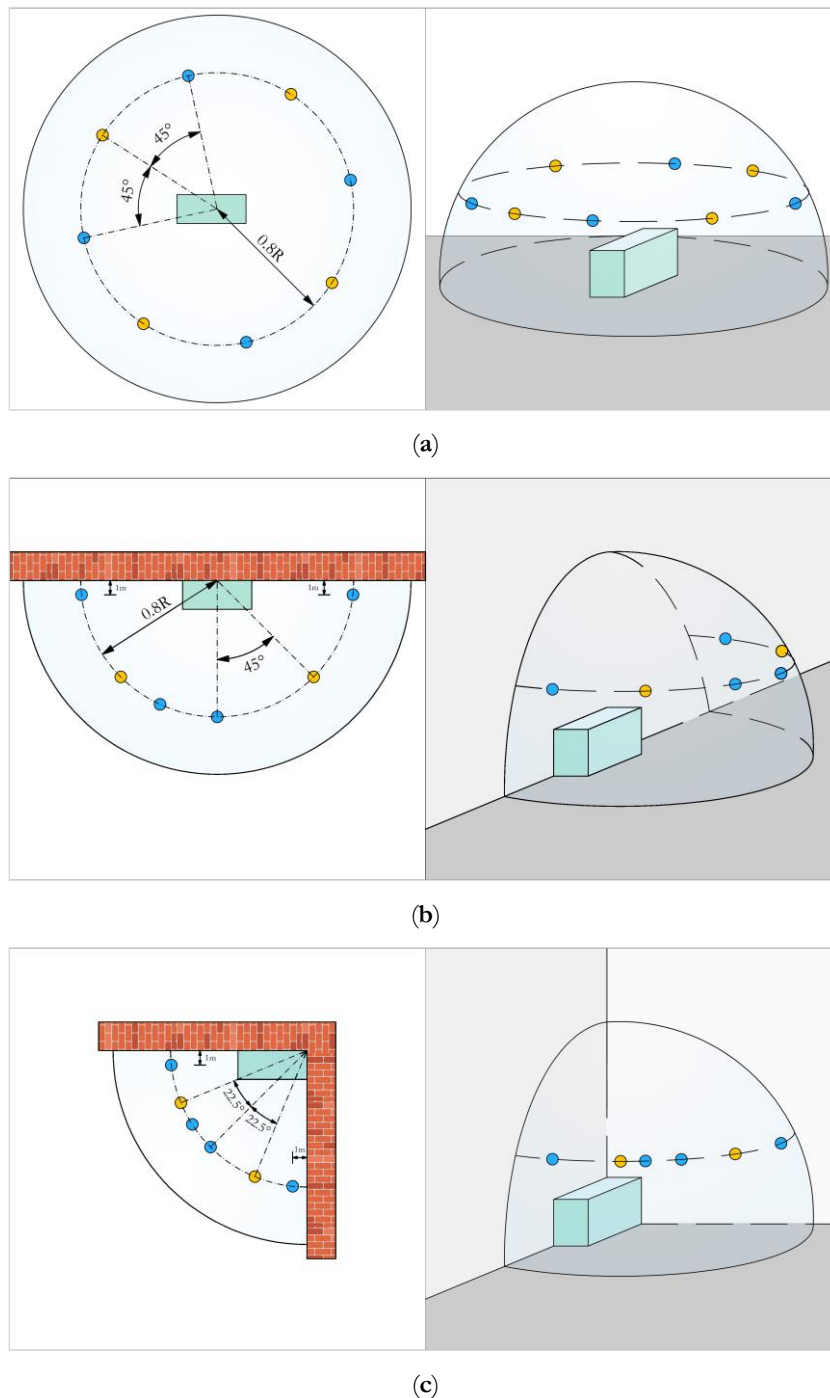


**Figure 5.** Spherical measurement surfaces and microphone positions around the reference box: (a) on one reflecting plane, (b) at two reflecting planes, and (c) at three reflecting planes. Blue circles present key, while orange circles present additional microphone positions.

The key microphone positions are placed on a circular path at a height of  $0.6 \times R$  and a horizontal distance from the sphere centre of  $0.8 \times R$ . The microphone height should be at least 1 m even if  $0.6 \times R < 1$  m, and the microphone height is limited to 10 m in cases when  $0.6 \times R > 10$  m. There are 4 key microphone positions. Key microphone position No. 1 is chosen as the position on the circular path at which the highest value of the overall A-weighted sound pressure level occurs. In case of symmetry in a horizontal plane, only one microphone position is needed. The rest of key positions are placed evenly distributed on the circular path. In cases when the difference between any two values of the overall A-weighted sound pressure level measured at the key microphone positions exceeds 6 dB, additional microphone positions are required (see [Figure 5](#)).

The source strength is calculated according to (6). With this method, it is also possible to obtain source-directional characteristics,  $\Delta L_{\Phi}$ :

$$\Delta L_{\Phi i} = (L_{pi} - K_i) \cdot \overline{L_p} + 3 \cdot n \quad (8)$$

where  $L_{pi}$  is the octave band sound pressure level at microphone position  $i$  (after correction for background noise), in dB,  $K_i$  is the environmental correction in microphone position  $i$ , in dB,  $\overline{L_p}$  is the energy average sound pressure level in dB defined in (7), and  $n = 0, 1, 2$  when one, two or three reflecting planes are present near the source, respectively.

### 2.2.2.2 Nordtest Box Method

The Nordtest Box Method defines microphone positions on the surface of the imaginary box which encloses the sound source under test. The distance from the sound source can be quite small. Hence, the application of the box method is applicable in “unfavourable” acoustic environment. The term “unfavourable” refers to cases where background noise levels are high or in the presence of reflecting object. With this method, it is not possible to obtain source-directional characteristics. The key and additional measurement positions are shown in [Figure 6](#), depending on number of reflecting planes the reference box terminates on.

The distance between measurement surface and sides of the reference box  $a$  must be larger than 0.15 m, but preferably as large as possible (distances larger than 1 m are recommended). According to the method, small distance  $a$  reduce the accuracy, especially at low frequencies. At the same time the necessary number of microphone positions becomes large. If  $a$  is shorter than half the smallest side length of the reference box, extra microphone positions at the midpoint of each free edge of the measurement surface are added. Following rules are applied:

- The heights of the key microphone positions:  $h_1 = (l_3 + a)/2$  and  $h_2 = l_3 + a$ ;
- The heights  $h_1$  and  $h_2$  should be at least 1 m and maximum 10 m;
- If  $(l_3 + a)/2 < 1$  m,  $h_1$  is chosen in the interval  $1 \text{ m} \leq h_1 \leq h_2$ ;
- If  $l_3 + a \geq 10$  m,  $h_2$  is chosen in the interval  $1 \text{ m} < h_2 \leq 10$  m;
- If  $(l_3 + a)/2 > 10$  m,  $1 \text{ m} < h_1 \leq 10$  m

Additional microphone positions are required if the difference between the overall A-weighted sound pressure levels measured at any two key microphone positions exceeds 6 dB and at the same time the distance measured along the measurement surface between any two adjacent key microphone positions exceed  $2a$  (see [Figure 6](#)).

The total source strength,  $L_w$ , in each octave band is calculated according to:

$$L_w = \overline{L_p} - E + 10 \cdot \log \frac{S}{S_0} \text{ [dB]} \quad (9)$$

where  $\overline{L_p}$ ,  $S$  and  $S_0$  are same as in (6), and  $E$  is correction due to near-field error defined in [Table 5](#).

### 2.2.2.3 Measurement Uncertainty

Standard deviations of the Nordtest method [31] are presented in Table 6. According to the Nordtest method, the standard deviations are based on measurements of sound strengths of broad band industrial noise sources. One should bear in mind that the measurement uncertainty is expected to larger if the noise contains pronounced discrete tones in on or more octave bands. Generally speaking, accurate results are expected if a low background noise and a favourable environment combined with a large measurement distance are provided.

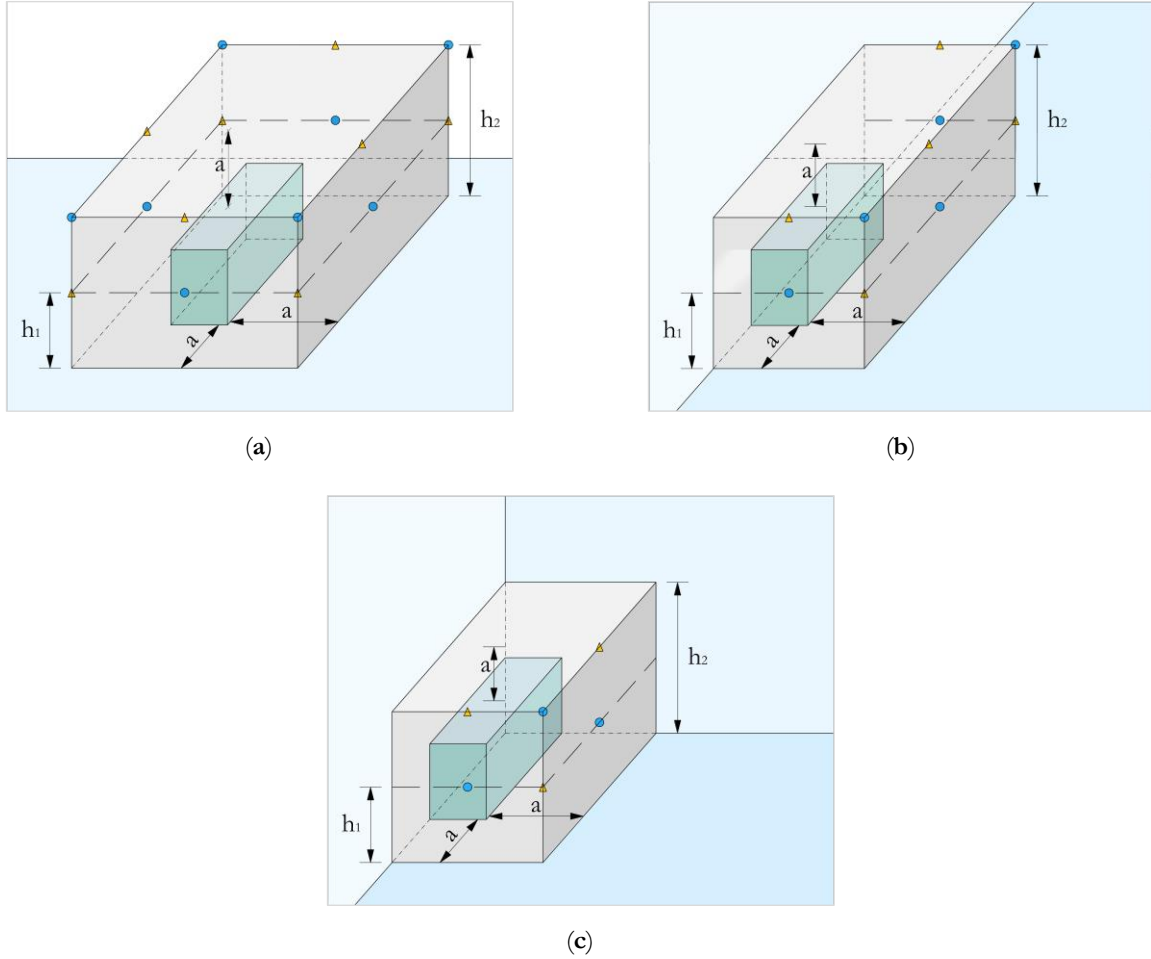


Figure 6. Parallelepipedal measurement surfaces and microphone positions around the reference box: (a) on one reflecting plane, (b) at two reflecting planes, and (c) at three reflecting planes. Blue circles present key, while orange triangles present additional microphone positions.

Table 5. Correction,  $E$ , due to near-field error ( $S$  – area of measurement box surface [ $\text{m}^2$ ],  $S_{ref}$  – area of reference box surface [ $\text{m}^2$ ]).

$S_{ref} / S$ [dB]	$E$ [dB]
$0 < S_{ref} / S \leq 0.4$	0
$0.4 < S_{ref} / S \leq 0.7$	1
$0.7 < S_{ref} / S \leq 0.9$	2
$0.9 < S_{ref} / S < 1$	3

Table 6. Standard deviations of measured sound strength of broad band industrial sources according to Nordtest method.

Frequency [Hz]	63	125	250–500	1000–4000	8000	Total A-weighted
Standard deviation [dB]	4	3	2	1.5	3	2

### 2.2.3 ISO 9614-1

Unlike sound pressure-based measurement methods described in previous sections, ISO 9614-1 [10] defines procedures for determination of sound power levels of a noise source from measurements of sound intensity. As in case of sound pressure-based measurement methods, measurement of sound intensity is done on a surface enclosing the source. The ISO 9614-1 is based on discrete-position sampling of the intensity field. The main advantage of the measurement of sound intensity is that it can be used in the presence of high levels of background noise generated by sources other than that under investigation, since only a normal component of sound intensity is measured. Due to limitations of measurement equipment, the measurements are usually restricted to one-third octave range 50–6300 Hz.

The normal sound intensity is measured on an initial measurement surface, which can be parallelepiped, hemisphere, cylinder or hemi-cylinder. The measurements are made at minimum of one position per square meter and at minimum of ten position distributed as uniformly as possible. If more than fifty measurement positions are required, a reduction to one position per 2 m<sup>2</sup> is allowed as long as the total number of measurement positions is not less than fifty. The sound power level of the noise source in each frequency band is calculated according to:

$$L_w = 10 \cdot \log \sum_{i=1}^N \frac{P_i}{P_0} \text{ [dB]} \quad (10)$$

where  $P_0$  is the reference sound power (10<sup>-12</sup> W),  $N$  is the total number of measurements and segments, and  $P_i$  is the partial sound power for segment  $i$  calculated according to:

$$P_i = I_{ni} \cdot S_i \quad (11)$$

where  $S_i$  is the area of segment  $i$ , and  $I_{ni} = I_0 \cdot 10^{XX/10}$  is the signed magnitude of the normal sound intensity component measured at position  $i$  on the measurement surface. If the normal sound intensity level  $L_{I_{ni}}$  for segment  $i$  is expressed as XX dB, the value of  $I_{ni}$  is calculated from:

$$I_{ni} = I_0 \cdot 10^{XX/10} \quad (12)$$

If the normal sound intensity level  $L_{I_{ni}}$  for segment  $i$  is expressed as (-)XX dB, the value of  $I_{ni}$  is calculated from:

$$I_{ni} = -I_0 \cdot 10^{XX/10} \quad (13)$$

#### 2.2.3.1 Measurement Uncertainty

Standard deviations of the ISO 9614-1 [10] are presented in Table 7. According to the ISO 9614-1 method, the stated uncertainties account for random errors associated with the measurement procedure, together with the maximum measurement bias error. Since there is no sufficient data below 50 Hz, but also bearing in mind limitations of measurement equipment, uncertainties are limited to one-third octave bands 50–6300 Hz.

**Table 7.** Standard deviations of measured sound power levels according to ISO 9614-1.

Octave band centre frequencies	One-third octave band centre frequencies	Standard deviations, s* Engineering (grade 2) [dB]
63–125	50–160	3
250–500	200–630	2
1000–4000	800–5000	1.5
	6300	2.5

\* The true value of the sound power level is to be expected with a certainty of 95 % in the range  $\pm 2s$  about the measured value.

## 2.3 Acoustic Scale Models

Acoustic scale models were first used in 1930s [41], but the main modelling principles have not changed until today. The major improvements have been reflected mostly in testing equipment [42] (e.g., miniature loudspeaker and other equipment working at ultrasound frequencies) and introduction of digital signal processing [43]. Scale modelling has been used to investigate different acoustic phenomena, such as phenomena in auditorium and architectural acoustics [44], traffic noise propagation [45], noise propagation in factories [46] and urban areas [47], and many others. Recently, scale modelling techniques were also used to assess the prehistoric acoustics (musical sounds and speech) of Stonehenge [48], among other things.

The scaling technique is based on two fundamental equations:

$$\text{Speed of sound} = \frac{\text{Distance}}{\text{Time}} = \text{Frequency} \times \text{Wavelength} \quad (14)$$

Since air is commonly used propagation medium in both full-size and scale models, the speed of sound remains the same in both cases. Thus, distance and time are reduced by the scale factor in the model, while the frequency is increased. This means that e.g., in a 1:10 scale model dimensions are decreased, and frequency is increased by a factor of 10.

The main advantage of scale modelling is to be found in the fact that the majority of acoustic phenomena in a scale model seem to be identical to phenomena in full-size models. However, certain attention should be paid to material properties and absorption of the air. The former can be overcome by careful selection of materials in the model which would match absorption characteristics of full-size materials. In the case of acoustically hard surfaces, the properties of the material remain identical in both scale models and full-size models. The latter could be eliminated by suitable choice of the scale factor, making sure that air humidity is within certain limit [44].

## 2.4 Experimental Setup

### 2.4.1 Scale model experiment

The measured object was built of a solid wood and had parallelepiped shape with dimensions  $0.6 \times 0.55 \times 0.3$  m. It consisted of four 1" tweeters (two pairs) mounted in the centre of an acoustically hard wooden base, with an angle between any two adjacent tweeters of approx.  $45^\circ$  (see Figure 7a). The first pair consisted of two *SB Acoustics SB26STAC-C000-4* tweeters that faced each other, while the second pair consisted of two *Peerless by Tymphany XT25TG30-04* tweeters aimed outwards. Since tweeters are known to be very directional sound sources, this configuration was chosen in order to provide as uniform sound dispersion in all directions as possible. Additionally, nine spherical shaped diffusers were mounted on the ceiling in order to provide as diffuse sound field inside the object as possible, as well to further support the uniform dispersion of sound energy radiated outwards.

According to specification sheets [49,50], both pairs of speakers had flat on axis frequency response in the frequency range approx. 700 – 40000 Hz, providing sound levels of approx. 90 dB at 1 m distance. In order to ensure safe operation of the speakers, two crossovers with crossover frequency of 500 Hz were designed and used with each pair of speakers. The crossovers were connected to the output of a custom power amplifier, which had a flat frequency response up to 100 kHz. The amplifier was connected to the output of *Steinberg UR22* audio interface, which supported sampling frequencies of up to 192 kHz. Microphone Brüel & Kjær type 4136, designed for high-frequency measurements, was used for acquisition of sound pressure levels around the measured object.

The shape of the object was selected to match a typical shape of floating river clubs. Two parallel side surfaces had openings with dimensions  $0.1 \times 0.1$  m (windows), one side surface had opening with dimensions  $0.1 \times 0.2$  m (door), while the last side surface had no openings. The object was constructed in a way so that ceiling and all side surfaces could disassemble, which allowed the characterisation of the object in different scenarios:

- Scenario 1 (S1) – Speaker cluster in a free space at one reflective plane (Figure 7a),
- Scenario 2 (S2) – Speaker cluster under reflective ceiling (Figure 7b), and
- Scenario 3 (S3) – Speaker cluster in enclosed wooden box with openings (Figure 7c).

For each scenario, three measurement methods were applied: ISO 3744, Nordtest Sphere and Nordtest Box. Application of the ISO 9614–1 measurement method was not possible due to inability of the intensity probe to cover the frequency range of interest. All measurements were performed in the open yard of a summer cottage outside Belgrade, Serbia, with the closest reflecting object several meters away.

The acoustically hard wooden base with dimensions  $2 \times 2$  m was used in order to support the farthest measurement positions, which were located 1 m away from the centre of the measured object. The flat wooden base played an important role in positioning the microphone at different measurement positions. Distribution of measurement positions for different characterisation methods is presented in Figure 8, together with corresponding heights.

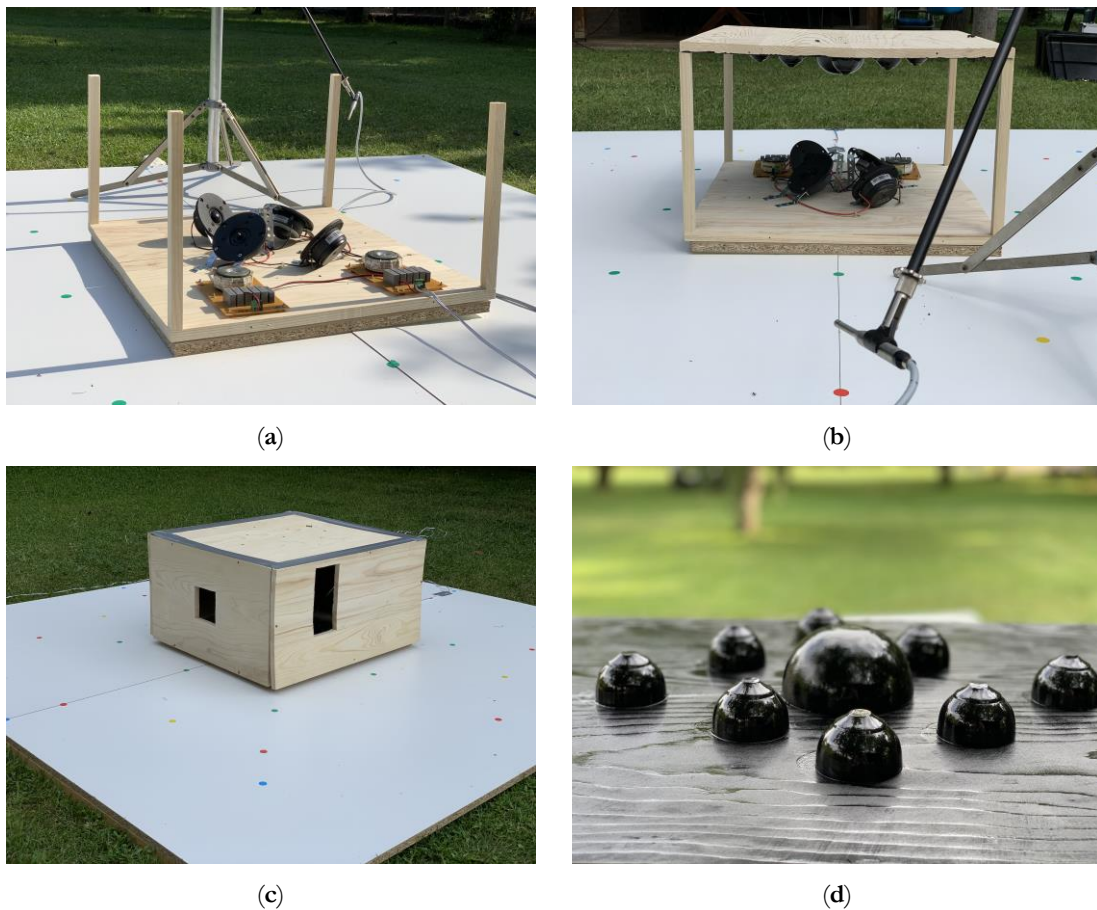


**Figure 7.** Scale model of floating river club used in different scenarios: (a) S1– Speakers in a free–field, (b) S2 – Speakers under reflective ceiling, (c) S3 – Speakers in enclosed wooden box with openings, and (d) Spherical shaped diffusers mounted in the ceiling.

In case of Nordtest Sphere method, eight measurement positions at single height  $h = 0.6$  m were used (red circles in Figure 8), while Nordtest Box method encompassed sixteen measurement positions at two heights,  $h_1 = 0.2$  m and  $h_2 = 0.4$  m (green circles in Figure 8). Therefore, each measurement position marked in Figure 8 was used twice, for two different heights. It should be noticed that only measurement positions 1–8 at  $h_1$  are marked in Figure 8. Measurement positions 9–16 at  $h_2$  can be obtained by converting position 1 to 9, 2 to 10, etc. Finally, ISO 3744 method contained twelve measurement positions at two different heights, eight measurement positions at  $h_3 = 0.15$  m (blue circles in Figure 8) and four measurement positions at  $h_4 = 0.71$  m (orange circles in Figure 8). In other words,

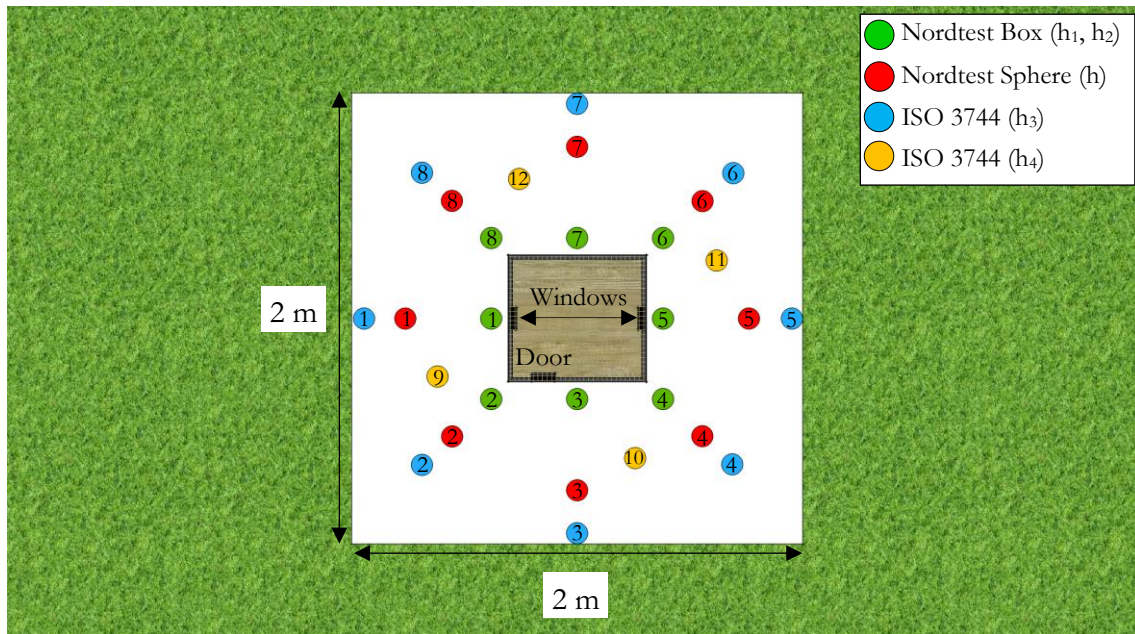


**Figure 8.** Distribution of microphone positions around the scale model of floating river clubs for different characterisation methods. Microphone heights varied between characterisation methods: Nordtest Sphere method ( $h = 0.6$  m), Nordtest Box method ( $h_1 = 0.2$  m,  $h_2 = 0.4$  m) and ISO 3744 ( $h_3 = 0.15$  m,  $h_4 = 0.71$  m).

both ISO 3744 and Nordtest Sphere methods contained different measurement positions on the imaginary sphere with radius  $R = 1$  m (see Section 2.2.1 and Section 2.2.2.1, respectively), while the Nordtest Box contained measurement positions on the imaginary parallelepiped located at distance  $a = 0.1$  m away from the object's side surfaces (see Section 2.2.2.2).

In order to provide frequency range of interest (one-third octave bands with central frequencies 630 – 31500 Hz) as well as suitable signal-to-noise ratio, frequency band spectra power levels were calculated from impulse responses recorded at different measurement positions. The measurements employed logarithmic sine sweep excitation signals with length of 5.5 s. Each impulse response was recorded by averaging three consecutive measurements. The sampling frequency of 192 kHz was used, allowing calculation of frequency band spectral power levels up to the loudspeaker's upper limit (~40 kHz). The measuring platform EASERA (AFMG, Berlin, Germany) was used for both excitation and data acquisition. The MATLAB (The MathWorks, Inc, Natick, Massachusetts, USA) computing environment was employed for evaluation purposes. The excitation level as well as microphone sensitivity were kept constant during all measurements. In that way, it was possible to make relative comparisons of determined sound power levels for different scenarios and measurement methods.

#### 2.4.2 Cottage with a Lightweight Façade

The measured object used in the experiment was a summer cottage with a structure equivalent to most floating river clubs in Belgrade, Serbia (see Figure 9). Namely, the interior of the cottage consisted of a single open-space area, with façade made of lightweight wooden boards in combination with doors, single glass partitions and open areas. This led to a non-uniform radiation of sound from different façade elements when noise source was operating inside the house, as in case of floating river clubs. The cottage had dimensions  $6 \times 5.4 \times 2.6$  m which matched dimensions of the scale model presented in Section 2.4.1, after rescaling them with the factor of 10. Additionally, the structure of the house was identical to scenario S3 in the scale model (see Figure 7c). The house was built on the spacious flat surface which allowed for easy implementation of different measurement methods, unlike the environment in which floating river clubs are located.

The cottage was characterised by implementation of three sound pressure-based, ISO 3744 [9] alternative hemispherical surface method, Nordtest Sphere and Nordtest Box methods [31], and one sound intensity-based, ISO 9614-1 [10], measurement methods. Sound pressure-based measurements were performed by using *Norsonic Nor140* sound level meter with *Nor1225* class 1 microphone. For sound



Figure 9. Summer cottage made of lightweight wooden boards used in the experiment.

intensity-based measurements *Briel and Kjaer PULSE* system *type 2270* with hand-held sound intensity probe was used. A custom dodecahedron loudspeaker was used as a noise source in all measurements, producing around 110 dBA indoors. The working range of the loudspeaker was limited to 100–3150 Hz. Stationary pink noise with duration of 30 s was used as excitation signal. The loudspeaker was placed approximately in the geometric centre of the house, at height 1.5 m above the floor. A window and entrance door were left open during the measurements in order to match scenario S3 in the scale model experiment, but also to resemble music performances on the floating river clubs. The measurement positions' distribution for all four measurement methods performed in this experiment are presented in Figure 10.

For both ISO 3744 and Nordtest Sphere methods measurement positions on the imaginary sphere with radius  $R = 10$  m was used, but with different distribution. The ISO 3744 alternative hemispherical surface method suggests twelve, while the Nordtest Sphere method suggests eight measurement positions, as explained earlier (see Figure 8). The ISO 3744 method contained twelve measurement positions at two different heights, eight measurement positions at  $h_1 = 1.5$  m (red circles in Figure 10a), and four measurement positions at  $h_2 = 7.1$  m (blue circles in Figure 10a). For Nordtest Sphere method, eight measurement positions at single height  $h = 6$  m were used (see Figure 10b).

For the Nordtest Box method a parallelepiped with the distance of  $a = 1$  m away from the house was used as a measurement surface. Measurement positions were distributed at two heights,  $h_1 = 1.8$  m and  $h_2 = 3.6$  m, as shown in Figure 10c. Total of 32 measurement positions were used. This characterisation method is recommended method for sources situated in less favourable acoustic environment, e.g., where the background noise level is high or in the presence of sound-reflecting obstacles, as described in Section 2.2.2.2.

For the intensity-based measurement, each side of the object was divided into rectangular elements with dimensions  $1 \times 1$  m. Sound intensity measurements were performed in the centre of each element, as shown in Figure 10d. Total of 84 measurement positions were used. First, sound power levels of each individual side partitions were determined. Then the measurements were performed over the roof area in the same manner. Finally, overall sound power level was determined by logarithmic average of individual sound power levels for each partition.

### 2.4.3 The Case of Floating River Clubs

The Nordtest Sphere method was applied to two floating river clubs, hereinafter referred to as 'Club 1' and 'Club 2', by implementation of sound pressure level measurements with *Norsonic Nor140*

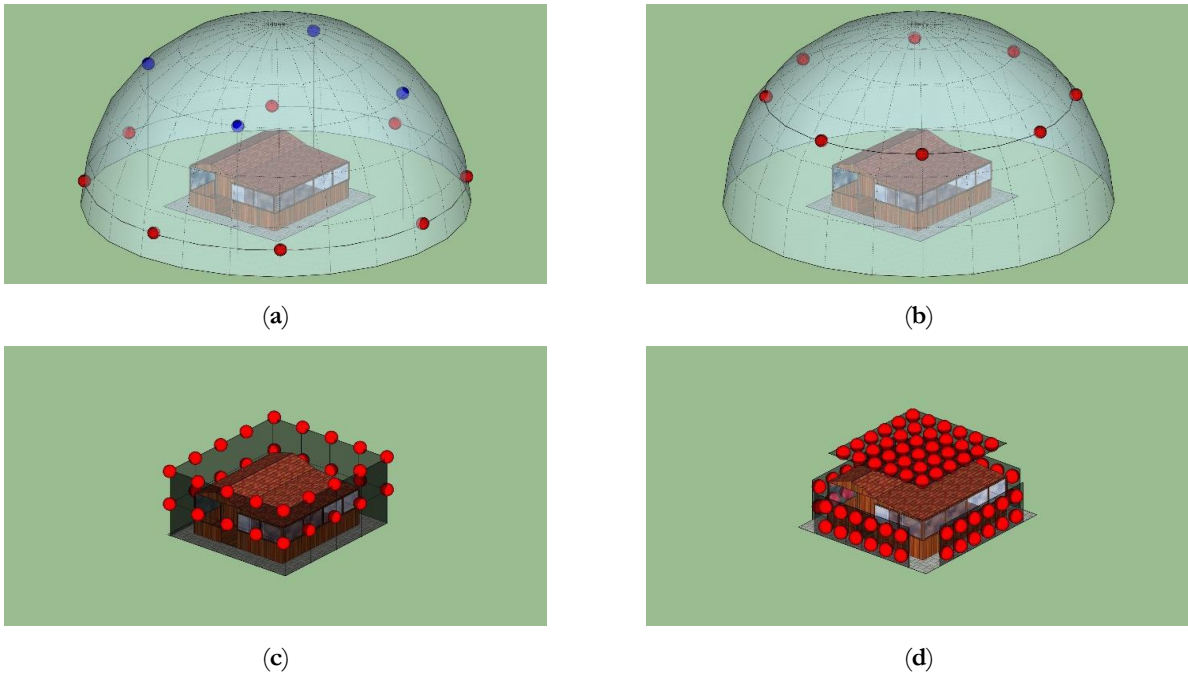


**Figure 10.** Distribution and of measurement positions for different sound power measurements: (a) ISO 3744 alternative hemispherical surface method, (b) Nordtest Sphere method, (c) Nordtest Box method, and (d) ISO 9614-1 sound intensity method.

sound level meter and *Nor1225* class 1 microphone. The sound pressure levels were measured at six measurement positions around the clubs (blue circles in [Figure 11](#) and [Figure 13](#)), at the distance of approx. 30 m away from the closest outer surface. Three measurement positions were located at the bank of the river, while the other three measurement positions were located on the river by help of a boat. The distance between clubs and measurement positions was determined with a laser rangefinder. The microphone was mounted at the adjustable rod, keeping the constant height of 10 m above the river level. A pink noise excitation signal with the length of 30 s was generated from clubs' audio systems at every measurement position, producing approx. 110 dBA indoors. Due to proximity of surrounding floating river clubs, measurements of sound pressure levels at two measurement positions between the clubs (orange circles at [Figure 11](#) and [Figure 13](#)), Club 1 and Club 2 and surrounding clubs, were not performed. Instead, the sound pressure levels were calculated as logarithmic average of the sound pressure levels measured at two closest measurement positions. All measurements were performed on Sunday morning, which was the quietest period of the week. Although both floating clubs were located in the vicinity to three bridges, the traffic over the bridges was low, producing background noise of approx. 35 dBA. The temperature was 30–35 °C, with the wind speed approx. 2.5 m/s and relative humidity 40–45 %.

Club 1 had a parallelepiped shape with dimensions approx.  $25 \times 15 \times 5$  m. Dance area was concentrated in the part of the club towards the river, see [Figure 11](#). Audio system consisted of eight *RCF ART 315* two-ways 15" speakers and six *KV2 AUDIO VHD4.18* single 18" subwoofers, uniformly distributed around the dance area. The club was built of a light wood and glass panels, with some completely open segments during opening hours as well as during the measurements. The radius of the imaginary sphere was approx.  $R = 42.5$  m, assuming the position of acoustic centre in the middle of the dance area. Appearance of the Club 1 with the surrounding is presented in [Figure 12](#).

Club 2 had a parallelepiped shape with dimensions  $20 \times 30 \times 9$  m. Dance area was located at the second floor of the club, at approx. 6 m above the river level, see [Figure 13](#). Audio system consisted of four custom designed three-way 15" speaker systems and four 18" subwoofers, with each loudspeaker-subwoofer pair located in the corner of the dance area and aimed towards the centre. The dance area was covered with a roof only partially, which made the audio system radiate sound energy in a nearly free-field conditions. Since the height of the microphone was kept the same, 10 m above the river level, this caused the microphone positions to be located approximately 4 m above the dance area.

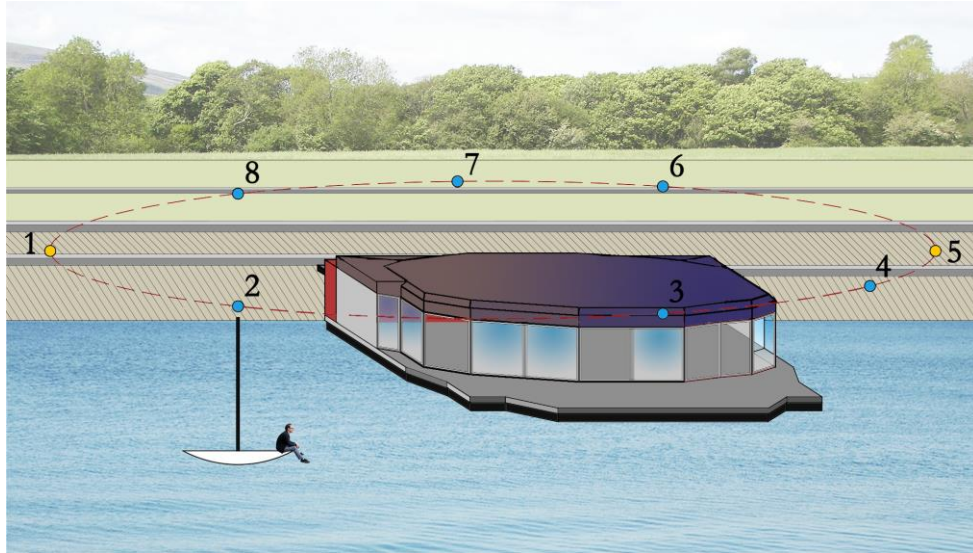


**Figure 11.** Illustration of the Club 1 located on the Sava river. Red area presents the entrance hall.



**Figure 12.** Photograph shows the boat with the measurement equipment in case of Club 1.

Therefore, the radius of the imaginary sphere was approx.  $R = 40$  m, assuming the acoustic centre in the middle of the dance area. Appearance of the Club 1 with the surrounding is presented in [Figure 14](#).

In order to verify application of the Nordtest Sphere method to Club 1 and Club 2, sound pressure levels were additionally measured at several control measurement positions in a far-field. The far-field measurements were performed in the normal direction against the opposite bank, keeping the same microphone height as in case of the Nordtest method i.e., 10 m above the river level. The measured sound pressure levels in a far-field were then compared to those calculated according to:

$$\overline{L_p} = L_w - 20 \cdot \log r - 8 \text{ dB [dB]} \quad (15)$$

where  $L_w$  is the sound strength level determined by implementation of the Nordtest method,  $r$  is the distance between measurement positions and acoustic centre of the clubs, while 8 dB correction is applied to sound sources close to a flat surface (radiation of acoustical energy to half of a sphere). The results are presented in the next section.

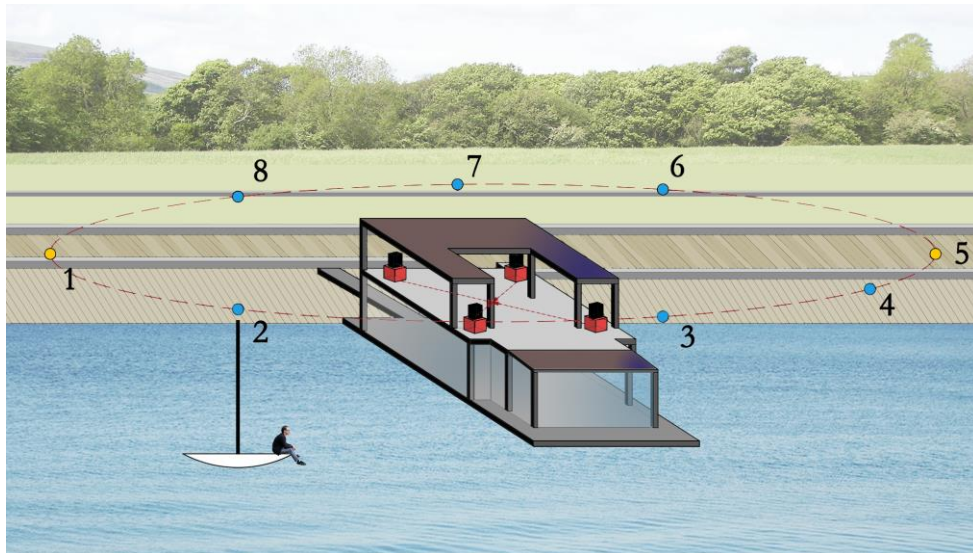


**Figure 13.** Illustration of the Club 2 located on the Sava river. Red cubes present subwoofers, while black cubes present three-way speaker systems.



**Figure 14.** Photograph shows the boat with the measurement equipment in case of Club 2.

## 2.5 Experimental Result and Discussions

The measurement methods for sound power level determination, presented in [Section 2.2](#), were implemented in different scenarios. First, a scale model of a typical floating river club was built in order to investigate possible differences in sound power levels when implementing different measurement methods. The differences were further investigated in case of a cottage with a lightweight façade equivalent to floating river clubs but located on the hard ground. In this way, practical difficulties related to measurements in specific environment characteristic for floating river clubs were avoided. The purpose of these investigations was to carry out a selection of an optimal sound power measurement method, which would be in line with the existing standards, and can be further applied to the specific environment of floating river clubs. Finally, the optimal measurement method was implemented in case of two floating river clubs.

### 2.5.1 A Scale Model Experiment

Frequency band spectral power levels were calculated in one-third octave bands with central frequencies 63–3150 Hz using (1) and (6). This frequency range corresponded to the frequency range 560–35500 Hz in the scale model experiment. The frequency range was chosen due to practical limitations of measurement equipment. Results obtained for different scenarios (S1–S3) are presented in [Figure 15–Figure 17](#) along with standard deviations described in [Section 2.2.1.1](#). Sound power levels determined by implementation of the ISO 3744 method were used here as a reference. The choice of the referent characterisation method was arbitrary, and the focus should be kept on relative differences between different characterisation methods.

A good agreement between sound power levels obtained by implementation of different characterisation methods in scenarios S1 and S2 was found. Most of the values presented in [Figure 15](#) and [Figure 16](#) lied within standard deviations of the ISO 3744 method, with few exceptions. The ISO 3744 standard deviations were slightly exceeded at 400 Hz, 630 Hz, 800 Hz and 3150 Hz in case of the Nordtest Sphere method, and at 630 Hz and 800 Hz in case of the Nordtest Box methods for scenario S1. For scenario S2, the deviations were exceeded at 125 Hz, 630 Hz, 800 Hz, 2500 Hz and 3150 Hz in case of the Nordtest method, as well as at 2500 Hz and 3150 Hz in case of the Nordtest Box method. However, the exceedances were less than 1 dB in all cases except at 3150 Hz in S2, where exceedances of about 1.7 dB were found for both the Nordtest Box and the Nordtest Sphere methods. Additionally, relative differences in overall sound power levels for S1 between Nordtest methods and the ISO 3744 were only 0.5 dB and 0.7 dB for the Nordtest Box and the Nordtest Sphere method, respectively. For S2, those differences were –0.2 dB and 0.2 dB for the Nordtest Box and the Nordtest Sphere method, respectively.

Unlike first two scenarios, scenario S3 showed a different trend (see [Figure 17](#)). Namely, a good agreement was obtained between the Nordtest Sphere and ISO 3744 methods. Here, all relative differences between the methods lied within standard deviations of the ISO 3744 method. However, relative differences between the Nordtest Box and the ISO 3744 methods diverged significantly after 315 Hz. This effect was even more pronounced at high frequencies starting from 1250 Hz. Still, a good agreement at low frequencies below 200 Hz was found for all methods, where the Nordtest Sphere and the Nordtest Box methods showed almost perfect match. While the overall levels for the Nordtest Sphere and ISO 3744 methods were identical, the Nordtest Box method overestimated the overall sound power level by 3.3 dB.

Three phenomena stood out from the presented results. First, a good agreement between all characterisation methods, in all scenarios, was obtained at low frequencies below 250 Hz. This was somehow unexpected in case of the Nordtest Box method, since the method itself cautions of reduced accuracy at low frequencies due to distribution of measurement positions in a vicinity of measured objects. Second, relative differences of sound power levels obtained in S2 suggested that all methods gave satisfying results in the whole frequency range. The results indicated that the choice of a characterisation method in case of floating river clubs with reflective roof and no side surfaces can be arbitrary. This

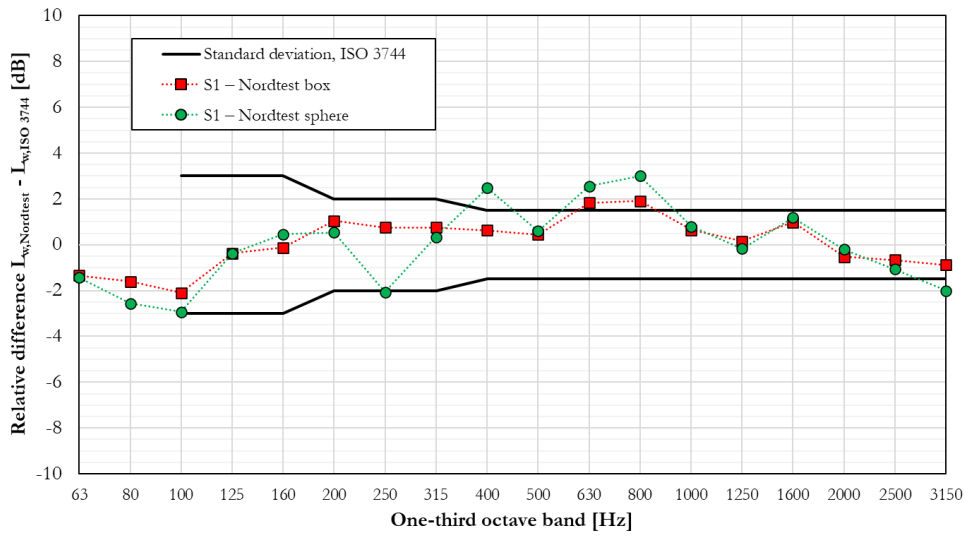


Figure 15. Relative sound power level differences between Nordtest methods and ISO 3744 method for S1.

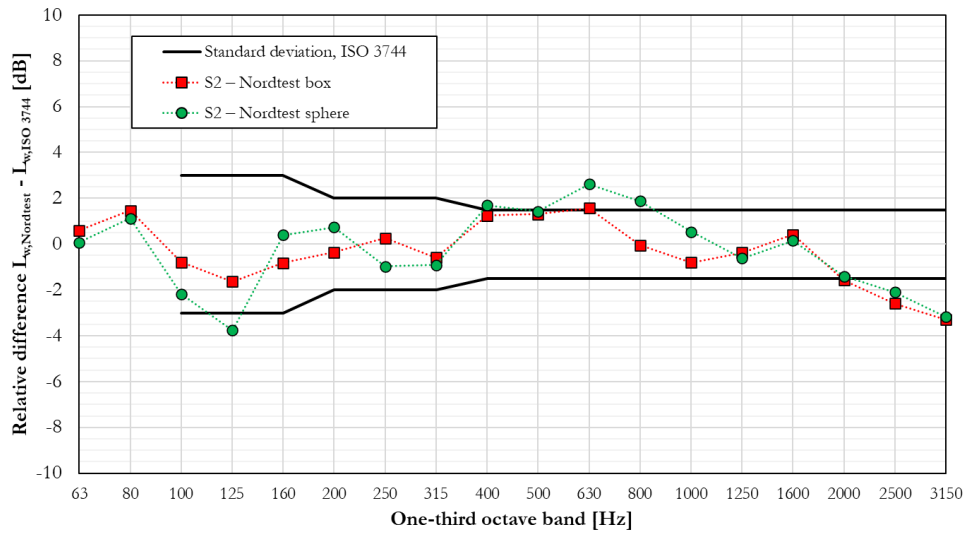


Figure 16. Relative sound power level differences between Nordtest methods and ISO 3744 method for S2.

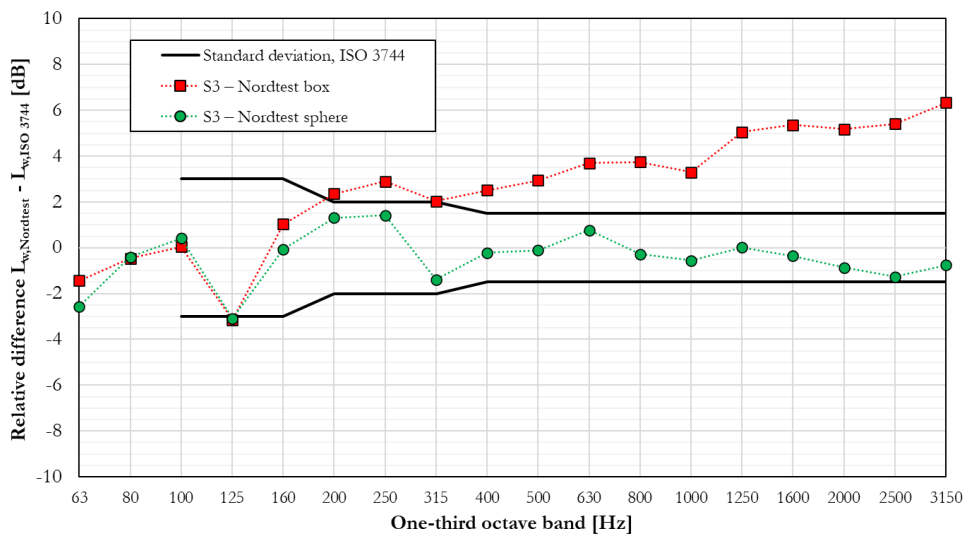


Figure 17. Relative sound power level differences between Nordtest methods and ISO 3744 method for S3.

indication was even applicable to S1. Finally, results obtained for S3, when both roof and side walls with high insulation properties were combined with side openings (i.e., windows and doors), recommended implementation of either ISO 3744 or Nordtest Sphere method. Implementation of the Nordtest Box method in this scenario overestimated the sound power level, decreasing the accuracy with increasing frequency from middle to high frequency range. In order to further investigate the overestimation of the sound power level, frequency band spectral power levels at individual microphones for all characterisation methods in S3 are presented in [Figure 18–Figure 20](#).

The highest overall spectral power level at single microphone position in [Figure 18– Figure 20](#) (mic. no. 1 in [Figure 18](#)) was normalized to 0 dB. All the other remaining overall spectral power levels were normalized accordingly, in such a way so as to enable to make relative comparison between them. The most noticeable feature of presented results was the shape of three curves in [Figure 18](#), i.e., mic. no. 1, mic. no. 3 and mic. no. 5. These three microphone positions exhibited significantly higher frequency band spectral power levels in the high frequency region compared to other microphone positions. Two microphone positions, mic. no. 1 and mic. no. 5, exhibited significantly higher frequency band spectral power in the middle frequency range as well. This trend was noticed only in the case of the Nordtest Box method. By analysing distribution of microphone positions in [Figure 8](#), it was found that these three microphone positions were located in front of side openings, i.e., two windows and the door. However, the energy radiated through the openings seemed to be “smeared out” in both ISO 3744 and Nordtest Sphere methods and thus the phenomenon was not captured. Different measurement positions captured different radiation components, where directivity of the source played an important role. Therefore, the overestimation of the sound power level in case of the Nordtest Box method in S3 was most likely a consequence of near–field measurement positions.

Signal–to–noise ratio (SNR) for all three scenarios is investigated in [Appendix A](#), where a range of SNR values obtained at individual measurement positions as well as an average SNR for different characterisation methods are presented. The SNR was found to be high, with average values higher than 30 dB for S1 and S2 and average values higher than 20 dB for S3. This was somehow expected, since impulse response measurements with logarithmic sine sweep excitation are known for better SNR than e.g., conventional measurements of sound pressure levels with pink noise excitation. Slightly lower SNR values at frequencies above 1600 Hz in S3 can be explained by high insulation properties of the solid wood used to build the model, in the given frequency range. The sound energy generated inside the object was significantly attenuated by the side walls, and the energy was radiated mostly through the openings.

### 2.5.2 Cottage with a Lightweight Façade

The sound power level differences obtained by applying different characterisation methods to a scale model of a typical floating river club, presented in the previous section, were further investigated in case of the summer cottage outside Belgrade, Serbia. Nordtest [\[31\]](#) and ISO 3744 [\[9\]](#) methods used in the scale model experiment were complemented with the ISO 9614–1 [\[10\]](#) sound intensity measurement in this case.

Sound levels were calculated in one–third octave bands with central frequencies 100–3150 Hz. The frequency range was chosen due to practical limitations of the loudspeaker’s working range as well as the intensity probe where 12 mm spacer between the two microphones was used. The results of sound power levels obtained by implementation of different characterisation methods are presented in [Figure 21](#), along with standard deviations of ISO 9614–1, described in [Section 2.2.3.1](#). The diagram presents relative differences between different characterisation methods where sound power levels determined by implementation of ISO 9614–1 were used as a reference. The reasoning behind this was that sound intensity measurements are least prone to impact of background noise and that the largest number of measurement positions was used. However, the choice of the referent characterisation method can be arbitrary, and the focus should be kept on relative differences between different characterisation methods. Absolute sound power levels were not of interest here, since they strongly depend on the type of the noise source operating indoors.

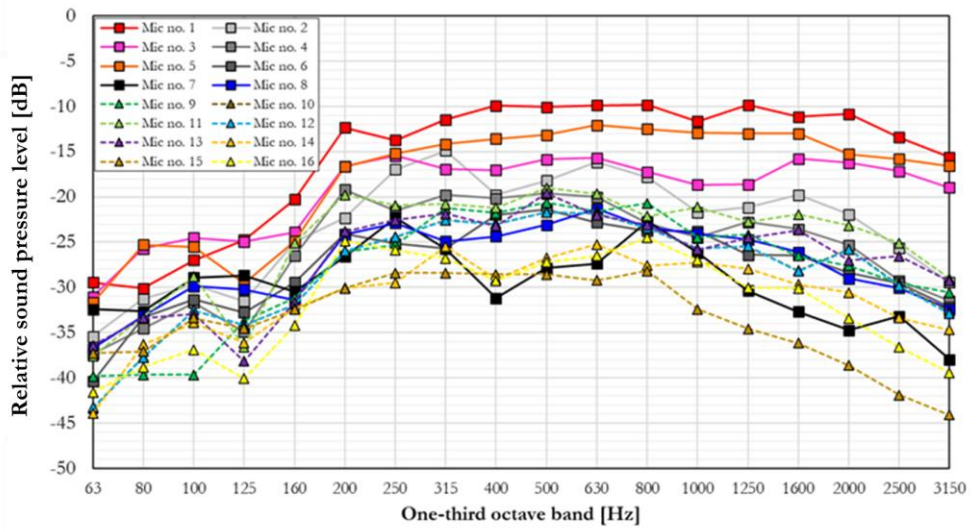


Figure 18. Relative sound pressure levels at individual microphones for the Nordtest Box method (S3).

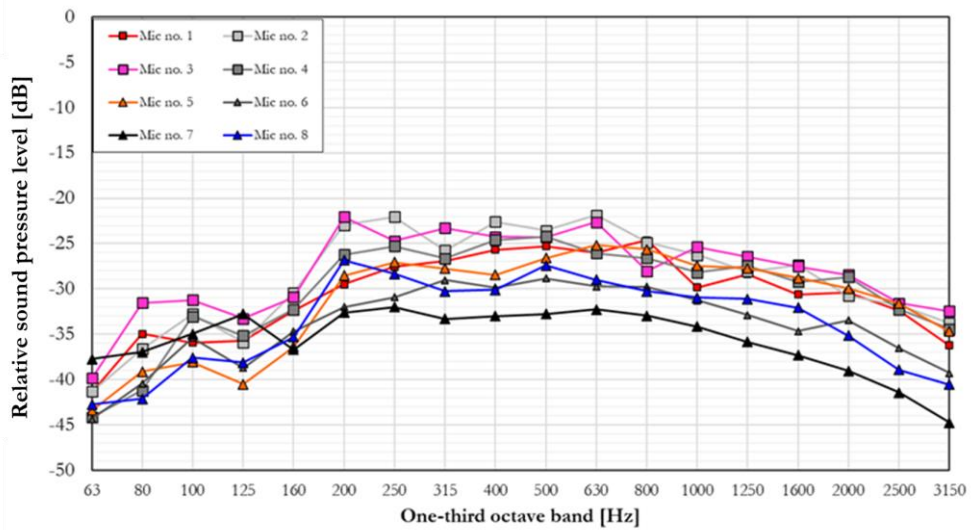


Figure 19. Relative sound pressure levels at individual microphones for the Nordtest Sphere method (S3).

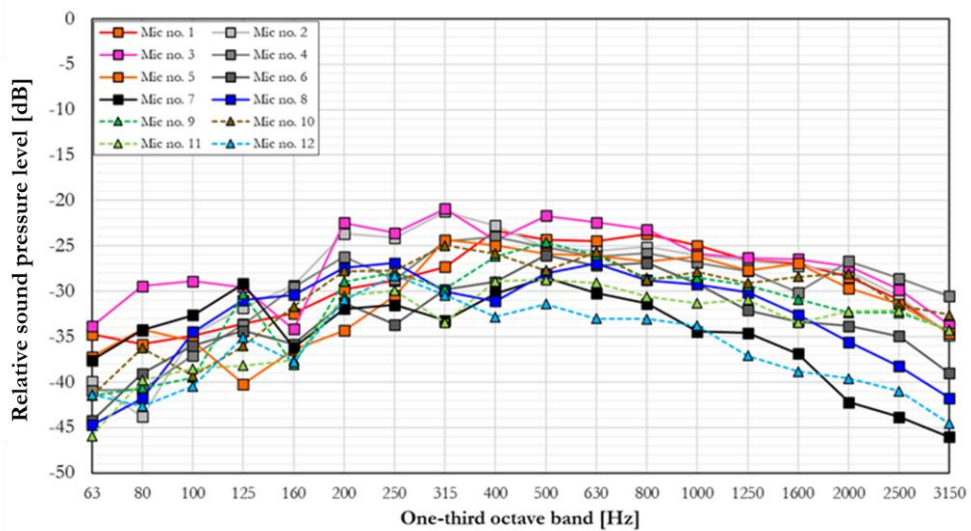


Figure 20. Relative sound pressure levels at individual microphones for the ISO 3744 method (S3).

A good agreement between sound power levels obtained by implementation of ISO 9614–1 and Nordtest Sphere was found. Most values of sound power levels obtained by implementation of Nordtest Sphere presented in Figure 21 lied within or slightly exceeded standard deviations of ISO 9614–1. The most noticeable exceedances occurred in the frequency range 250–500 Hz, with values between 0.7–2.5 dB. In this frequency range, ISO 3744 exhibited slightly better matching with ISO 9614–1, where relative differences in sound power levels were displayed around standard deviations of ISO 9614–1. Additionally, a good agreement between ISO 3744 and ISO 9614–1 was obtained at frequencies below 250 Hz. However, compared to ISO 9614–1, ISO 3744 overestimated sound power levels at higher frequencies, starting from 630 Hz and upwards. Relative differences in overall sound power levels between Nordtest Sphere and ISO 9614–1 as well as between ISO 3744 and ISO 9614–1 were identical and equal to 3.2 dB.

Unlike Nordtest Sphere and ISO 3744, Nordtest Box overestimated sound power levels obtained by ISO 9614–1 at almost all frequencies. The deviations varied in the range 4.7–8 dB. The only exception is 100 Hz, where sound power value obtained by Nordtest Box matched standard deviation of ISO 9614–1. The overall sound power level obtained by Nordtest Box overestimated the sound power level obtained by ISO 9614–1 by 6.4 dB.

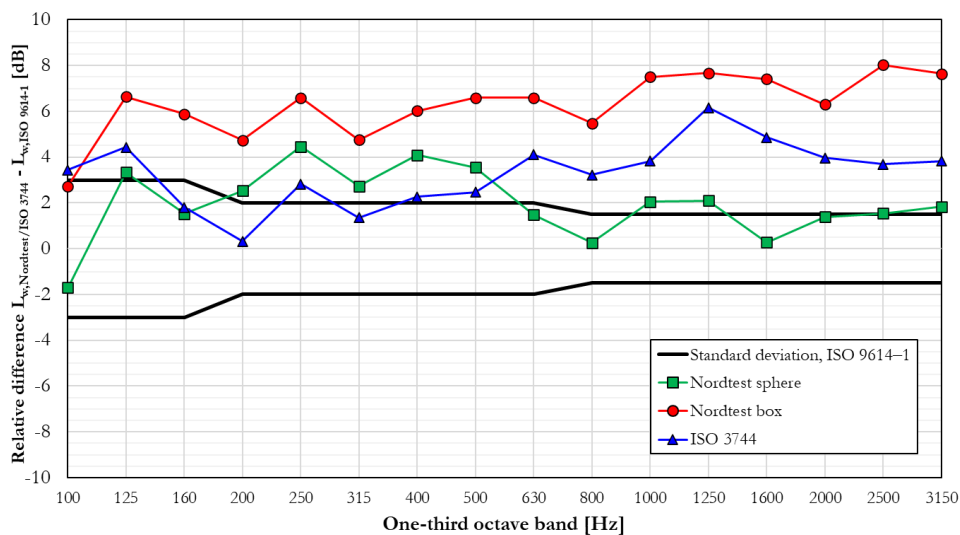


Figure 21. Relative differences between sound power levels obtained by sound pressure–based measurements (ISO 3744 and Nordtest methods) and ISO 9614–1 sound intensity measurement (taken as a reference).

The results presented in Figure 21 confirmed, for the most part, findings from scenario S3 in the scale model experiment. On the one hand, Nordtest Box was found again to overestimate sound power levels compared to Nordtest Sphere and ISO 3744. In this experiment, the overestimation of sound power levels was further supported by comparison to ISO 9614–1. On the other hand, a good agreement between Nordtest Sphere and ISO 3744 was found, where identical overall sound power levels were obtained. The lowest sound power levels in case of ISO 9614–1 could be explained by the probe orientation normal to the side walls. Consequently, contribution of sound energy radiated from other directions was neglected.

In the scale model experiment, the roof and side partitions sound insulation was significantly higher compared to the experiment with the cottage, given the insulation properties of the material used to build the model and the frequency range of the excitation. However, in practice, materials with low sound insulation properties are used and sound components transmitted through side partitions have a greater contribution to sound levels outside the object, as in case of the cottage. In addition to this, the ceiling sound insulation often has much better sound insulation properties than side partition. Consequently, sound components radiated upwards are reflected towards side partitions and openings, which further increase sound energy outside the object. This was confirmed by implementation of sound intensity measurements above the roof, in the same manner as for side partitions. Obtained sound power

level of the roof was approx. 10 dB lower compared to sound power levels of side partitions and the overall sound power level of the object increased by 0.2 dB, making the contribution of the roof negligible.

The differences of sound power levels demonstrated in [Figure 17](#) and [Figure 21](#) were a consequence of applied measurement techniques. It is believed that the obtained differences occurred due to specificity of the measured objects, primarily a non-homogeneity of its surface including some completely open areas. Applied characterisation methods act differently to such specific noise radiation where different distribution of measurement positions contributes differently to determination of sound power levels. However, even under such circumstances, differences between Nordtest Sphere and ISO 3744 lied mostly within standard deviations of ISO 3744.

### 2.5.3 Floating River Clubs

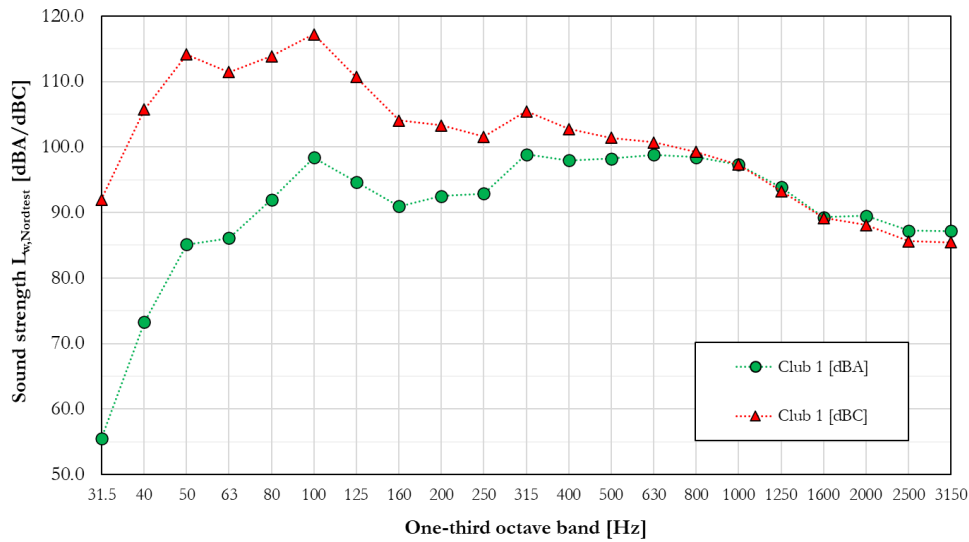
Results presented in [Section 2.5.1](#) and [Section 2.5.2](#) justified the implementation of Nordtest Sphere in case of floating river clubs. The Nordtest method recommends a minimum number of measurement positions compared to other methods, at the same time providing identical accuracy with ISO 3744. Therefore, Nortest method has been applied to two different types of floating river clubs on the Sava river in the central part of Belgrade, Serbia. The results of the characterisation have been further investigated by measurements of sound pressure levels at control measurement positions in a far-field.

Sound strength levels were calculated in one-third octave bands with central frequencies 31.5–3150 Hz. This frequency range was chosen to cover the specific noise from floating river clubs with powerful audio systems. The standard frequency range 100–3150 Hz, often used in building acoustics, was extended to account for low frequency noise from these objects. The results of sound strength levels obtained by applying the Nordtest Sphere method to Club 1 and Club 2 are presented in [Figure 22a](#) and [Figure 22b](#), respectively. The diagram presents both A-weighted and C-weighted values. Background noise correction was applied to all measurements.

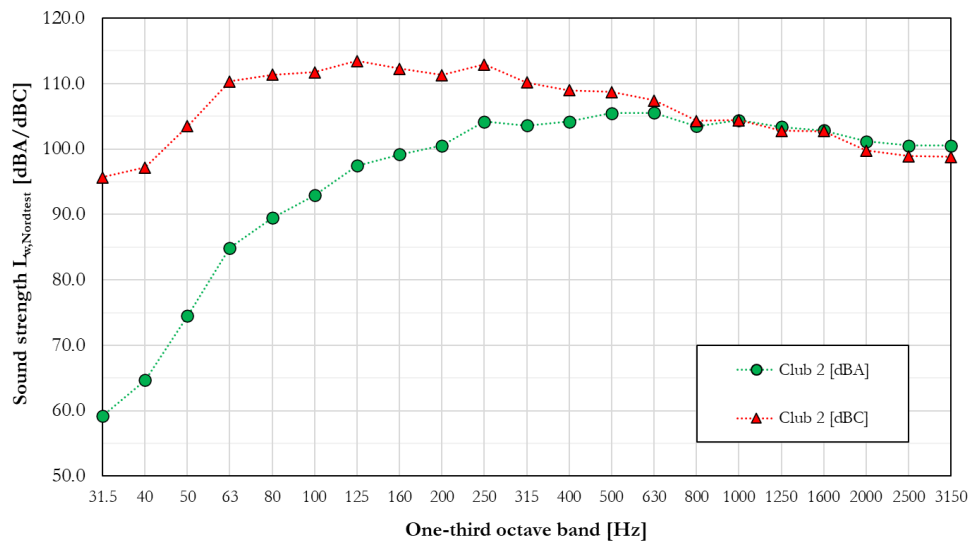
The overall A-weighted and C-weighted sound strength levels for Club 1 were found to be 108 dBA and 121.7 dBC, respectively. For Club 2, the overall A-weighted and C-weighted sound strength levels were found to be 114.8 dBA and 122 dBC, respectively. In both cases, the differences between C-weighted and A-weighted sound strength levels indicate significant energy of the radiated noise at low frequencies. Furthermore, the differences in sound strength levels between the clubs were above all a consequence of different types and numbers of loudspeakers. Because of this and other differences such as different constructions and dimensions, the clubs were analysed independently one from another.

The sound strength levels were further used to calculate sound pressure levels at control positions in a far-field. Namely, sound pressure levels were calculated by (15) and compared to those obtained from far-field measurements. Unlike sound strength levels presented in [Figure 22](#), calculated by averaging sound pressure levels at all measurement positions around the clubs, the sound strength levels used to calculate sound pressure levels at control measurement positions were calculated just from measurement positions in the direction of the control measurement positions. Correspondingly, directional characteristics of the clubs were taken into account. In this way, it was possible to validate the values obtained by applying Nordtest Sphere and introduce necessary corrections. The results are presented in [Figure 23](#) for Club 1 and Club 2, respectively.

In case of the Club 1, a good agreement was found between measured and calculated sound pressure levels starting from 80 Hz and upwards, at all measurement positions. Slightly larger differences appeared in the middle frequency range 200–400 Hz, where calculated values of sound pressure levels overestimated the measured ones. The differences varied between control measurement positions, but they were most noticeable at distances  $d=80$  m,  $d=185$  m and  $d=215$  m. At frequencies above 400 Hz, the agreement was excellent at all frequencies and all distances except in the frequency range 2000–3150 Hz at the distance  $d=215$  m. In this frequency range, measured values of sound pressure levels slightly overestimated calculated ones. Finally, the most noticeable feature of [Figure 23](#) was higher values



(a)

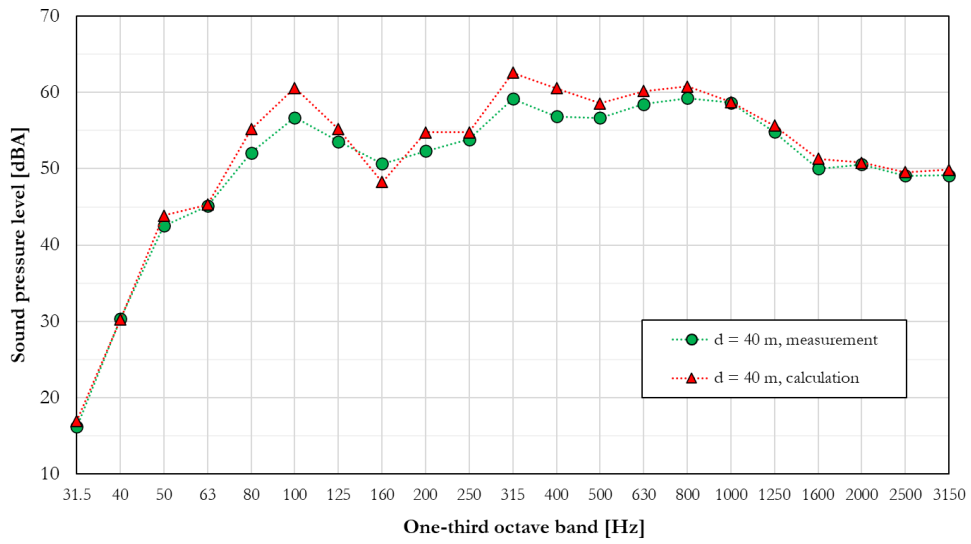


(b)

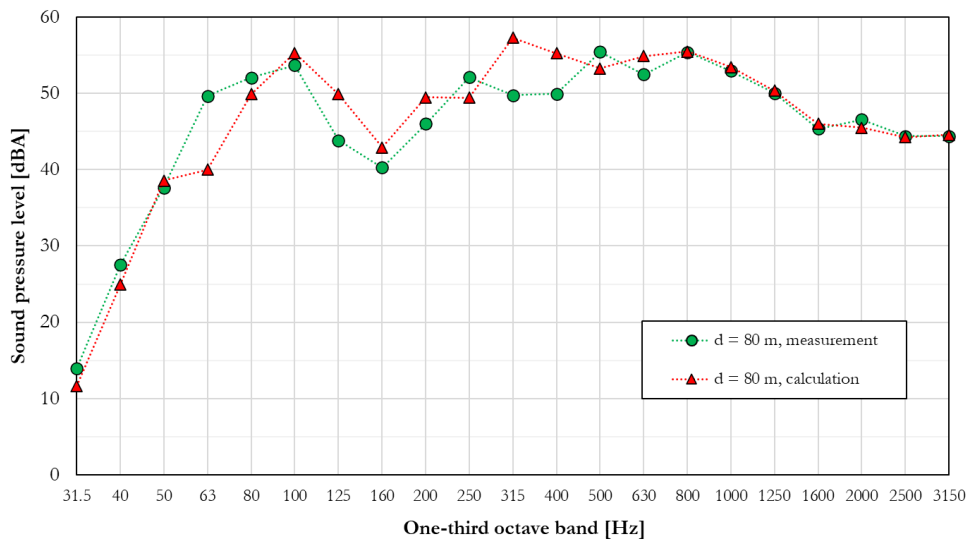
**Figure 22.** Sound strength levels obtained by implementation of the Nordtest Sphere method on: (a) Club 1, and (b) Club 2.

of measured sound pressure levels compared to calculated sound pressure levels at low frequencies below 80 Hz. Furthermore, differences between measured and calculated sound pressure levels expressed general tendency to increase with the increment of a distance.

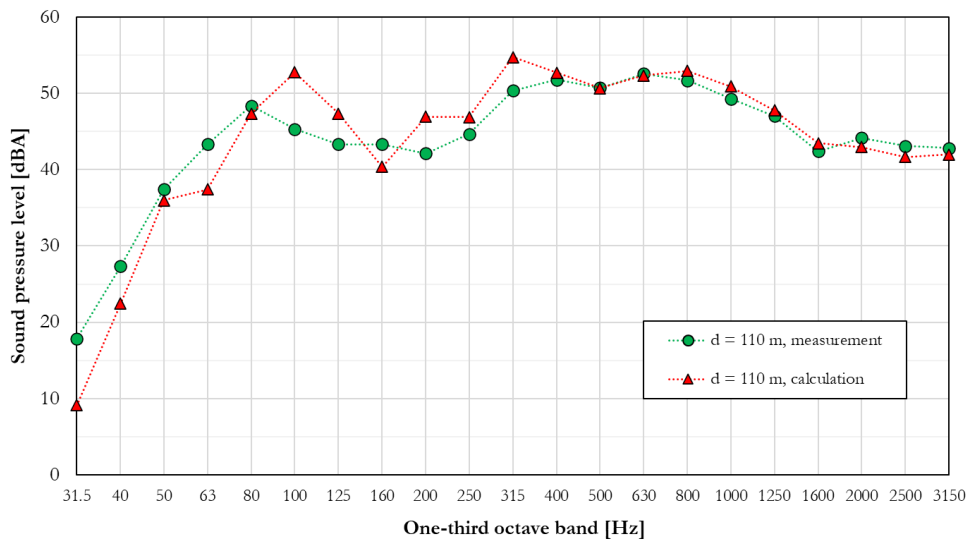
In case of the Club 2, a good agreement was found between measured and calculated sound pressure levels starting from 125 Hz and upwards, at all measurement positions. Slightly larger differences appeared in the frequency range 250–315 Hz at distance  $d=140$  m, as well as in the frequency range 400–500 Hz at distance  $d=175$  m. As in case of the Club 1, a certain mismatch between measured and calculated sound pressure levels was found at low frequencies. While a good agreement between the measured and calculated sound pressure levels was found at low frequencies below 125 Hz at distance  $d=175$  m, except at 63 Hz, a mismatch was found at all frequencies below 125 Hz at distance  $d=140$  m. The values of sound pressure levels at control measurement positions in a far-field, presented in [Figure 23](#) and [Figure 24](#), were calculated under assumption that floating river clubs can be considered as point noise sources, which is a very simple approximation of the complex noise sources such floating river clubs are. Furthermore, all sound propagation phenomena such as sound refraction, air absorption, influence of air humidity, etc., were not taken into account. Finally, the calculations of sound pressure levels at control measurement positions were based on the sound strength levels calculated from



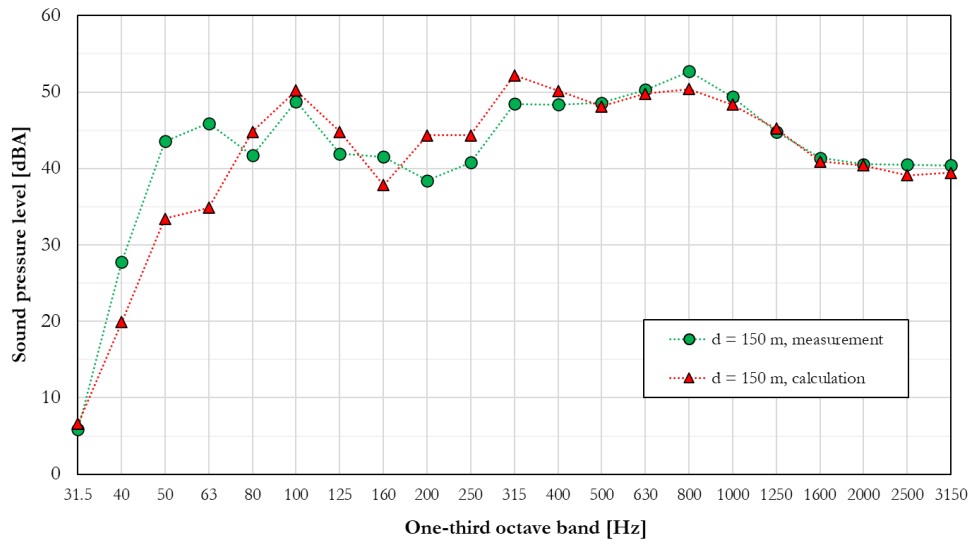
(a)



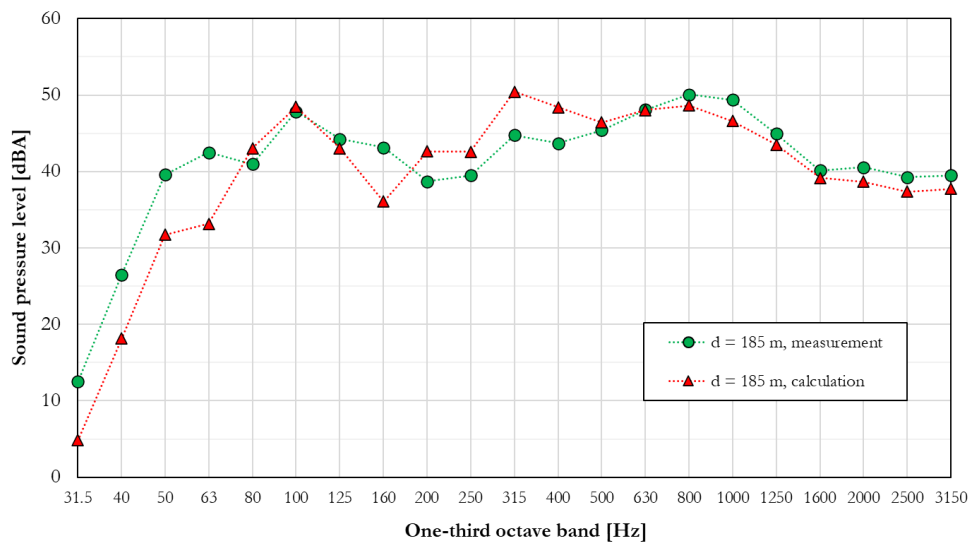
(b)



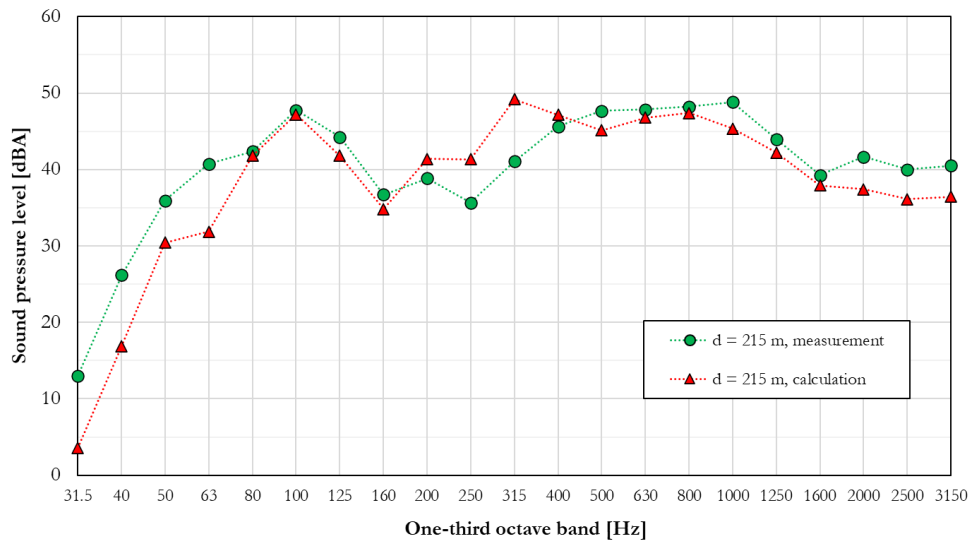
(c)



(d)

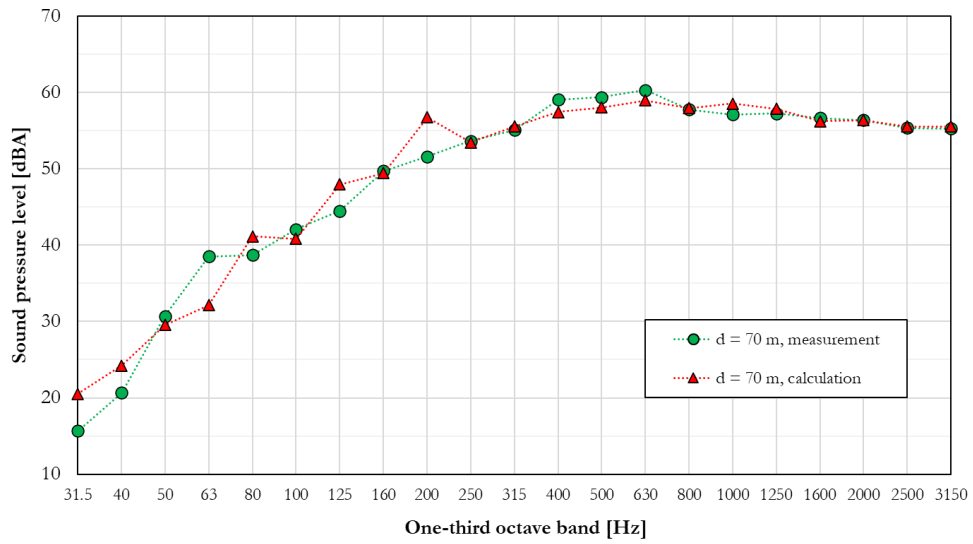


(e)

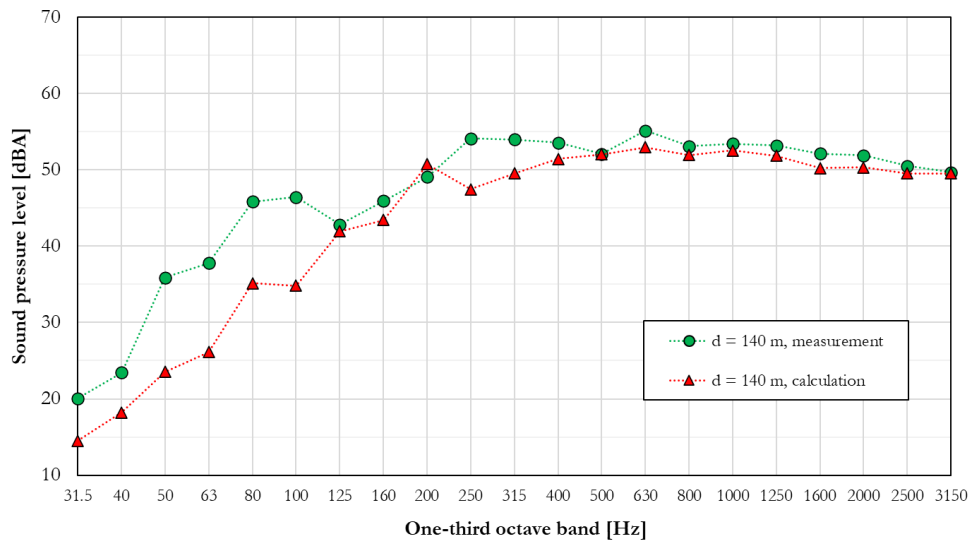


(f)

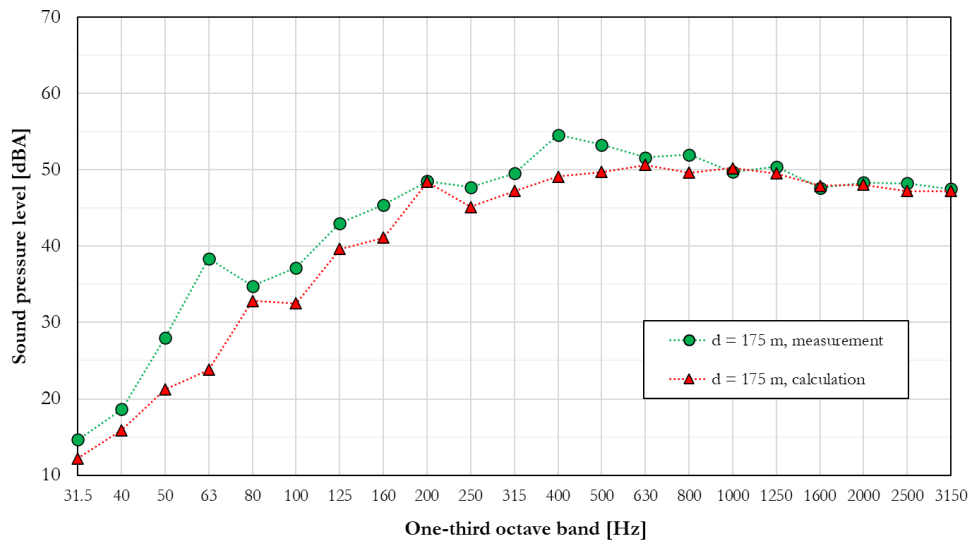
**Figure 23.** Comparison of measured and calculated sound pressure levels at different control measurement positions in a far-field for Club 1.



(a)



(b)



(c)

Figure 24. Comparison of measured and calculated sound pressure levels at different control measurement positions in a far-field for Club 2.

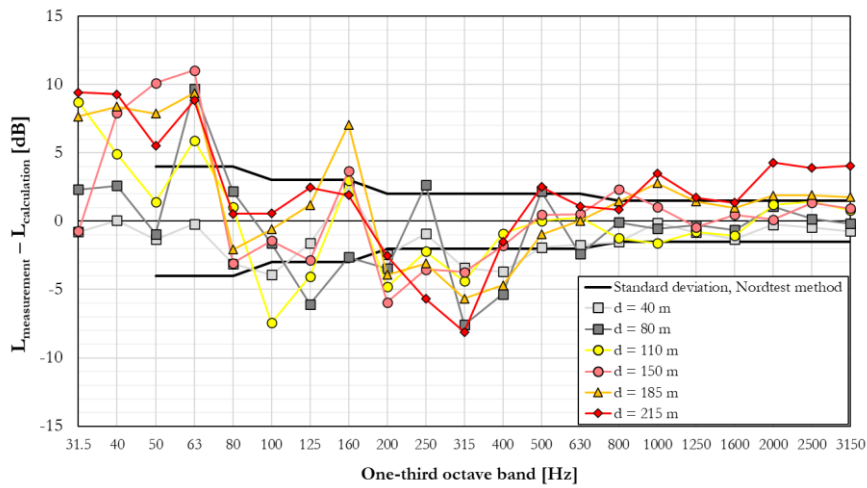
measurement positions at height of 10 m above the river level i.e., under a specific radiation angle. Yet, the angle of the radiated noise was different at control measurements positions, since the microphone height was kept the same. All this might have had an influence on the differences between calculated and measured sound pressure levels at control measurement positions. However, the simple calculation model was chosen with intention to facilitate the calculation of noise from floating river clubs as much as possible in order to easily implement it in the practice. Therefore, the differences were considered only for those initial assumptions.

It is important to mention that sound pressure levels at far-field measurement positions for the Club 2 were calculated for acoustic centre between two back loudspeaker-subwoofer pairs. The absence of the roof excluded existence of a diffuse sound field, leading to directional radiation of back and front loudspeaker-subwoofer pair and their different contribution to sound levels measured at far-field measurement positions. The orientation of two front loudspeaker-subwoofer pairs, i.e., those closer to the far-field measurement position, made their contribution at far-field measurement positions negligible.

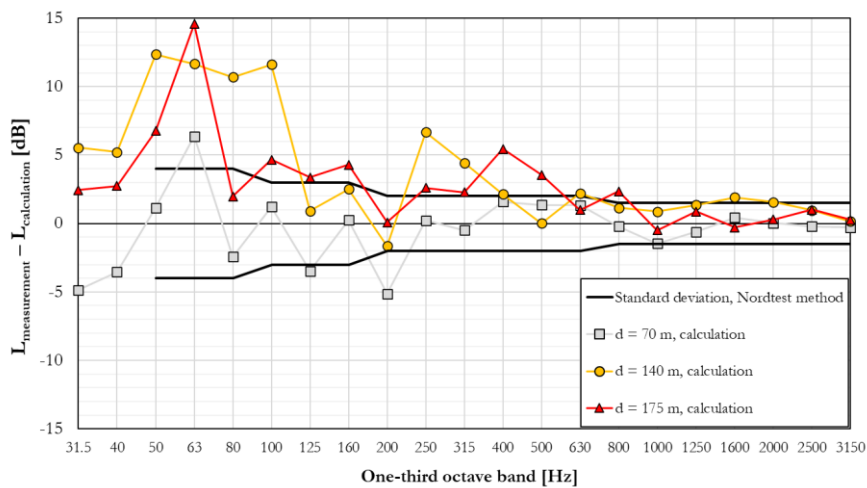
In order to make results presented in [Figure 23](#) and [Figure 24](#) more evident, relative differences between measured and calculated sound pressure levels at control measurement positions in a far-field are presented in [Figure 25a–b](#) for Club 1 and Club 2, respectively. The relative differences are presented together with standard deviations of the Nordtest Sphere method, earlier explained in [Section 2.2.2.3](#). Despite all calculation simplifications described above and characteristic properties of the clubs described in [Section 2.4.3](#), the differences between measured and calculated sound pressure levels at control measurement positions in a far-field lied mostly within or around standard deviations of the Nordtest method for both clubs. However, two phenomena were visible: a slight mismatch between measured and calculated sound pressure levels at middle frequencies and higher values of the measured sound pressure levels at low frequencies. Slightly higher sound pressure levels at frequencies 2000–3150 Hz for distance  $d=215$  m in case of the Club 1 were probably obtained due to a background noise since the measurement under the actual measurement. Still, the mismatch at high frequencies has not been found to be a trend but rather an isolated case, therefore not requiring further discussion.

A mismatch between measured and calculated sound pressure levels at middle frequencies was further investigated in terms of interferences between direct and water reflected sound at control measurement positions. Namely, due to significantly higher density than air, water is considered as acoustically reflective surface and can produce strong reflections. A phenomenon called ‘comb filter’ occurs when direct sound interferes with strong reflections, causing constructive and destructive interference. On the one hand, destructive interference occurs at frequencies at which a path difference between the direct and reflected sound equals an odd product of half of the wavelength. On the other hand, constructive interference occurs at frequencies at which a path difference between the direct and reflected sound equals an even product of half of the wavelength. For both the Club 1 and Club 2, frequencies at which positive and negative interferences would be expected were calculated and compared with differences presented in [Figure 25](#). Nevertheless, no visible effect of comb filtering was found at expected frequencies. A possible reason for this could be the fact that the large number of loudspeakers produced multiple reflections which either shifted or masked the effect of comb filtering. Additionally, sound pressure levels at control measurement positions were recorded in one-third octave band which can further masks the effect of comb filtering, especially if comb filtering effect occurred in narrowband frequency region. As explained earlier, a mismatch at middle frequencies could have occurred due to different radiation angles between measurement positions under implementation of Nordtest Sphere and measurements in a far-field. Additional reason could be different influence of openings on measurement positions in the vicinity of the object and at larger distances.

Differences between measured and calculated sound pressure levels at low frequencies were even more pronounced than differences at middle frequencies. Measurements showed approx. 10 dB higher values compared to calculations in a wider frequency range. The differences were more noticeable in case of the Club 1, where sound pressure levels were measured at more control measurement points compared to case of the Club 2. In the former case, the differences were obtained in frequency range 31.5–63 Hz.



(a)



(b)

**Figure 25.** Relative differences between measured and calculated sound pressure levels at different control measurement positions in a free-field for (a) Club 1, and (b) Club 2.

In the latter case, the differences were obtained in the frequency range 50–100 Hz. The differences expressed general tendency to increase with the increment of a distance in case of the Club 1. The same trend was observed in case of Club 2 at 63 Hz, but the differences were contained in a narrower frequency range in this case. Since possible endangered receivers will mostly be located at the opposite side of the river, control measurement positions at larger distances should be used as a reference here.

Despite abovementioned frequency-dependant discrepancies between measured and calculated sound pressure levels at control measurement positions, lower discrepancies between total sound pressure levels were obtained. The absolute differences in total sound pressure levels lied in the range 0.5–2.1 dB at all control measurement positions in case of the Club 1, while the differences in case of the Club 2 lied in the range 0.1–1.9 dB.

# Chapter 3

## Indoor Noise of Entertainment Premises

In the previous section, floating river clubs were introduced as an example of specific sources of entertainment noise and characterisation of their outdoor noise was presented. The characterisation of the outdoor noise is important when assessing their influence in an urban environment. However, in order to account for transmission of the entertainment noise through building partitions into surrounding objects and environment, a character of their indoor noise must be known. Also, there is a correlation between the indoor and outdoor noise, i.e., one can be calculated from another if properties of building partitions are known. For that reason, analysis of the indoor sound level spectra for different types of entertainment premises, including floating river clubs, has been presented in this section. Additionally, the sound level spectra have been used to rate airborne sound insulation of building elements with single-number quantities and spectrum adaptation terms. The analysis has been based on the results of a monitoring performed in typical representatives of those premises. The results presented in this section have been published in [32].

### 3.1 Introductory Remarks

Frequency-dependent descriptors are used for rating the airborne sound insulation, which are further converted into single-number quantities according to ISO 717-1 standard [19]. The single-number quantities are followed with their spectrum adaptation terms,  $C$  and  $C_{tr}$ , calculated from two different sound level spectra. The former describes noise sources inside the building (A-weighted pink noise), while the latter describes traffic outside the building (A-weighted urban traffic noise). As stated by the standard itself, spectra of the most common indoor and outdoor noise sources lie in the range between those two spectra.

Single-number quantities and spectrum adaptation terms are calculated using one-third octave bands within the range 100–3150 Hz. However, a wider frequency range 50–5000 Hz is often used to account for noise sources capable of emitting low-frequency noise. It has been demonstrated [16,17] that low-frequency noise is less tolerated and perceived as more annoying than other types of noise. Since the low-frequency hearing threshold differs between individuals, an objective method which calculates the average of the hearing thresholds included in standards and in the literature is suggested [51] in order to assess the noise annoyance. Also, the low-frequency content is important for better correlation with a subjective assessment of sound insulation [52]. Therefore, an enlarged frequency range is particularly important when rating the sound insulation with respect to entertainment noise. Using a limited frequency range or wrong reference spectrum could lead to inappropriate rating of sound insulation and underestimation of possible protection methods.

Recently, a study [53] investigated that even reference spectra of modern home audio systems with bass music exceed that of urban traffic noise. This is in sharp contrast with the classification presented in the ISO 717-1 standard [19], namely, the standard suggests  $C_{tr}$  as a relevant spectrum adaptation term when rating airborne sound insulation against disco music. It is, however, reasonable to assume that many entertainment premises produce noise with strong bass content, the spectrum of which might introduce higher sound levels at lower frequencies than those which had been suggested. Additionally, the term “disco music” suggested by the ISO standard [19] is a more general term and requires further classification regarding the type of premise where the noise is originating from.

In order to authentically reproduce recorded music at low frequencies, modern audio systems in discotheques usually employ several subwoofers. Generally, subwoofers operate in the frequency region between 20 and 200 Hz, but in audio systems they are adjusted to reproduce the sound below 100 Hz. Also, there is a general tendency to enhance the listeners’ experience by setting the sound spectral level in the low-frequency region higher than in other frequency regions. This logic is supported by the

technical guidelines provided by Dolby laboratories [54], where a 10 dB higher subwoofer level than in the rest of the frequency region is proposed.

### 3.2 Spectrum Adaptation Terms According to ISO 717–1

The international ISO 717–1 standard [19] defines single–number quantities for airborne sound insulation in buildings and of building elements, take into consideration two typical sound level spectra (noise sources inside a building and traffic outside a building) and gives rules for determining those quantities from both laboratory and *in situ* measurements of sound insulation. To take the characteristics of particular sound spectra into account, single–number values are presented together with spectrum adaptation terms. Reference values for sound insulation to calculate single–number values and sound level spectra to calculate the adaptation terms are presented in Table 8 below. The values of sound level spectra presented in Table 8 are A–weighted and the overall spectrum level is normalized to 0 dB. They are also given for enlarged frequency range, since those are valid for characterizing the acoustic property of a building element against low–frequency noise. However, frequency range for which spectrum adaptation terms are calculated can be easily adjusted, taking care that the overall spectrum for adjusted frequency range is still normalized to 0 dB.

**Table 8.** Reference values for airborne sound insulation and sound level spectra to calculate the adaptation terms for enlarged frequency range [19].

Frequency	Reference values	Spectrum No. 1	Spectrum No. 2
Hz	dB	to calculate $C$	to calculate $C_r$
		dB	dB
50		–41	–25
63		–37	–23
80		–34	–21
100	33	–30	–20
125	36	–27	–20
160	39	–24	–18
200	42	–22	–16
250	45	–20	–15
315	48	–18	–14
400	51	–16	–13
500	52	–14	–12
630	53	–13	–11
800	54	–12	–9
1000	55	–11	–8
1250	56	–10	–9
1600	56	–10	–10
2000	56	–10	–11
2500	56	–10	–13
3150	56	–10	–15
4000		–10	–16
5000		–10	–18

First, frequency–dependant descriptors (such as  $R, R', D_n, D_{nT}$ , etc.) obtained from measurements are compared to reference values presented in Table 8. The reference curve is shifted in increments of 1 dB towards the measured curve until the sum of unfavourable deviations i.e., when the result of measurements is less than the reference value, is as large as possible but no more than 32 dB. Then the single–number value presents the value, in decibels, of the reference curve at 500 Hz after shifting it in accordance with previously described procedure.

Second, spectrum adaptation terms are calculated from values given in Table 8 from following equations:

$$C_j = X_{Aj} - X_W \quad (16)$$

where  $j$  denotes the sound spectra (No. 1 or No. 2),  $X_W$  denotes the single–number value, and  $X_{Aj}$  is calculated from:

$$X_{Aj} = -10 \log \sum 10^{(L_{ij}-X_i)/10} \text{ dB} \quad (17)$$

in which  $i$  denotes the subscript for the one–third–octave bands,  $L_{ij}$  are the levels given in Table 8, and  $X_i$  denotes frequency–dependant descriptor at the measuring frequency  $i$ , given to one decimal place.

The resulting spectrum adaptation term is an integer, and it is written as  $C$  or  $C_{tr}$ , when calculated with spectrum No. 1 and spectrum No. 2, respectively. Since spectrum adaptation terms can be calculated for different frequency ranges, this should also be stated as a subscript (e.g.,  $C_{tr, 50-5000}$ ). To choose appropriate spectrum adaptation term, Table 9 is used as a guideline to assess the sound insulation with regard to different noise sources.

At the end, the calculated spectrum adaptation terms are presented together with the single–number values. The common way of doing this is by using parentheses, as shown below:

$$R_w (C; C_{tr}) = 35 (0; -2)$$

Requirements in building codes are usually defined as the sum of single–number value and the relevant spectrum adaptation term. One possible application of spectrum adaptation term  $C$  is when calculating airborne sound insulation between apartments within the same building, while application of spectrum adaptation term  $C_{tr}$  is when calculating airborne sound insulation of facades.

**Table 9.** Different types of noise source attached to the spectrum adaptation terms  $C$  and  $C_{tr}$  [19].

Type of noise source	Relevant spectrum adaptation term
Living activities (talking, music, radio, TV)	
Children playing	
Railway traffic at medium and high speed	$C$
Highway road traffic at >80 km/ha	(spectrum No. 1)
Jet aircraft, short distance	
Factories emitting mainly medium– and high–frequency noise	
Urban road traffic	
Railway traffic at low speeds	
Aircraft, propeller driven	$C_{tr}$
Jet aircraft, large distance	(spectrum No. 2)
Disco music	
Factories emitting mainly low and medium frequency noise	

### 3.3 Experimental Setup

Noise monitoring was conducted in 17 entertainment premises located in Belgrade, Serbia and Stockholm, Sweden. The majority of measurements have been performed in order to illustrate a case of recorded music, while three of them were performed during live performances. The study was focused on three main types of premises:

- (1) Bars and pubs,
- (2) Clubs, and
- (3) Discotheques.

A total of five entertainment premises of type (1) and a total of six entertainment premises for each of types (2) and (3) were monitored. This classification has been introduced for the purpose of this study, and it is based solely on the type of dominant noise source in the entertainment premises. Bars and pubs were selected in a way that they were part of a residential building, presenting a real-life scenario. The music played from audio systems producing moderate background noise levels mixed with the noise of patrons talking to each other was common for all bars and pubs [55]. It was the people, i.e., patrons' conversations that presented a dominant source of noise in this type of entertainment premises. Contrary to that, clubs and discotheques selected for this study produced significant music sound levels, while the patrons' noise contribution was negligible. The main difference between these two types of entertainment premises was that discotheques had more complex audio systems with several independent subwoofers producing significant sound levels at low frequencies. Namely, the audio system in discotheques was configured for recorded music with pronounced low-frequency content. On the other hand, clubs had audio systems configured for linear reproduction of music, which is usually employed in live performances. So, while the focus in discotheques was on enhanced patron's experience, the focus in clubs was on the music reproduction accuracy.

Three measurements in clubs were performed during live performances, with two of them being weddings. The music bands in the weddings used similar type of audio systems found in other measurements performed in clubs. Two measurements in discotheques were performed on floating river clubs which, as a rule, do not have walls but rather open side surfaces. Except for those two special cases, all entertainment premises under study comprised heavyweight partitions.

The measurements were performed during busy hours, mostly on weekends, where sound levels of produced music were expected to be significant. No attentional changes of produced sound levels were perceived during the measurements. The measurements were performed in agreement with clubs' owners, thus making sure that there was no fear of inspection among employees and hence no potential reduction of sound levels.

For monitoring purposes, a *Norsonic Nor140* sound level meter with a *Nor1225* class 1 omnidirectional microphone (Norsonic AS, Tranby, Norway) was used. The integrated averaged sound pressure level,  $L_{eq}$ , was recorded in a 1 h period with time resolution of 1 s. The microphone positions were carefully chosen in the areas with patrons in which the quality of the reproduced music had been tuned by sound engineers, in case of clubs and discotheques. The distance of the microphone in reference to loudspeakers of the audio system varied between venues but was never closer than 3 m. The microphone was set at the height of 1.2–1.5 m.

In order to investigate the influence of different sound spectra on spectrum adaptation terms, these terms were calculated for four different types of building elements (BE) together with the single-number quantities. The BEs used in the study were the following:

- (1) Heavy partition (BE 1) – Concrete panel with thickness of 200 mm and surface mass of 468 kg/m<sup>2</sup>,
- (2) Light partition (BE 2) – 2 × 12.5 mm gypsum board, acoustic steel studs (stud spacing 450 mm), mineral wool (60 kg/m<sup>3</sup>) with thickness of 95 mm, 2 × 12.5 mm gypsum board,

- (3) Heavy and light partition combined (BE 3) – Concrete panel with thickness of 200 mm, acoustic steel studs (stud spacing 450 mm), mineral wool (60 kg/m<sup>3</sup>) with thickness of 95 mm, 2 × 12.5 mm gypsum board, and
- (4) Cinema partition (BE 4) – 3 × 15mm gypsum board, 100 mm glass wool, 210 mm air gap, 100mm glass wool, 3 × 15mm gypsum board.

Sound reduction indices,  $R_w$ , were calculated in the standardised frequency range 100 – 3150 Hz, while  $R_w$  indices, presented together with spectrum adaptation terms, were calculated for the extended frequency range 50–5000 Hz.

### 3.4 Experimental Results and Discussions

Sound level spectra of recorded indoor entertainment signals were calculated for the extended frequency range, i.e., in one-third octave bands with central frequencies 50–5000 Hz. The spectra were A-weighted and normalized to 0 dB, as described in the ISO 717-1 standard [19]. The recorded sound level spectra were compared with two reference spectra, for noise sources inside the building (Spectrum No. 1) and traffic outside the building (Spectrum No. 2), also defined by the same standard. The results are shown in Figure 26.

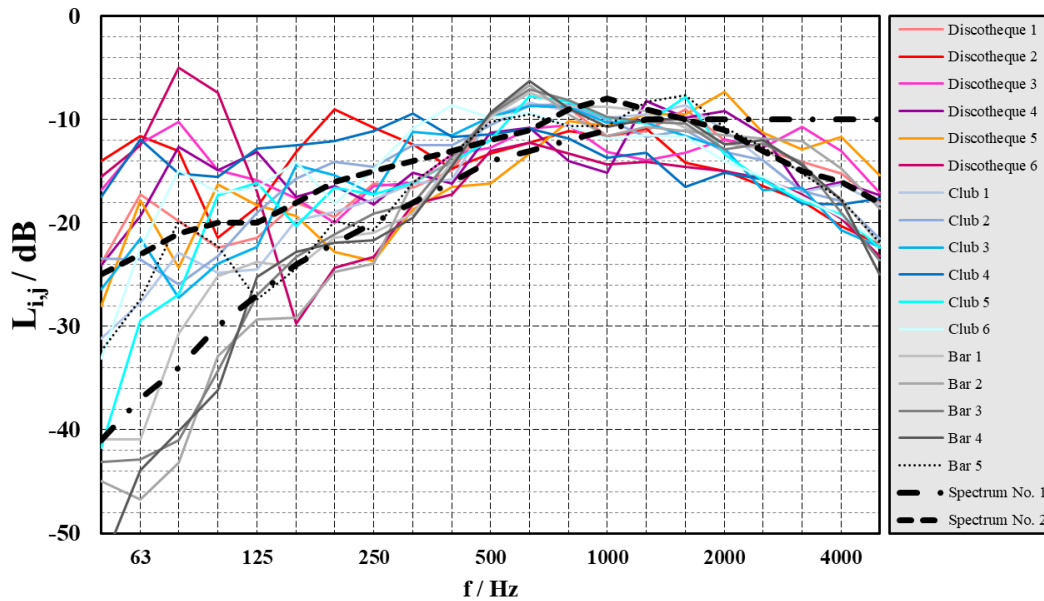


**Figure 26.** Sound level spectra of different entertainment premises to calculate spectrum adaptation terms. Spectra are A-weighted and normalized to 0 dB. [32]

The results presented in Figure 26 show diversity among recorded sound spectra. Most of the recorded spectra are located around two standardised sound spectra, Spectrum No. 1 and Spectrum No. 2, with few of them displaying large deviations at lower frequencies below 160 Hz. As a special case, the measurements “Discotheque 4” and “Discotheque 5” were performed on floating river clubs with no wall partitions. The absence of wall partitions in this case might have influenced the indoor sound field; however, pronounced low-frequency content still prevailed. All other measurements were performed in enclosed premises in accordance with descriptions given in Section 3.3. Additionally, the measurements “Club 1,” “Club 5,” and “Club 6” were performed during live performances of music bands.

In order to better understand diversity of recorded signals, sound spectra were averaged for different types of entertainment premises included in the study. The results are shown in Figure 27. An average sound level spectrum for bars and pubs corresponded to the reference spectrum for noise sources

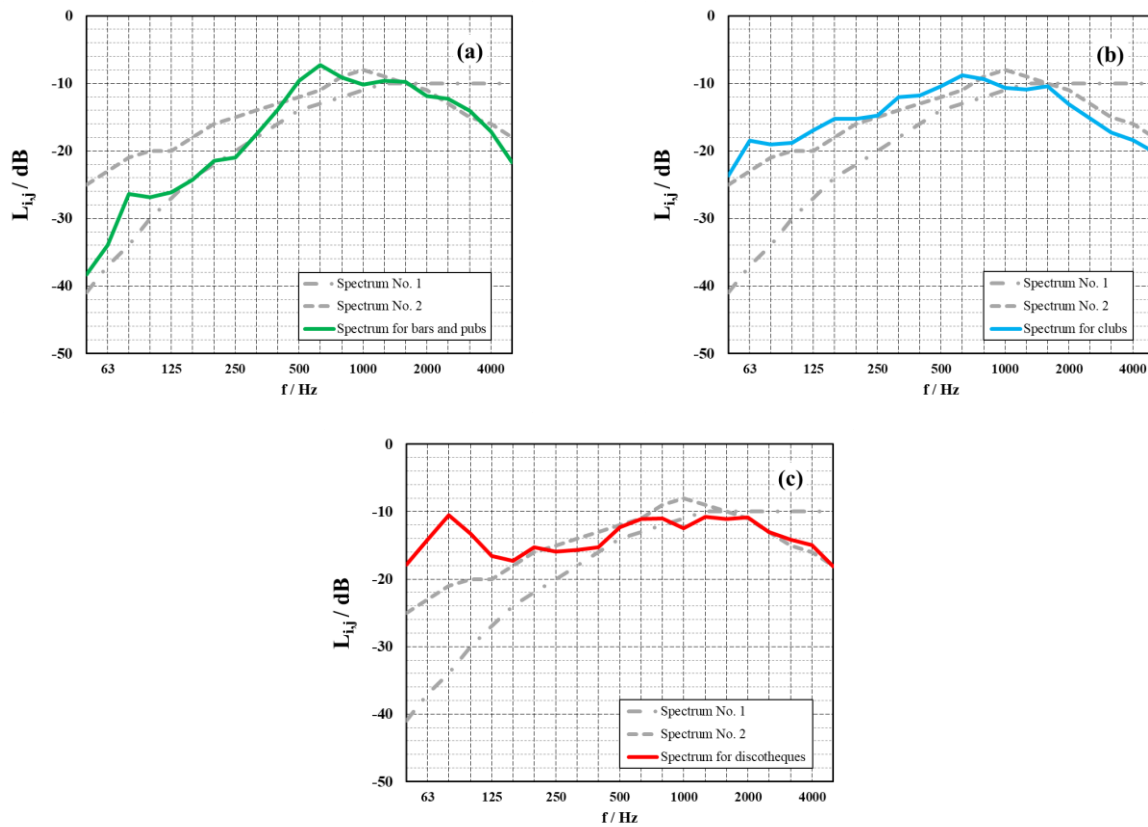


**Figure 27.** Average sound level spectra for different types of entertainment premises. Spectra are weighted and normalized to 0 dB. [32]

inside the building up to one-third octave band with the central frequency of 1600 Hz, see [Figure 27a](#). This has been expected to a certain extent since human speech was the dominant source of noise in this type of entertainment premises. The peak at 630 Hz supported this statement. No sources of low-frequency noise, such as subwoofers, were found in any of the bars and pubs included in the study. On the other hand, an average sound level spectrum for clubs corresponded to the reference spectrum for urban traffic, see [Figure 27b](#). This result supported the recommendation of the ISO 717-1 standard [19] for disco music. The term disco music, suggested by the standard, is rather general and could lead to a misinterpretation in terms of reference sound level spectra if different types of entertainment premises were considered. The same type of low-frequency music could be reproduced in different types of entertainment premises, but it is mainly an audio system that will determine the shape of noise level spectra. Even though the same type of music was reproduced in some clubs and discotheques used in the study, results indicated strong differences at low frequencies. Therefore, the average sound level spectrum for discotheques followed the sound level spectrum for urban traffic noise starting from a one-third octave band with the central frequency of 160 Hz, but there were strong deviations in lower one-third octave bands, see [Figure 27c](#).

The average sound level spectrum for discotheques shown in [Figure 27c](#) can be explained by a characteristic detail: a pronounced peak in the frequency region around 80 Hz. This made a noticeable difference when compared to the other spectra. The shape of a peak was recognized as a typical frequency response of a subwoofer used in audio systems [54]. Based on those facts as well as measurement results shown in [Figure 27c](#), a new sound level spectrum for discotheques has been proposed and shown in [Figure 28](#). Its shape was a combination of two sound level spectra. In the case of the above 125 Hz level, the average spectrum measured in discotheques was approximated by the standardised sound level spectrum for urban traffic noise proposed by ISO 717-1 [19]. The only difference between the modified spectrum shown in [Figure 28](#) and the standardised level spectrum above 125 Hz was in the frequency range 500–2000 Hz, where the modified spectrum exhibited a flat tendency. In the frequency range below 125 Hz, a pronounced peak in the modified spectrum was shaped according to the proposed

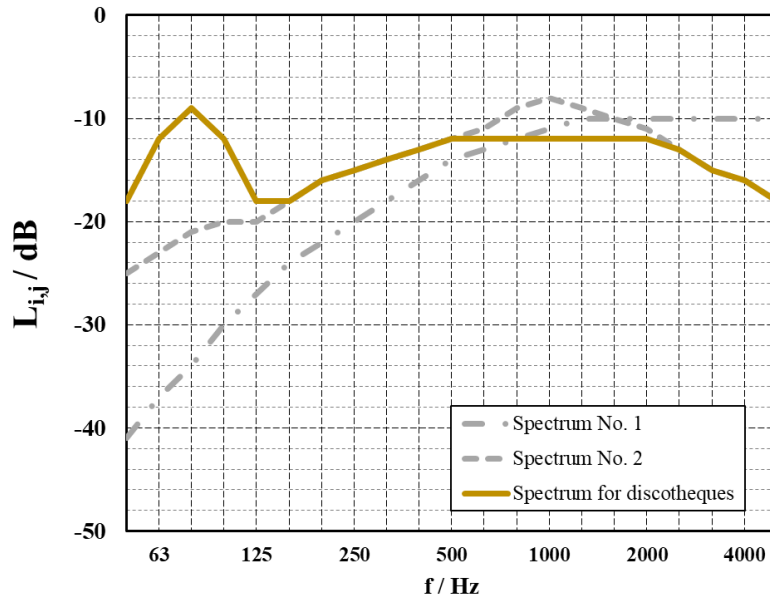


**Figure 28.** Proposed sound level spectrum for discotheques. Spectrum is A-weighted and normalized to 0 dB. [32]

characteristics of a subwoofer loudspeaker in audio systems, as presented in the Dolby manual [54]. Thus, an approximate 10 dB higher spectral level of subwoofer reproduction has been proposed relative to the spectral level of higher frequencies. At the same time, care was taken that the overall sound level of the modified spectra was still normalized to 0 dB, as in the case of two standardised spectra. The values of the proposed spectrum are presented in Table 10.

In Table 11, the results of the influence of different sound level spectra on spectrum adaptation terms for four partitions specified in Section 3.3 are presented. The results shown in Table 11 indicated the possible miscalculation of single-number quantities if the wrong sound level spectra were used. The influence of the calculated spectrum adaptation terms on the sound reduction index  $R_w$  was significant. Differences between  $R_w$  values calculated for spectrum adaptation term  $C_{tr}$  suggested by the ISO 717-1 standard [19] and  $C_{sub}$  calculated from average sound level spectrum presented in Figure 28 varied 4–11 dB between different BEs.

**Table 10.** Sound level spectrum to calculate the spectrum adaptation terms  $C_{sub}$ . Spectrum is A-weighted, normalized to 0 dB and presented in enlarged frequency range. [32]

Frequency	Spectrum to calculate $C_{sub}$
Hz	dB
50	-18
63	-12
80	-9
100	-12
125	-18
160	-18
200	-16
250	-15
315	-14
400	-13
500	-12
630	-12
800	-12
1000	-12
1250	-12
1600	-12
2000	-12
2500	-13
3150	-15
4000	-16
5000	-18

**Table 11.** Comparison of single-number quantities with different spectrum adaptation terms. Values are presented in dB. [32]

Partition	$R_w$	$C_{50-5000}$	$C_{tr, 50-5000}$	$C_{sub, 50-5000}^*$	$R_w + C_{sub, 50-5000}^*$
BE 1	59	-1	-6	-10	49
BE 2	57	-11	-24	-35	22
BE 3	71	-4	-17	-26	45
BE 4	77	-4	-17	-26	51

\* Spectrum adaptation term  $C_{sub}$  was calculated by using proposed sound level spectrum for discotheques shown in Figure 28.

# Chapter 4

## Outdoor Noise of Moored Ships

In this section, characterisation of noise from moored ships, as another source of low-frequency noise, has been investigated. The characterisation has been performed by help of the NEPTUNES measurement protocol [56], which combines near-field and far-field measurements to fully characterise the noise from moored ships. The NEPTUNES protocol has been explained and applied to four moored ships in the area of Stockholm, Sweden. The results of the characterisation have been discussed from the aspect of the low-frequency noise produced by funnel outlets of the auxiliary engines, as the most dominant low-frequency noise source on a ship. Finally, a need for corrections in the low-frequency range when applying near-field measurements has been pointed out.

### 4.1 Introductory Remarks

In the recent years, expansion of marine traffic, development of residential areas and increased interest of people to live around ports have led to concerns of authorities regarding airborne noise emissions from ships and their determination to take actions. In some cases, arrival terminals lie in central parts of cities and present a challenge when it comes to low-frequency noise annoyance in residential areas around the ports, especially if there has been a need for an increased number of ships. In order to investigate the influence of increased marine traffic on surrounding in different scenarios, a consistent characterisation method between ports is needed.

The measurement methods to determine sound power level of a noise source [9,10,31], described in Section 2.2, are rather general and can be applied to different types of noise sources, and so in the case of moored ships. However, these methods can be applied merely to common noise sources on board (e.g., ventilation inlets/outlets, containers, etc.), while an additional measurement method for characterisation of funnel outlets [57], as the most dominant low-frequency noise sources, is also required. Besides measurements on board, the low-frequency nature of funnel outlets entails additional measurement positions in a far-field, from which a correction to near-field measurements can be applied.

In order to standardise characterisation of moored ships, the international project NEPTUNES (Noise Exploration Program to Understand Noise Emitted by Moored ships) [56] has been initiated by eleven ports in Northwest Europe, Australia and Canada. A new measurement protocol, which refers to different types of ships, has been developed. Recently, noise labels were proposed based on measurements of 29 moored ships by following the NEPTUNES measurement protocol [58]. The noise labels give ports opportunity to define port fees and implement appropriate measures in residential areas around the ports.

### 4.2 Neptunes Measurement Procedure

The NEPTUNES measurement protocol [58] establishes a uniform and worldwide applicable measurement procedures to implement noise measurements on individual ships. In this way, it is possible to perform noise measurements in a same manner and compare results obtained from different ports and by different persons. More specifically, the measurements are performed as a combination of sound emission measurements on board of the ships i.e., near-field measurements, and at certain distances from the ships i.e., far-field measurements. The following ship types are particularly interesting in measurements:

- (a) Container ships,
- (b) Cruise ships,
- (c) Tankers,

- (d) RoRo / RoPax,
- (e) Bulk carriers, and
- (f) General cargo / service vessel.

In general, individual noise sources that can be found on board of the ships are diverse. Some noise sources exist at all ship types, while others exist only at certain ship types. The most common noise sources to be measured are:

- (1) The funnel outlet of the auxiliary engines,
- (2) The opening of engine room ventilation inlet and outlet,
- (3) The opening of the cargo holds ventilation and air conditionings inlet and outlet,
- (4) The opening of the ventilation and air condition of passenger rooms,
- (5) Cooled containers / reefers,
- (6) Pumps on deck, and
- (7) Water pumps on deck.

It should be noted, however, that measurements of sound radiation from the ship's hull, water falling from the ship into the sea and cars driving over a ramp are optional and based on the subjective assessment.

Basically, all moored ships are equipped with at least one main and two auxiliary engines. On the one hand, main engines are used to drive ships and mostly used in the course of docking and sailing out. On the other hand, auxiliary engines are used to run electrical consumers on board (e.g., pumps, air conditioners, etc.) when ships are moored. While almost all individual noise sources described above can be characterised by using some of the measurement methods already described in [Section 2.2](#), funnel outlets of auxiliary engines present the most dominant low-frequency noise source on a ship and require a special approach which is described below.

#### 4.2.1 Characterisation of the Funnel Outlet in a Near-Field

The measurement of sound power levels of funnel outlets is implemented according to DIN 45635–47 [57]. As presented in [Figure 29](#), sound pressure levels are measured at two measurement positions, M1 and M2. The measurement positions can be distributed arbitrarily in the horizontal direction since directivity is expected to be same in that direction. The distance from the wall of funnel outlets is 1 m. If possible, additional measurements at greater distances from the funnel outlet (e.g., 5–10 m) are performed and compared to that at the distance of 1 m. Surface areas  $S_1$  (hemisphere above the horizontal plane of the funnel outlet) and  $S_2$  (hemisphere below the horizontal plane of the funnel outlet), shown in [Figure 29](#), are calculated according to:

$$S_1 = 2 \cdot \pi \cdot r_s^2 \quad (18)$$

and

$$S_2 = 2 \cdot \pi \cdot r_s \cdot \sqrt{r_s^2 - r_k^2} \quad (19)$$

with  $r_s = r_0 + 1\text{m}$ ,  $70^\circ \leq \varphi_1 \leq 80^\circ$ , and  $100^\circ \leq \varphi_2 \leq 110^\circ$ .

The sound power level of funnel outlets is calculated separately for measurement surfaces  $S_1$  and  $S_2$  according to:

$$L_{WA} = L_{Aeq} - K + 10 \cdot \log \frac{S}{S_0} \text{ dBA} \quad (20)$$

where  $L_{Aeq}$  is the A-weighted equivalent continuous sound pressure level averaged over the measurement surface area  $S$  ( $m^2$ ),  $S_0$  is the reference surface of  $1 m^2$ , and  $K$  is the correction factor for background noise.

Then, the total sound power level of the funnel outlet is:

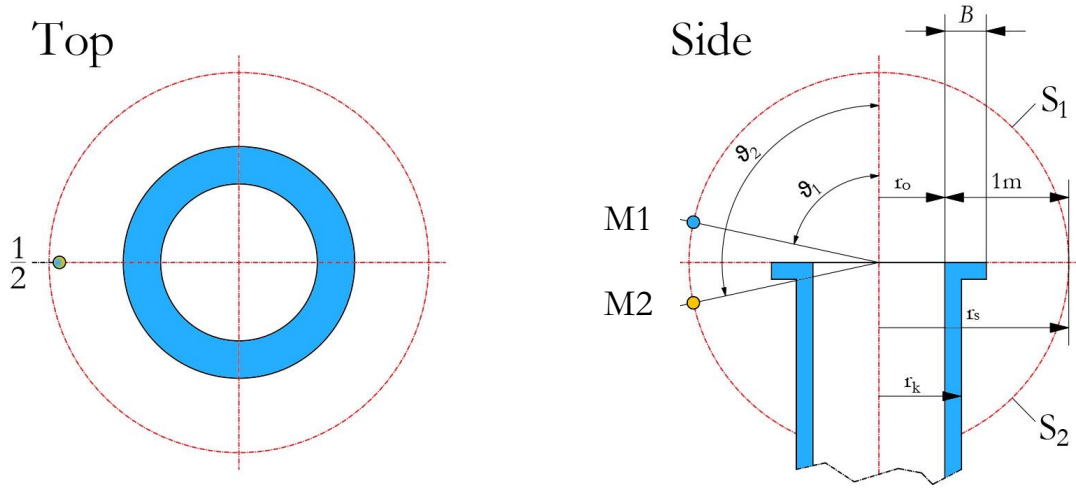


**Figure 29.** Measurement positions for determination of sound power levels of funnel outlets.

$$L_{WA,funnel} = 10 \cdot \log \left( 10^{\frac{L_{WA,1}}{10}} + 10^{\frac{L_{WA,2}}{10}} \right) \text{ dBA} \quad (21)$$

where  $L_{WA,1}$  and  $L_{WA,2}$  are the sound power levels calculated for two measurement positions from Figure 29, M1 and M2, according to (18), (19) and (20).

#### 4.2.2 Measurements in a Far-Field

The measurement of sound pressure level at a certain distance from the ship serve to assess the overall sound emission of the ship. Additionally, they indicate the presence of the low-frequency components which are not detected from the measurements on board. It is possible to introduce necessary corrections in the sound power level calculations by means of comparing two measurements. These corrections are mostly expected when calculating sound power levels of funnel outlets, as the most dominant low-frequency noise source.

The measurements at a certain distance from the ship should be performed at three measurement positions:

- MP1 – Sideways from the funnel outlet,
- MP2 – In the middle of the ship bow and the centre of the ship, and
- MP3 – Sideways from the stern or behind the stern of the ship.

Different positions for MP2 and MP3 should be chosen in case when funnel outlet lies within less than 10 m to MP2 and MP3. All positions should be chosen in a way that there is a clear line of sight between microphone and funnel outlets. The placement of the measurement positions is illustrated in Figure 30 below. The height of the measurement positions should be at least  $h_m = 6 \text{ m}$  above the quay ground. Also, the measurement position MP1 is chosen in a way that the angle ( $\alpha$ ) between the direct distance to the funnel outlet ( $d_c$ ) and the horizontal distance ( $d_h$ ) lies in a range  $5^\circ \leq \alpha \leq 20^\circ$ . The measurement duration at each measurement position should be longer than 2 min.

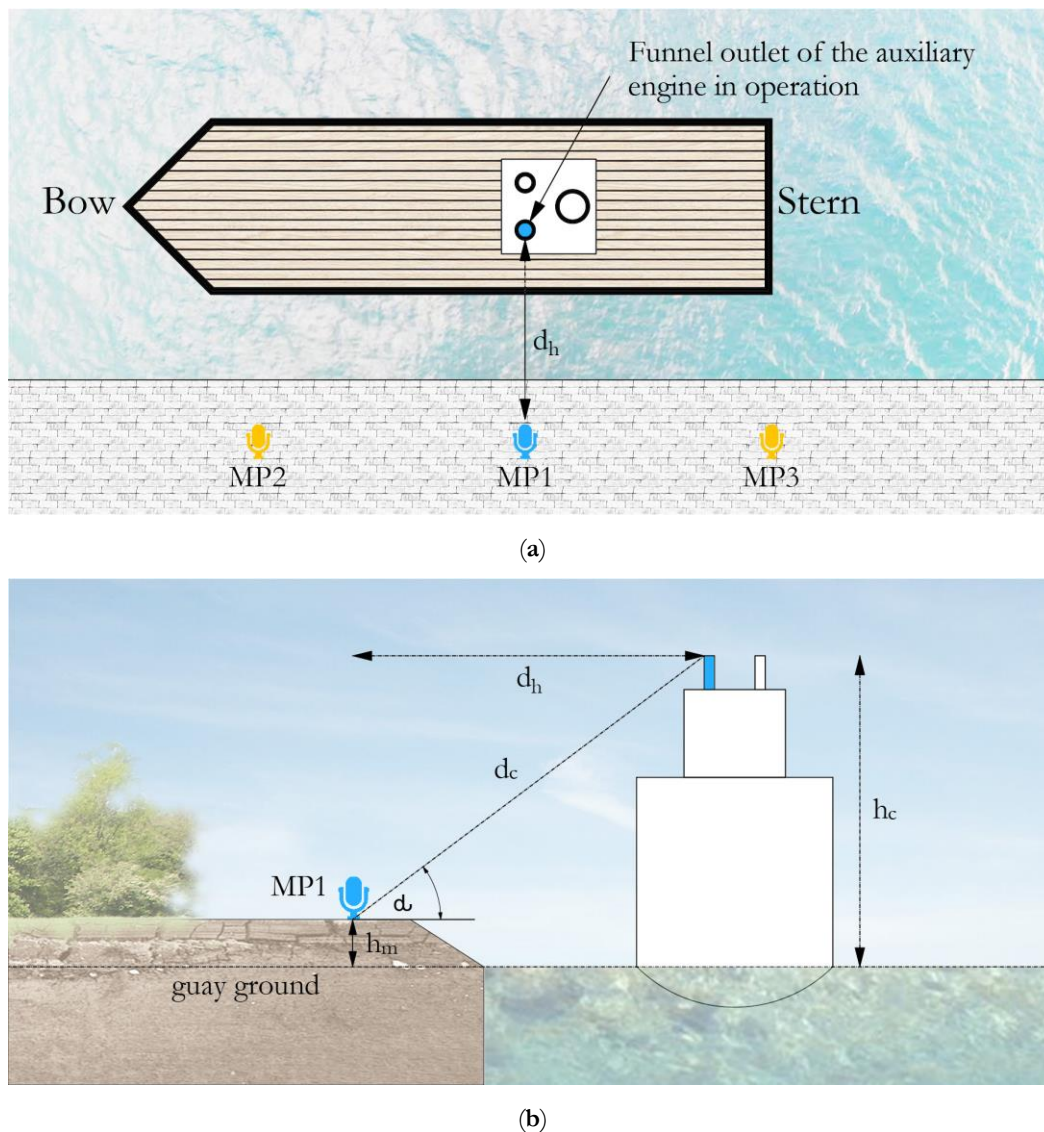


**Figure 30.** Measurement positions at a certain distance from the ship: (a) Placement of the measurement positions at horizontal distance  $d_h$ . (b) Relative position of position MP1 to the funnel outlet in operation.

### 4.3 Emission Measurement Methods

The sound emission measurements were applied to four moored ships by following the NEPTUNES measurement protocol [56], described in the previous section. The measurements took place in ports around and in the city area of Stockholm, Sweden. Technical specifications of the ships included in the study are presented in Table 12.

**Table 12.** Technical specifications of the ships characterised by the NEPTUNES measurement protocol [56].

Name	Type	Number of auxiliary motors	Active auxiliary motors when moored	Power of moored ship [kW]	Width [m]	Length [m]	Capacity
Ship 1	RoRo/RoPax	3	2	650	30.5	219	192
Ship 2	RoRo/RoPax	3	1	770	26.6	161	1300
Ship 3	RoRo	2	1	230	22.7	139	12
Ship 4	Cruise ship	4	2	9400	51.7	325	3963

Near-field and far-field measurements of sound pressure levels were performed during ships' normal operational conditions when they were moored i.e., with only auxiliary engines in operation. First, the near-field measurements were used to calculate sound power levels of funnel outlets according to (18), (19) and (20). Then, the near-field sound power levels were used to calculate sound pressure levels at measurement positions in a far-field. This was performed by employing the SoundPLAN noise software [6], together with the ISO 9613-2 [59] calculation method. In the calculation model, funnel outlet was considered a point source radiating acoustical energy in all direction i.e., full sphere radiation. The calculations were performed with three reflections. Terrain between ships and far-field measurement positions was considered acoustically reflective. Terrain data was obtained from a service for laser terrain mapping. Finally, the calculated sound pressure levels in a far-field were compared to measured sound pressure levels at the same measurement positions.

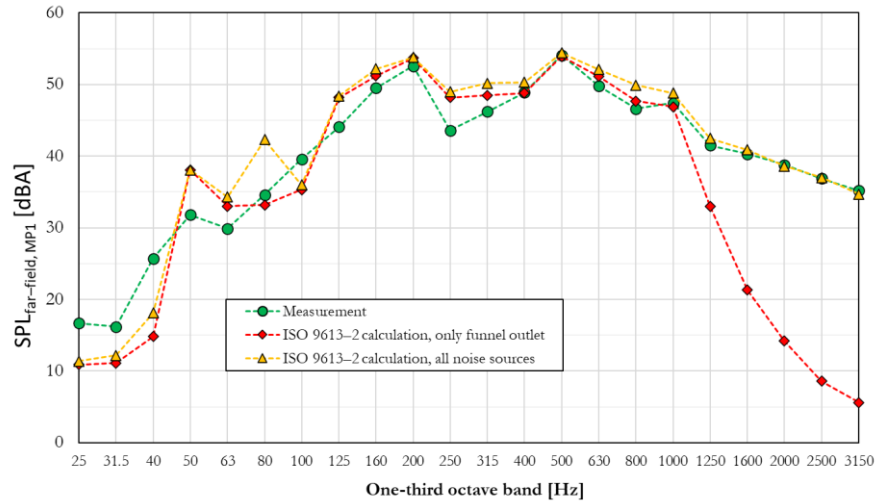
The near-field measurements were performed at distances approx. 1–2 m from the funnel outlets, except in case of Ship 4 where distance of approximately 15–20 m was used. The reason for this is the fact that the funnel outlet in case of Ship 4 was an outlet cluster with dimensions of approx.  $18 \times 15 \times 15$  m, compared to single outlets in case of other ships. The far-field measurements were performed at distances 65–380 m from the ships, depending on their position and terrain configuration. The distance between the far-field measurement positions and ships was determined with a laser rangefinder. Whenever it was possible, the far-field measurement positions were chosen in such way so that a contribution of other noise sources was minimised i.e., performing measurements on the side of ships where no or very few other noise sources had been detected. The height of a microphone during far-field measurements was 6 m above the ground, as recommended by the NEPTUNES measurement protocol [56]. Although there were other noise sources operating on board, the most dominant low-frequency and, in most cases, mid-frequency noise source was assessed to be funnel outlet of the auxiliary engine.

In case of Ship 1, two measurements positions, MP1 and MP3, were chosen at distances approximately 120 m from the ship, just on the opposite sides of the ship. Both measurement positions were located at  $h_M=6$  m, while the funnel outlet was located at approx.  $h_C=37$  m. In case of Ship 2, two measurement positions, MP1 and MP2, were chosen at distances approx. 110 m and 135 m from the ship, respectively. Both measurement positions were located on the same side of the ship. Position MP1 was located at  $h_M=11$  m, while MP2 was located on a hill at  $h_M=25$  m. The funnel outlet was located at approx.  $h_C=50$  m. In case of Ship 3, two measurement positions, MP1 and MP2, were chosen on the same side of the ship at distances approx. 65 m from the ship. Position MP1 was chosen sideways from the funnel outlet at  $h_M=11$  m. Position MP2 was chosen sideways of the bow at  $h_M=13$  m. The funnel outlet was located at approx.  $h_C=26$  m. In case of Ship 4, two measurement positions, MP1 and MP2, were chosen on the same side of the ship at distances 380 m and 330 m from the ship, respectively. Same height  $h_M=6$  m was used for both measurement positions.

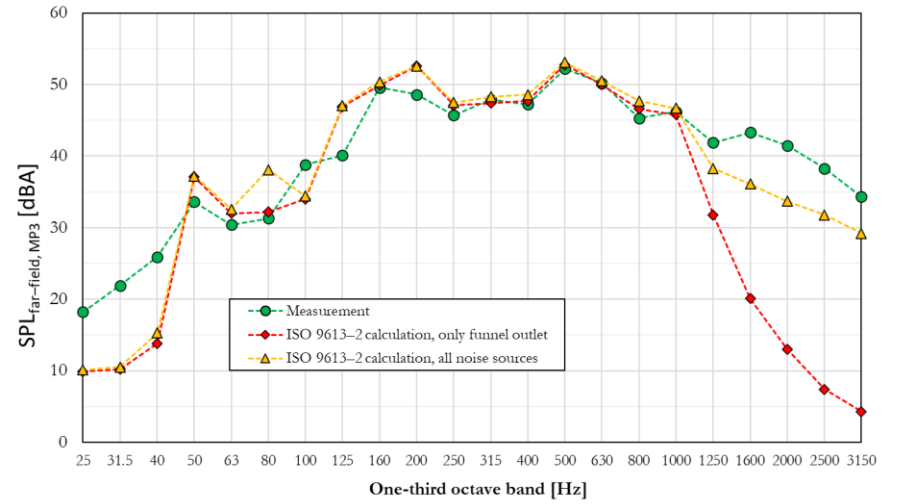
## 4.4 Experimental Results and Discussions

The measured and calculated sound pressure levels at measurement positions in a far-field are presented in Figure 31–34. The sound pressure levels were calculated for each ship in two scenarios: with only funnel outlet in operation, and with funnel outlet and other noise sources in operation. In this way, it was possible to investigate the influence of other noise sources on sound pressure levels at measurement positions in a far-field. Sound power levels of all noise sources for individual ships, which contributed to sound pressure levels at measurement positions in a far-field, are presented in Appendix B.

In three cases, funnel outlets emitted a pronounced low-frequency noise from a single outlet (Figure 31–34), where three characteristic regions were observed. First, the low-frequency region 25–40 Hz, where measured sound pressure levels exhibited greater values compared to calculated. Second, a generally good agreement between measured and calculated sound pressure levels was obtained in the frequency range approximately 50–1000 Hz, 50–400 Hz and 50–800 Hz for Ship 1, Ship 2 and Ship 3,

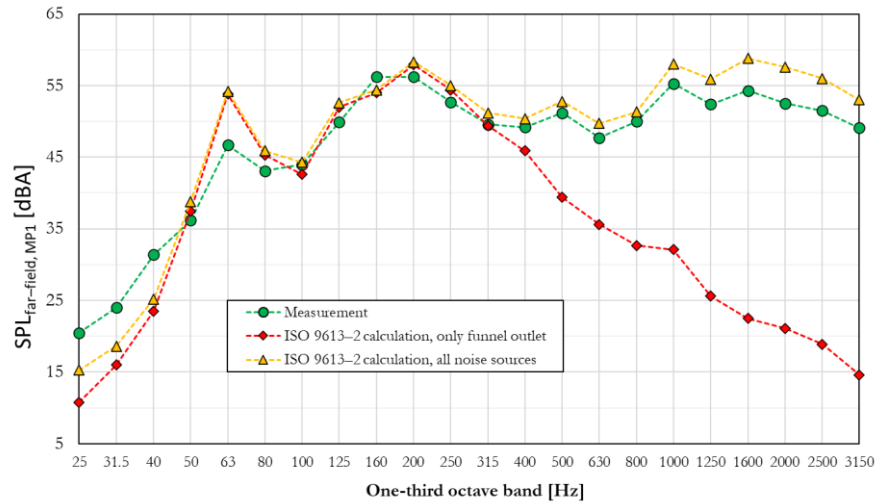


(a) Measurement position MP1

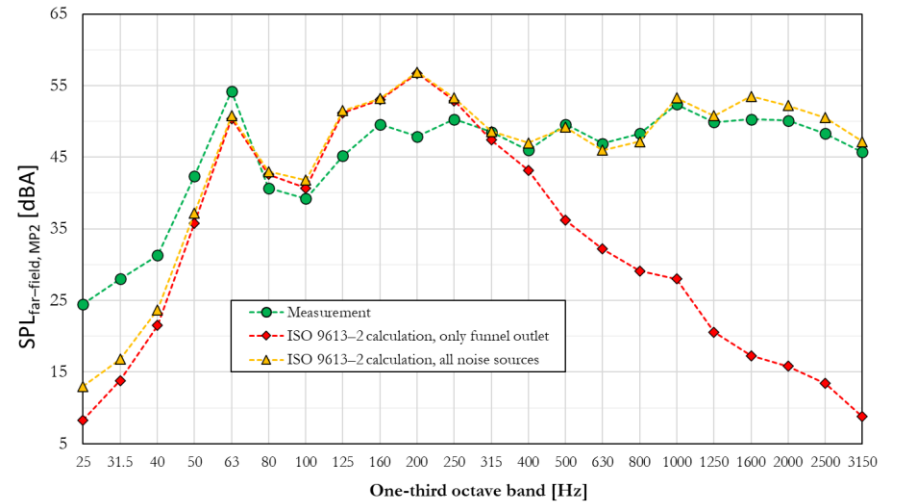


(b) Measurement position MP3

Figure 31. Comparison of measured and calculated sound pressure level in far-field obtained at different measurement positions for ship 1.

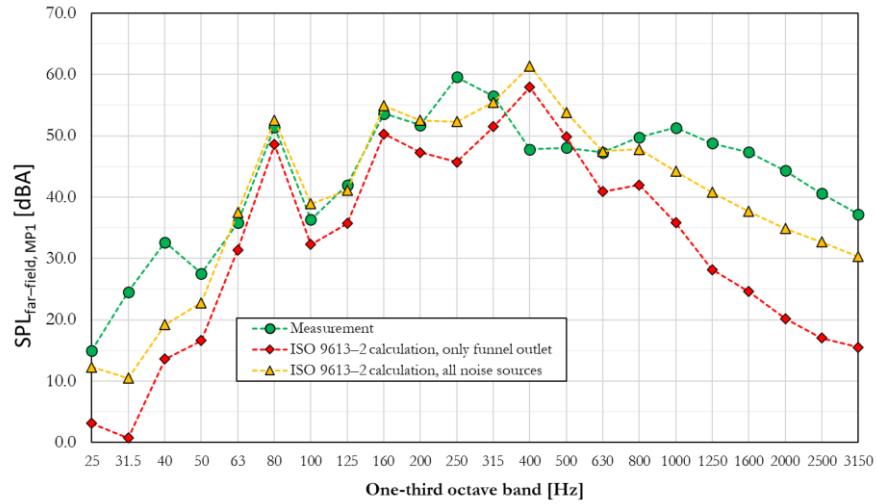


(c) Measurement position MP1

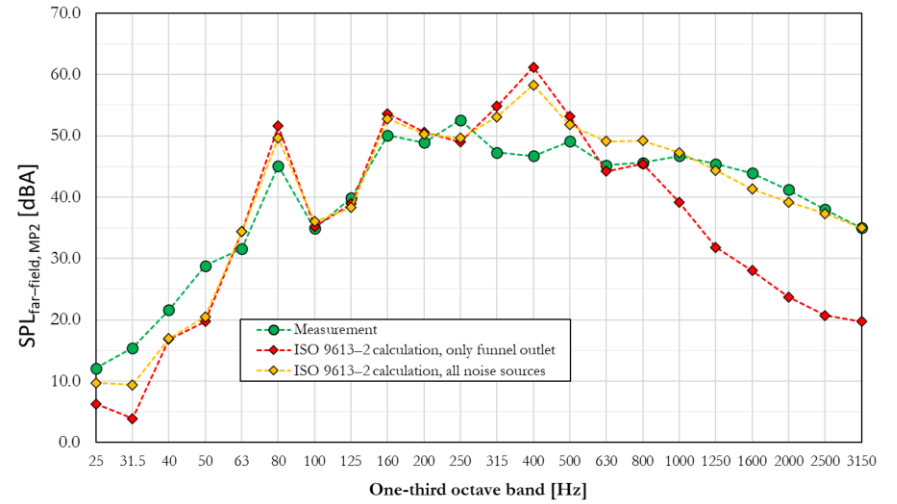


(d) Measurement position MP2

Figure 32. Comparison of measured and calculated sound pressure level in far-field obtained at different measurement positions for ship 2.

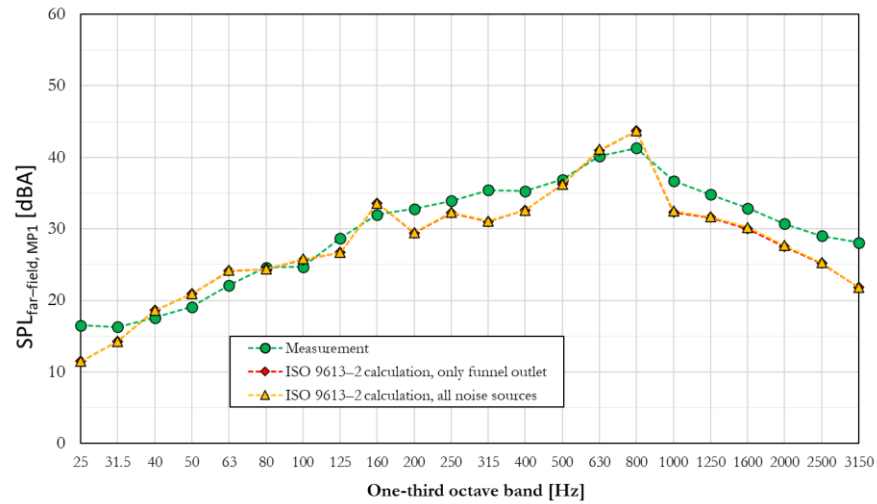


(a) Measurement position MP1

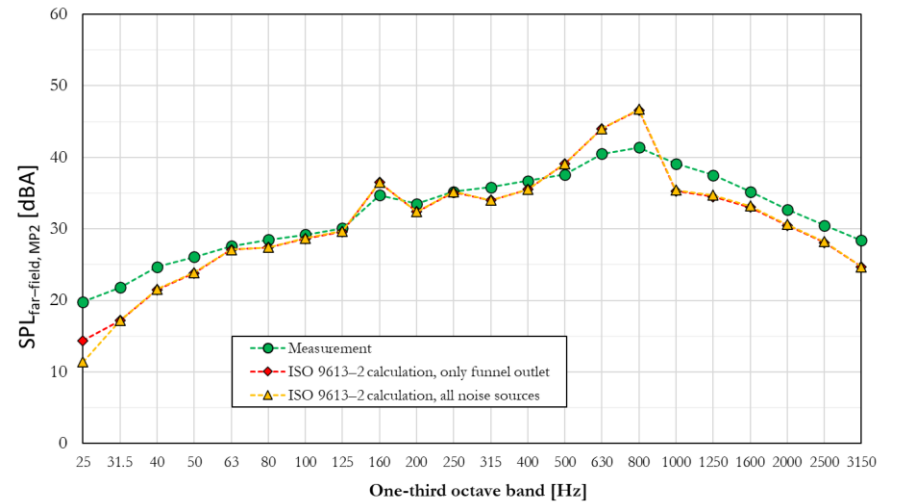


(b) Measurement position MP2

Figure 33. Comparison of measured and calculated sound pressure level in far-field obtained at different measurement positions for ship 3.



(c) Measurement position MP1



(d) Measurement position MP2

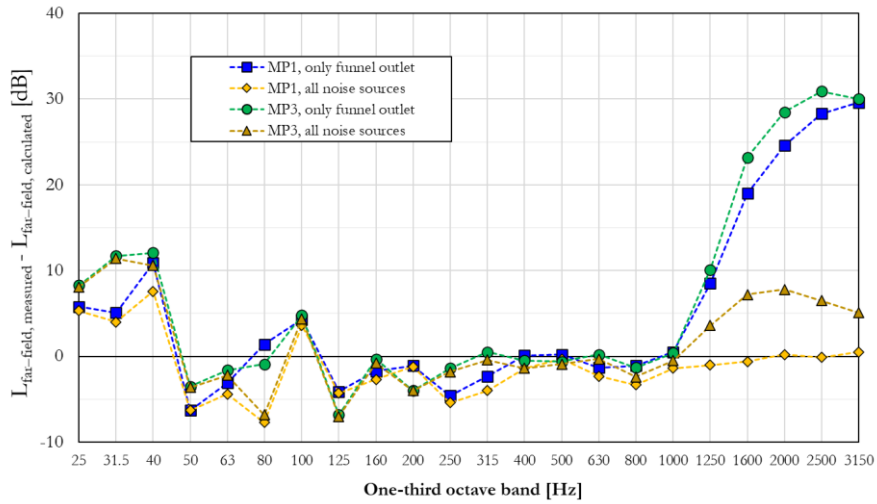
Figure 34. Comparison of measured and calculated sound pressure level in far-field obtained at different measurement positions for ship 4.

respectively. Finally, a large disagreement between measured and calculated sound pressure levels was obtained in the higher range in all three cases, when only funnel outlets were used for calculation of the sound pressure levels in a far-field. When all noise sources on a ship were included in the calculations, the agreement between measured and calculated sound pressure levels was significantly improved. In the last case presented in [Figure 34](#), funnel outlet emitted a broadband noise from an outlet cluster rather than a single outlet. For this reason, this has been considered as isolated case compared to other three cases.

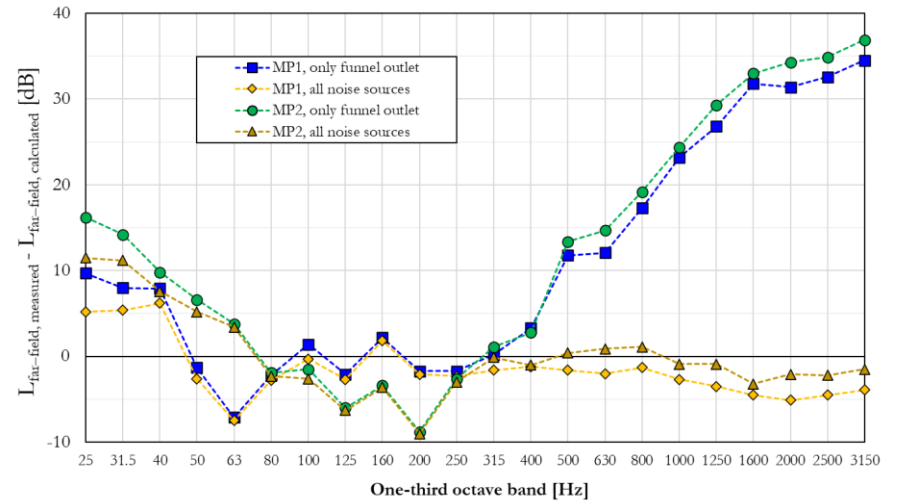
Relative differences of measured and calculated sound pressure levels at measurement positions in a far-field are presented in [Figure 35](#) so as to make results in [Figure 31–34](#) more evident. Furthermore, the results presented in [Figure 35](#) showed that most near-field measurements in case of Ship 1, Ship 2 and Ship 3 underestimated sound power levels of the ships by 4–14 dB in the frequency range 25–40 Hz. The differences were obtained in case when sound pressure levels at measurement positions in a far-field were calculated with all noise sources in operation. A possible explanation for this lies in the fact that in the region very close to funnel outlet the sound field is uncertain, and the funnel outlet cannot be considered a point source at such close distances. With the aim of considering funnel outlet a point source, measurements should be carried out at distances several wavelengths away. In case of low-frequency noise produced by funnel outlets the distance become larger than 7 m for frequencies below 50 Hz. This distance is significantly larger than the distance recommended by the NEPTUNES measurement protocol. In the frequency range approximately 50–1000 Hz, 50–400 Hz and 50–800 Hz for Ship 1, Ship 2 and Ship 3, respectively, a good agreement was obtained in all three cases with few exceptions. The exceptions were most noticeable in case of Ship 3, where deviations between measured and calculated sound pressure levels at measurement points in a far-field were most likely a consequence of inability to perform near-field measurements at positions M1 and M2 (see [Figure 29](#)) due to safety reasons. Namely, the funnel outlet in this case was aimed at an angle of 90° (not upwards as in all other cases) and the near-field measurement was performed opposite to direction of the noise radiation (at an angle of 180°), where the exit to the roof was located. Therefore, sound pressure levels in a far-field were measured for different radiation angles. In this case, the directivity of the funnel outlet in the observed frequency range might have played a significant role. Finally, a good agreement between measured and calculated sound pressure levels in a far-field at higher frequencies was obtained for most measurement points when all noise sources were included in the calculations. Here, other activities in the ports (e.g., other ships, transportation vehicles, human activities etc.) might have interfered with far-field measurements and led to deviations obtained at MP3 in [Figure 35a](#) as well as MP1 in [Figure 35c](#). Higher values of measured sound pressure levels than calculated goes in favour of that.

In the fourth case, presented in [Figure 34](#) and [Figure 35d](#), a good agreement between measured and calculated sound pressure levels was obtained in the whole frequency range. Here, a size of the funnel outlet was large, and the position of acoustical centre was unclear. Therefore, a near-field characterisation was performed at distance approximately 20 m away from the funnel outlet. It is important to mention that the near-field characterisation was performed in the direction of the bow, not sideways towards measurement positions in a far-field. Moreover, far-field characterisation was performed at distances 330 m and 380 m from the ship, which is significantly larger compared to other three ships. Additionally, the far-field measurement positions were located in a very quiet area, far away from other potential noise sources. As a result, a good agreement between far-field and near-field sound pressure levels was obtained in the whole frequency range and hence no need for introducing any corrections.

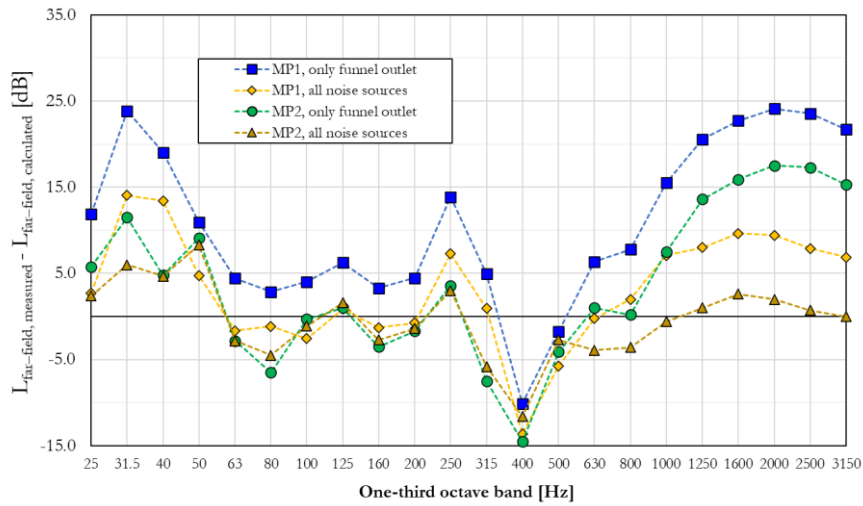
The results presented in [Figure 31–34](#) showed the importance of the measurement position in a far-field and indicated a need to introduce a low-frequency correction in the near-field measurements. This is also in agreement with results obtained in [Section 2.5.3](#). Selection of measurement positions in a far-field affects the values of low-frequency corrections and should be done carefully. In addition to measurement positions in a far-field, one or more control points can be used to monitor the operation of ships during their characterisation. In that case, a change in operation conditions can be detected and necessary corrections can be applied. The NEPTUNES measurement protocol is the first and important step for further analyses of noise from moored ships i.e., for calculation of their noise in different scenarios as well as for taking measures.



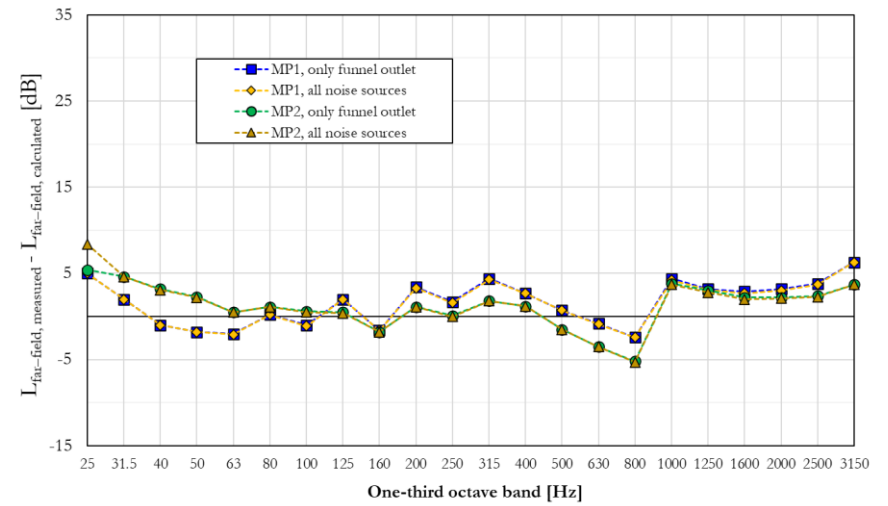
(a) Ship 1



(b) Ship 2



(c) Ship 3



(d) Ship 4

Figure 35. Relative differences between measured and calculated sound pressure levels in far-field obtained for different ships and measurement positions.

## Part II

### Protection Methods

The second part of this dissertation starts with an overview of acoustic properties of noise barriers (Section 5.1), followed by key measurement standards and their principles: *in situ* (Section 5.2) and laboratory (Section 5.3) measurement methods. Noise barrier are the most common protection method in urban environments against noise from road traffic, railway traffic, industry, etc., and therefore investigated in this dissertation. Then, the measurement methods are applied to two different types of noise barriers – a conventional sound absorbing barrier and a prototype of sound absorbing sonic crystal (Section 5.4). The research of sonic crystals as noise barriers has emerged in the literature during the last two decades and therefore investigated in this dissertation as protection method in case of noise from specific noise sources. Finally, the results are presented as both frequency-dependant and single-number values of sound insulation and sound reflection (Section 5.5).

# Chapter 5

## Acoustic Properties of Noise Barrier

### 5.1 Introductory Remarks

The most common type of noise barriers is *screen-type* (i.e., *conventional*) noise barrier. This type of noise barriers is built as a continuous and rigid flat wall made of materials such as concrete, steel, wood, methacrylate, etc. The acoustic performance of such noise barriers is mostly dependant on its shape [60], height [61] and density [62]. A drawback of this type of noise barriers is the fact that foundation costs significantly increase with increment of barrier height. Another disadvantage is high resistance to air and water flow, together with loss of sunlight and visual dominance [63]. Additionally, barrier panels are connected by using posts, which are often responsible for leakage and therefore cause a drop in acoustic performance of the barrier [30]. Finally, they must be very weight and tall in order to be efficient against the low-frequency noise. In order to improve sound insulation and absorption properties of conventional noise barriers at low frequencies, resonant elements are used [64].

As an alternative to conventional noise barriers, a special type of noise barriers called *sonic crystal* (SC), has been investigated in the last two decades. This type of noise barriers consists of sound scatterers periodically arranged in a lattice. Their most important characteristic is ability to prevent sound propagation in certain frequency bands, called *band gaps*. This is possible due to a mechanism called *Bragg scattering*, which is the destructive interference between the sound reflected from different scatterers in the lattice. Experimental characterisation of acoustic band gaps was first investigated in 1995 within a kinematic sculpture made by Eusebio Sempere, which is exhibited at the Juan March Foundation in Madrid [65]. A few years later, the results were confirmed in a laboratory environment [66,67], where the existence of complete and partial band gaps was associated with the lattice symmetry and its filling fraction. Afterwards, wider and frequency-tuneable band gaps were shown to be feasible by changing the spatial arrangement and the mechanical properties of scatterers [68,69].

Compared to conventional noise barriers, SCs do not necessarily need foundations since they show almost no resistance to air and water flow. However, a word of caution regarding this property is warranted. When the velocity of air is above a certain cut-off, the generated flow noise can quench the band gaps [70]. SCs are also lighter compared to traditional noise barriers and have great aesthetic potential. Additionally, there are no posts in case of SCs and thus no weaknesses in their acoustic properties in that sense. Nevertheless, there are very few practical implementations of SCs outside laboratory environments [71,72], mostly because of fabrication costs. However, the costs could be substantially reduced through mass production.

Experimental data show that a periodic arrangement of metallic cylinders in air provides sound attenuation of up to 25 dB [66,71–75], which could compete with traditional noise barriers. At band gap frequencies, simultaneous low transmittance and high reflectance are expected due to Bragg scattering. Unfortunately, the band gaps produced by SCs made of rigid cylinders are confined to a relatively narrow band of frequencies. Outside the band gaps, attenuation is very poor, making the use of SCs infeasible against broadband noise. Hence, additional physical mechanisms should be involved in order to achieve broadband attenuation. In that sense, the use of absorbing material covering the scatterers and local resonant phenomena have been recently proposed [75–82]. In this way, it is possible to obtain barriers whose frequency-dependent attenuation is more uniform and, in some cases, to enhance their overall performance.

There are numerous different ways to characterise noise barriers, especially when it comes to SCs. In most of the investigated research, this was done by implementing different non-standardised measurement techniques. One possible way of characterisation is presented in [65,71], where finite size barrier samples are characterised in anechoic chambers. However, the transmitted component was not

isolated in these examples since diffraction components over the barrier's top edge and around its sides were included. This means that the measured attenuation values should be considered as indicative rather than precise. This could have been avoided if a *time-windowing technique* was used. This approach was employed in [80], but under reverberant field conditions. A time window length of 6 ms was used, which was not enough to exclude diffraction over the top of 1 m long barrier sample. Also, one of the most common way to characterise noise barriers is to employ traditional *ISO 140-3* [83] and *ISO 354* [84] laboratory measurements. These two versions are recently replaced with their supplemented versions relevant for noise barriers, *1793-2* [85] and *EN 1793-1* [86], respectively. Although widely used to define specification of noise barriers, these methods are implemented under diffuse field conditions which contrasts with directional sound field under which noise barriers are usually exposed. Additionally, some researchers [87–89] claimed that the sound absorption coefficient measured in a reverberation room could be strongly affected by the sample size.

Apart from characterisation methods presented above, a research project name *Adrienne* (1995–1997) [90] was funded by the European Commission to develop a new test method for measuring intrinsic properties of noise reducing devices *in situ*. During the 3-years project, research team managed to produce innovative techniques to test airborne sound insulation and sound reflection of noise barriers, but also to reduce the lowest reliable frequency from 400 Hz to 200 Hz. After this, verification of the methods was performed [30,91] and a first version of European standard was released [92]. This very first version included methods for determining both *in situ* airborne sound insulation and sound reflection properties of noise barriers. More recently, *QUIESST* research project (2009–2012) [93] provided examples of best practices and recommendations on these *in situ* methods. Finally, the test method for determining *in situ* values of airborne sound insulation, *EN 1793-6* [29], and the test method for determining *in situ* values of sound reflection, *EN 1793-5* [28], were issued as independent European standards. By applying an appropriate windowing technique, *EN 1793-6* [29] accounts for transmitted components only, while dismissing diffracted and sound reflected components from the ground and other objects located nearby. Similarly, the windowing technique in the case of *EN 1793-5* [28] excludes components other than those reflected from the barrier itself.

The above-mentioned *in situ* measurement methods have many advantages over traditional *EN 1793-1* [26] and *1793-2* [27] laboratory measurements. As mentioned before, the laboratory measurements have been developed for testing building elements and require measurements to be done inside specially designed rooms under diffuse sound field conditions. In contrary, *in situ* measurements are mostly performed in front of noise barriers and use directional sound field. The latter is expected to be more realistic since noise barriers are rarely installed in diffuse field conditions. An exception are semi- or fully closed spaces such as tunnels [94]. Although results obtained by implementation of laboratory and *in situ* measurement techniques are not directly comparable, some correlation between them was discovered [30,95,96]. In general, laboratory measurements exhibit lower sound insulation and higher sound absorption values compared to *in situ* measurements.

The *in situ* methods have thoroughly been tested with traditional noise barriers [30,91,96–101], while their applicability in the case of SCs is still uncertain. Recently, Morandi et al. [33] characterised an SC noise barrier made of polyvinyl chloride (PVC) rods with a lattice constant of 0.2 m, by implementing standardised *EN 1793-5* [28] and *EN 1793-6* [29] methods. They showed that the values of the sound insulation index (*SI*) and the reflection index (*RI*) strongly depend on the measurement configuration, attaining maximum values of about 24 dB for *SI* and around 1 (on the decimal scale) for *RI* in the Bragg band gap. While the *EN 1793-6* [29] method allows calculation of the intrinsic airborne sound insulation, the method itself restricted the applicability to SCs with no more than three rows of cylinders in the lattice. This is due to inability of the temporal window to include all reflections with a significant spectral content. For sound reflection measurements, correlation between the number of rows and the measured data was found to be poor, according to [33, Fig. 7]. Another example of implementation of *in situ* methods on SCs is investigated in [102]. In this case, a real-sized SC sample with three rows of SC elements made of six concentric resonant PVC pipes was characterised in an anechoic chamber according

to EN 1793–6 [29]. It was shown that by including resonant elements, instead of solid cylinders, an overall performance of the SC barrier was improved. However, it should be noted that sample size of  $2 \times 1 \times 0.5$  m allowed for diffraction around its sides, although a time–windowing technique was employed.

This part of dissertation is organized as follows. First, a description of *in situ* methods employed to characterise two noise barriers, a conventional and a SC noise barrier, has been presented in Section 5.2. Laboratory methods used to obtain acoustic properties of the conventional noise barrier, which are later compared with those obtained by the *in situ* methods, have been described Section 5.3. Then, a comprehensive report on the experimental results for these two types of noise barriers has been presented in Section 5.5. Although results of a sound reflection measurement for the conventional noise barrier presented in Section 5.5.1.2 had previously been investigated in [103], measurement results presented in this work have been obtained for different barrier element. Additionally, results presented here have been used to complement sound insulation measurements presented in Section 5.5.1.1. The main results of this part of dissertation have been presented in Section 5.5.2, where results of characterisation of a sonic crystal barrier have been described. These results, together with detailed theoretical analysis, have been published in [34].

## 5.2 Measurement Methods

### 5.2.1 In Situ Measurement Methods

European standards EN 1793–6 [29] and EN 1793–5 [28] specify measurement methods for *in situ* assessment of sound insulation and reflection performance, respectively, of road traffic noise–reducing devices. The methods are used to check intrinsic characteristics of airborne sound insulation and sound reflection of noise–reducing devices to be installed along roads and those already in place. They are also applied to examine barrier design specifications, verifying long–term barrier performance, and facilitating interactive designing of new products. Such measurements are widely accepted as a common way of noise–reducing device characterisation. One of the advantages of the *in situ* methods over traditional laboratory measurements, EN 1793–1 [26] and EN 1793–2 [27], is that they can be undertaken in the presence of traffic background noise. This is possible by using deterministic excitation signals in combination with impulse–response measurement techniques. Also, *in situ* measurements assume a directional sound field compared to a diffuse field in the case of laboratory measurements, since the former is more realistic. Thus, the results are comparable but not identical [30,95,96].

*In situ* methods use the same principles and equipment for both sound insulation and reflection measurements. The main principles of the methods are explained in more details below, in connection with the actual SC barrier sample whose characterisation results are presented in Section 5.4.2. However, the principles are identical for the conventional barrier sample presented in Section 5.4.1.

#### 5.2.1.1 In Situ measurements of Airborne Sound Insulation of Noise Barriers

Two impulse–response measurements are the basis of the *in situ* insulation method. The first is performed in a free–field without a noise barrier and the second with a noise barrier (see Figure 36). Both measurements are carried out keeping the same loudspeaker–to–receiver distance, calculated by summing the loudspeaker–to–barrier ( $d_s$ ) and barrier–to–receiver ( $d_M$ ) distances with the thickness of the noise barrier ( $t_B$ ). Both loudspeaker–to–barrier and barrier–to–receiver distances are defined by the method itself and the values are 1 m and 0.25 m, respectively. The receiver consists of a  $3 \times 3$  microphone grid (M1–M9), with any two adjacent microphones spaced 0.4 m apart.

When performing a measurement in the presence of a noise barrier, the sound emitted by the sound source is partly reflected, partly absorbed, partly transmitted, and partly diffracted by the barrier itself. To calculate the intrinsic characteristic of the barrier, all sound components, except those directly transmitted through the barrier, are discarded. This refers to both diffracted and ground–reflected sound waves (see Figure 36b). It is achieved by applying a specially designed temporal window called the *Adrienne*

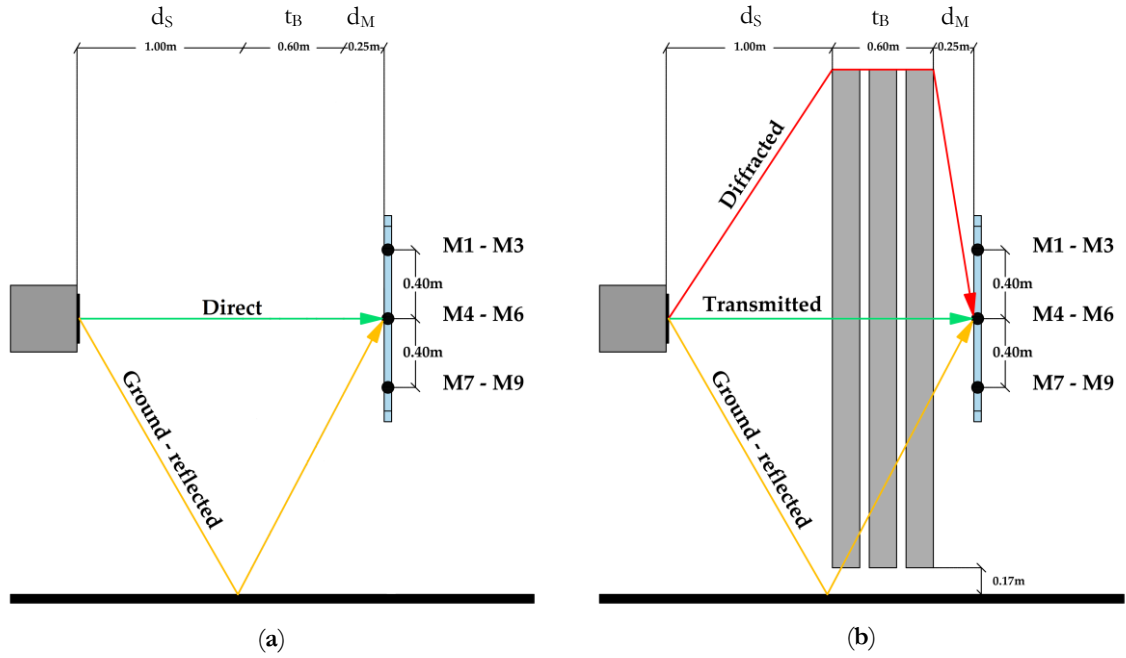


**Figure 36.** Illustration of experimental setup for implementation of standardised EN 1793-6 [29] measurement method at the microphone position M5: (a) without a noise barrier; (b) in the presence of a noise barrier.

temporal window. Finally, the energies of the time windowed impulse responses are calculated and compared to those from the free-field measurement. The measured data are averaged over all nine microphones and a specific quantity called the *sound insulation index* ( $SI$ ) is evaluated from:

$$SI_j(\text{dB}) = -10 \cdot \log \left\{ \frac{1}{n} \sum_{k=1}^n \frac{\int_{\Delta f_j} |F[h_{t,k}(t) \cdot w_{t,k}(t)]|^2 df}{\int_{\Delta f_j} |F[h_{i,k}(t) \cdot w_{i,k}(t)]|^2 df} \right\} \quad (22)$$

where  $h_{i,k}(t)$  is the free-field impulse-response at the  $k$ -th microphone position,  $h_{t,k}(t)$  is the impulse-response at the  $k$ -th microphone position with the barrier in between,  $w_{i,k}(t)$  and  $w_{t,k}(t)$  are the time windows (*Adrienne* temporal windows) for the free-field and the transmitted components, respectively, at the  $k$ -th microphone position, and  $F$  denotes the *Fourier transform*. Finally, index  $j$  denotes the  $j$ -th one-third octave frequency band with bandwidth  $\Delta f_j$  and the integer  $n$  ( $n = 9$ ) defines the number of microphone positions.

*Adrienne* temporal window consists of a leading edge having a left-half *Blackman-Harris* shape with a fixed length of 0.5 ms, a flat portion and a trailing edge having a right-half *Blackman-Harris* shape (see Figure 37). The lengths of the flat portion and the right-half *Blackman-Harris* portion should have a ratio of 7:3. The position where the flat portion of the *Adrienne* temporal window begins is called the marker position (MP). *Adrienne* temporal window is placed so as its MP begins 0.2 ms before the direct component peak of the measured impulse response. This is done for each single microphone in the microphone grid. Changing the microphone position, MP is placed at slightly different time instants.

The size of the barrier affects the width of the *Adrienne* temporal window as well as the lowest reliable frequency  $f_{\text{MIN}}$  at which the barrier can be characterised. On the first hand, this stems from the fact that the low-frequency limit of the EN 1793-6 [29] *in situ* insulation method is inversely proportional to the width of the *Adrienne* temporal window. As an indication of the low-frequency limit, the first notch in the magnitude spectrum of the *Adrienne* window is used [96]. On the other hand, the width of the *Adrienne* window depends on the temporal delay between direct sound and diffracted/ground reflected sound. The size of the barrier will affect the temporal delay and, thus, the width of the *Adrienne* window and low-frequency limit  $f_{\text{MIN}}$ . The larger barrier sample, the lower  $f_{\text{MIN}}$ , hence the wider frequency range of  $SI$  is investigated. The influence of the size of the barrier is well explained in [104]. To calculate the

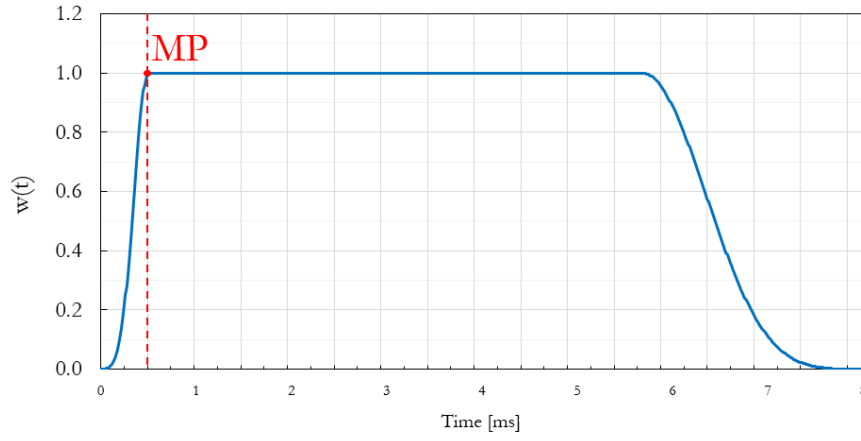


**Figure 37.** *Adrienne* temporal window with length of 7.9 ms, with marker position MP.

width of the *Adrienne* temporal window, the lowest latencies between the diffracted and ground-reflected sound need to be determined relative to the transmitted sound, for all individual microphone positions. To simplify the calculation of the width of the *Adrienne* temporal window, it is assumed in this dissertation that all sound components at three individual microphones in the same row of the microphone grid arrived at the same time.

*Single-number ratings* are calculated in addition to the frequency-dependent *SI* indices defined in (22). The single-number ratings are defined by EN 1793-6 [29] standard and present a standard way of rating the performance of noise barriers. They were introduced because there was a need to categorise the airborne sound insulation performance of noise barriers. In that way, formulation of acoustic requirements in noise barrier specification was simplified. In general, three single-number values are derived: One for acoustic elements, one for posts, and a global rating. A post is defined here as a pillar holding two adjacent acoustic elements together. The single-number rating for barrier elements  $DL_{SI,E}$ , in decibels, is defined as:

$$DL_{SI,E} = -10 \cdot \log \left[ \frac{\sum_{i=m}^{18} 10^{0,1L_i} \cdot 10^{-0,1SI_{E,i}}}{\sum_{i=m}^{18} 10^{0,1L_i}} \right] \quad (23)$$

where  $SI_{E,i}$  is the sound insulation index measured in the  $i^{\text{th}}$  one-third octave band,  $m = 4$  is the number of the lowest reliable one-third octave frequency band, and  $L_i$  is the value of the normalized traffic noise spectrum, defined in EN 1793-3 [105], in the  $i^{\text{th}}$  one-third octave band.

In the same manner, the single-number ratings across posts  $DL_{SI,P}$ , in decibels, is defined as:

$$DL_{SI,P} = -10 \cdot \log \left[ \frac{\sum_{i=m}^{18} 10^{0,1L_i} \cdot 10^{-0,1SI_{P,i}}}{\sum_{i=m}^{18} 10^{0,1L_i}} \right] \quad (24)$$

where  $SI_{P,i}$  is the sound insulation index measured in the  $i^{\text{th}}$  one-third octave band,  $m = 4$  is the number of the lowest reliable one-third octave frequency band, and  $L_i$  is the value of the normalized traffic noise spectrum, defined in EN 1793-3 [105], in the  $i^{\text{th}}$  one-third octave band.

To calculate the global single-number rating for a barrier sample  $DL_{SI,G}$ , a logarithmic average between single-number ratings for the barrier element and the post is calculated according to:

$$DL_{SI,G} = -10 \cdot \log \left[ \frac{10^{-0,1DL_{SI,E}} + 10^{-0,1DL_{SI,P}}}{2} \right] \quad (25)$$

where  $DL_{SI,E}$  is the single-number rating for barrier elements and  $DL_{SI,P}$  is the single-number rating for posts.

In addition to single-number ratings, it is a common practice to categorise the airborne sound insulation performance of a noise barrier. This is done by using categories defined by the EN 1793–6 [29] standard, as listed in Table 13 below. The purpose of categories is further simplification of rating the performance of noise barriers, besides single-number ratings. It is often used in tender documentation, having an important market role in many projects where noise barriers are needed as a protection method.

**Table 13.** Categories of airborne sound insulation according to [29].

Category	Single-number rating [dB]
D0	Not determined
D1	<16
D2	16 to 27
D3	28 to 36
D4	>36

### 5.2.1.2 In Situ measurements of Sound Reflection of Noise Barriers

The measurement of sound reflection is also based on two impulse-response measurements, but for different configurations (see Figure 38). Namely, both loudspeaker and microphone grid are placed on the same side of the sample being tested ( $t_B$ ), at distances  $d_s = 1.5$  m and  $d_M = 0.25$  m from the sample, respectively. The windowing technique in this case is applied in a similar manner as described in Section 5.2.1, but unlike the *SI* measurement, only the ground-reflected sound wave is discarded (see Figure 38b). By comparing the energies of the reflected component of the impulse response taken in front of the sample and the incident component of the free-field impulse responses this method defines a specific quantity called the *reflection index* (*RI*):

$$RI_j(\text{dB}) = \frac{1}{n_j} \sum_{k=1}^{n_j} \left[ \frac{\int_{\Delta f_j} |F[h_{r,k}(t) \cdot w_{r,k}(t)]|^2 df}{\int_{\Delta f_j} |F[h_{i,k}(t) \cdot w_{i,k}(t)]|^2 df} \cdot C_{geo,k} \cdot C_{dir,k}(\Delta f_j) \cdot C_{gain,k}(\Delta f_g) \right] \quad (26)$$

where  $h_{i,k}(t)$  is the incident reference component of the free-field impulse response at the  $k$ -th measurement position,  $h_{r,k}(t)$  is the reflected component of the impulse response taken in front of the sample at the  $k$ -th measurement position,  $w_{i,k}(t)$  and  $w_{r,k}(t)$  are the time windows (*Adrienne* temporal windows) for the free-field and the reflected components, respectively, at the  $k$ -th microphone position,  $F$  denotes the *Fourier transform*,  $j$  is the index of the  $j$ -th one-third octave frequency band,  $n_j$  is the number of microphone positions on which to average ( $n_j \geq 6$ ), and  $\Delta f_j$  is the width of the  $j$ -th one-third octave band frequency band. For the  $k$ -th microphone position,  $C_{geo,k}$  is the correction factor for geometrical divergence and  $C_{dir,k}$  is the correction factor for sound source directivity. Finally,  $C_{gain,k}$  is the correction factor to account for any change in the amplification settings of the loudspeaker and the sensitivity settings of the individual microphones, when the measurement configuration is changed from free-field to in front of the sample or vice versa, with frequency range  $\Delta f_g$  expressed in one-third octave frequency bands between 500 Hz and 2 kHz.

The *signal subtraction technique* [100] is applied to separate a reflected component on each microphone of the grid. The technique disregards direct sound waves from both the free-field and the measurement with the barrier. It is also important to point out that the *RI* index is a quantity different from the sound absorption coefficient obtained by the laboratory method EN 1793–1 [26]. However, these two quantities can be converted into each other, taking the complement to one. Even though the two methods imply different sound fields (directional field in the *in situ* and diffuse field in the laboratory method), there is a certain correlation between them, as described in [30,95,96].

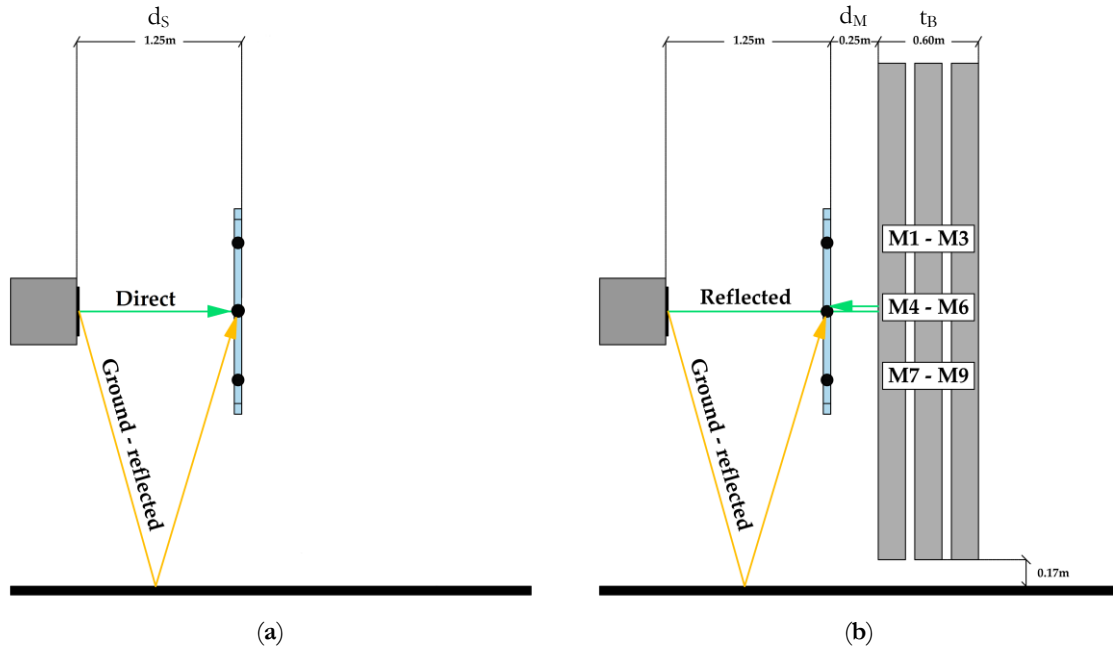


**Figure 38.** Illustration of experimental setup for implementation of standardised EN 1793-5 [28] measurement method at the microphone position M5: (a) without a noise barrier; (b) in the presence of a noise barrier.

As in the case of the sound insulation measurement, a single-number rating  $DL_{RI}$  is delivered in addition to the frequency-dependent  $RI$  indices presented in (26) to indicate the performance of the product. The individual sound reflection indices are weighted according to the normalized traffic noise spectrum defined in EN 1793-3 [105]. The higher single-number rating, the higher reflective properties of the barrier. The single-number rating of sound reflection  $DL_{RI}$ , in decibels, is defined as:

$$DL_{RI} = -10 \cdot \log \left[ \frac{\sum_{i=m}^{18} RI_i \cdot 10^{0,1L_i}}{\sum_{i=m}^{18} 10^{0,1L_i}} \right] \quad (27)$$

where  $RI_i$  is the sound reflection index measured in the  $i^{\text{th}}$  one-third octave band,  $m$  is the number of the lowest reliable one-third octave frequency band, and  $L_i$  is the value of the normalized traffic noise spectrum, defined in EN 1793-3 [105], in the  $i^{\text{th}}$  one-third octave band.

### 5.2.1.3 Calculation of Signal-To-Noise Ratio

According to EN 1793-6 [29] and EN 1793-5 [28], the effective signal-to-noise ratio ( $SNR$ ) should be greater than 10 dB over the frequency range of measurements. The calculation of the effective  $SNR$  is needed to ensure that  $SI$  and  $RI$  measurements are not influenced by the background noise. This is mainly important in cases when measurements are implemented in the presence of the existing traffic noise.

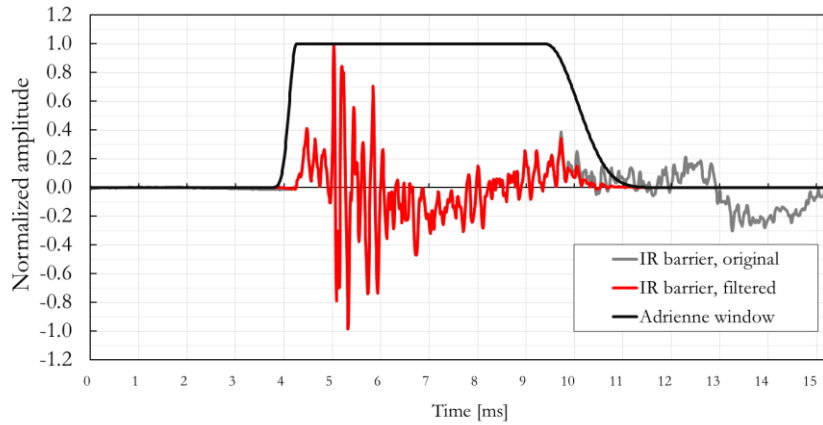
One possible way to calculate  $SNR$  is proposed in [100], where  $SNR$  is calculated according to formula:

$$SNR_{SI,k,j} = 10 \cdot \log \frac{\int_{\Delta f_j} |F[h_k(t) \cdot w_{\text{signal},k(t)}]|^2 df}{\int_{\Delta f_j} |F[h_k(t) \cdot w_{\text{noise},k(t)}]|^2 df} \quad (28)$$

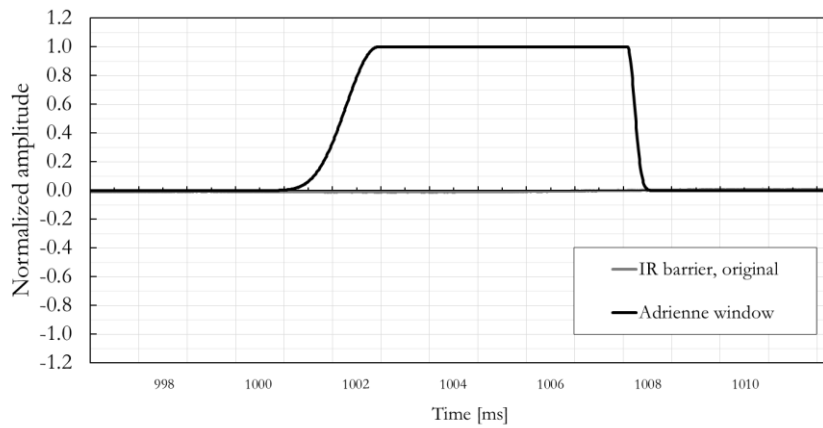
where  $h_k(t)$  is the measured impulse-response at the  $k$ -th microphone position,  $w_{\text{signal},k(t)}$  is the *Adrienne* temporal window used for evaluation of the “signal” segment of the impulse response (identical to that used for evaluation of  $SI$ ),  $w_{\text{noise},k(t)}$  is the *Adrienne* temporal window used for evaluation of the “noise” segment of the impulse response (placed between 0 ms and 3.5 ms),  $F$  denotes the *Fourier*

transform, while index  $j$  denotes the  $j$ -th one-third octave frequency band with bandwidth  $\Delta f_j$ . Finally, the integer  $k$  defines the microphone position ( $k = 1, \dots, 9$ ).

On the one hand, the energy of the “signal” segment of the impulse response in (28) is calculated from the transmitted component (see Figure 39a). On the other hand, it should be noted that the calculation method of  $SNR$  proposed in [100] recommends placement of the *Adrienne* temporal window between 0 ms and 3.5 ms (the moment of arrival of the transmitted component of the impulse response) for calculation of energy of the “noise” segment, which limits the investigated  $SNR$  from one-third octave bands centred at 400 Hz. In order to improve the low-frequency limit, another calculation method is presented in [101]. Here, the “noise” segment is taken from the impulse response tail (see Figure 39b). In this case, the length of the *Adrienne* temporal window is same as in  $SI$  and  $SNR$  evaluation, making the investigated frequency range same.



(a)



(b)

**Figure 39.** Application of signal-to-noise ratio ( $SNR$ ) calculation for  $SI$  measurements presented in [101] for: (a) “signal”, and (b) “noise” segment of the impulse response.

Calculation of the effective  $SNR$  according to (28) is done for each one-third octave frequency band at individual microphone positions. However,  $SNR$  could be calculated as a single-number for each microphone position just by applying summation in the whole frequency range instead of in each one-third octave frequency band. Additionally, a single-number value of  $SNR$  for the whole measurement can be calculated as logarithmic average of single-numbers.

While the effective  $SNR$  in  $SI$  measurements is influenced by the low magnitude of transmitted sound components in case of highly insulating noise barriers,  $SNR$  in  $RI$  measurements is influenced by the low magnitude of the reflected sound components in case of highly absorptive noise barriers. The energy of the “signal” segment of the impulse response in  $RI$  measurements is calculated from the

reflected component (see Figure 40), while the energy of the “noise” segment is taken from the impulse response tail in a same manner as in case of *SI* measurements.

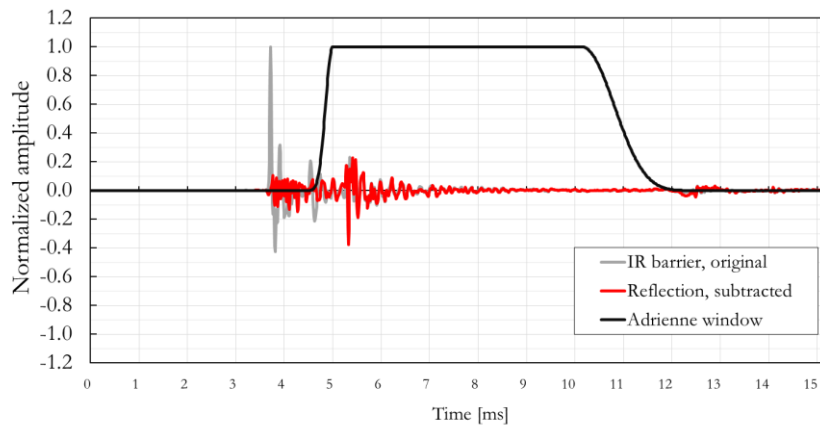


**Figure 40.** Application of signal-to-noise ratio (*SNR*) calculation for *RI* measurements for “signal” segment of the subtracted signal.

## 5.2.2 Laboratory Measurement Methods

European standards *EN 1793–2* [27] and *EN 1793–1* [26] specify laboratory measurement methods for qualifying the intrinsic sound insulation and absorption performance, respectively, of road traffic noise-reducing devices to be used in reverberant conditions. While *in situ* methods described in the previous section are used to determine intrinsic characteristics for noise reducing devices to be installed on roads in non-reverberant conditions, the laboratory methods are used for noise reducing devices to be installed e.g., inside tunnels, deep trenches and under covers. Both methods are in accordance with the previous versions *ISO 140–3* [83] and *ISO 354* [84]. The main principles of the methods are explained below.

### 5.2.2.1 Laboratory Measurement of Airborne Sound Insulation of Noise Barriers

Averaged sound pressure levels in two adjacent rooms, called the *source room* and the *receiving room*, are the basis of the laboratory airborne sound insulation method. The rooms are separated by an opening where the test specimen is inserted. The test specimen should be mounted in the same manner as it is used in practice. In other words, same connections and seals between element components are employed. The leakage of sound on flanking paths is suppressed by using edge supports. At least one post connecting two adjacent panels is included, where posts are used in practice. The length of the panel on one side of the post must be at least 2 m long. The side of the panel facing the traffic should face the source room.

A loudspeaker in the source room is used to produce a continuous broadband excitation signal. At least two loudspeaker positions are recommended. For each loudspeaker positions, sound pressure levels at minimum five measurement positions are measured in both the source and the receiving room. Finally, average sound pressure levels in both rooms are obtained and a specific quantity called the *sound reduction index*, *R*, is evaluated from:

$$R(\text{dB}) = L_{p,1,j} - L_{p,2,j} + 10 \cdot \log \frac{S}{A_j} \quad (29)$$

where  $L_{p,1,j}$  is the average sound pressure level in the source room (dB),  $L_{p,2,j}$  is the average sound pressure level in the receiving room (dB),  $S$  is the area of the test specimen ( $\text{m}^2$ ),  $A_j$  is the equivalent absorption area in the receiving room ( $\text{m}^2$ ) and index  $j$  denotes the  $j$ -th one-third octave frequency band from 100 Hz to 5000 Hz.

A single-number rating,  $DL_R$ , is calculated in addition to frequency-dependent noise reduction indices in order to indicate the performance of the test element:

$$DL_R = -10 \cdot \log \left| \frac{\sum_{i=1}^{18} 10^{0,1L_i} \cdot 10^{-0,1R_i}}{\sum_{i=1}^{18} 10^{0,1L_i}} \right| \quad (30)$$

where  $R_i$  is the sound reduction index measured in the  $i^{\text{th}}$  one-third octave band, and  $L_i$  is the value of the normalized traffic noise spectrum, defined in EN 1793-3 [105], in the  $i^{\text{th}}$  one-third octave band.

The single-number rating of airborne sound insulation is investigated after being rounded to the nearest integer. In addition to the single-number rating, sound insulation performance is categorised by using categories listed in Table 14 below. This is done from the same reasons as stated in Section 5.2.1.1.

**Table 14.** Categories of airborne sound insulation [27].

Category	$DL_R$ [dB]
B0	Not determined
B1	<15
B2	15 to 24
B3	25 to 34
B4	>34

#### 5.2.2.2 Laboratory measurements of Sound Absorption of Noise Barriers

Two measurements of average reverberation times, with and without the test specimen, are the basis of the laboratory sound absorption measurement. The measurements are performed in a reverberation room, which closely approximates a diffuse sound field condition. Hence, sound-absorbing characteristic of the specimen is obtained as average over all angles of incidence i.e., at random incidence. A specific quantity called the *sound absorption index*,  $\alpha_s$ , is evaluated from:

$$\alpha_s = \frac{A_T}{S} \quad (31)$$

$$A_T = 55.3V \left( \frac{1}{c_2 T_2} - \frac{1}{c_1 T_1} \right) - 4V(m_2 - m_1) \quad (32)$$

where  $A_T$  is the equivalent sound absorption area of the test specimen ( $\text{m}^2$ ),  $S$  is the area of the test specimen ( $\text{m}^2$ ),  $c_1$  and  $c_2$  are the propagation speeds of sound in air at the temperature  $t_1$  and  $t_2$ , respectively,  $T_1$  and  $T_2$  are the mean reverberation times of the room in each frequency band without and with the test specimen, respectively,  $V$  is the volume of the empty reverberation room ( $\text{m}^3$ ), and  $m_1$  and  $m_2$  are the power attenuation coefficients calculated according to ISO 9613-1 [106] using the climatic conditions that have been present in the empty reverberation room during the measurements. The sound absorption index  $\alpha_s$  is presented in one-third octave frequency bands from 100 Hz to 5000 Hz. Accurate measurements in lower one-third octave frequency bands, below 100 Hz, are difficult due to modal density of the reverberation room.

Reverberation time is calculated by using either *direct method* or *indirect method*. The direct method i.e., the interrupted noise method, is result of a statistical process and several decay curves are averaged at one microphone/loudspeaker position. In contrary, indirect method i.e., the integrated impulse response method, is not prone to statistical deviations and hence no averaging is needed. The total number of spatially independent decay curves should be at least 12, which is obtained by using at least three microphone and two loudspeaker positions.

## 5.3 Experimental Setup

The measuring equipment used to carry out both airborne sound insulation and sound reflection measurements consisted of a *Roland Studio-Capture* multichannel sound card, *Mackie SRM150* single driver loudspeaker, and nine *NTI Audio M4261* microphones supported by a custom-made aluminium frame. The measuring platform *EASERA* (AFMG, Berlin, Germany) was used for both excitation and data acquisition. The *MATLAB* (The MathWorks, Inc, Natick, Massachusetts, USA) computing environment was employed for evaluation purposes. Car battery was used as power supply in case where no electricity was available.

Measurements were performed by using logarithmic sine sweep excitation signals with a length of 5.5 s. Each impulse response was recorded by averaging three consecutive measurements. In order to record as good quality of impulse responses as possible, the highest sampling frequency of 96 000 Hz supported by the sound card was used.

Measurement procedures described in [Section 5.2.1](#) are based on ratios of power spectra obtained from impulse responses measured under same conditions and with same equipment for individual noise barriers. Therefore, high accuracy measurement equipment is not needed. However, according to EN 1793-6 [29] and EN 1793-5 [28] measurement standards, sound source should consist of a single loudspeaker driver, have a smooth magnitude of the frequency response throughout the measurement frequency range and impulse response with a length not greater than 3 ms. In order to check these requirements, free-field measurement was performed. Results are shown in [Figure 41](#) below.

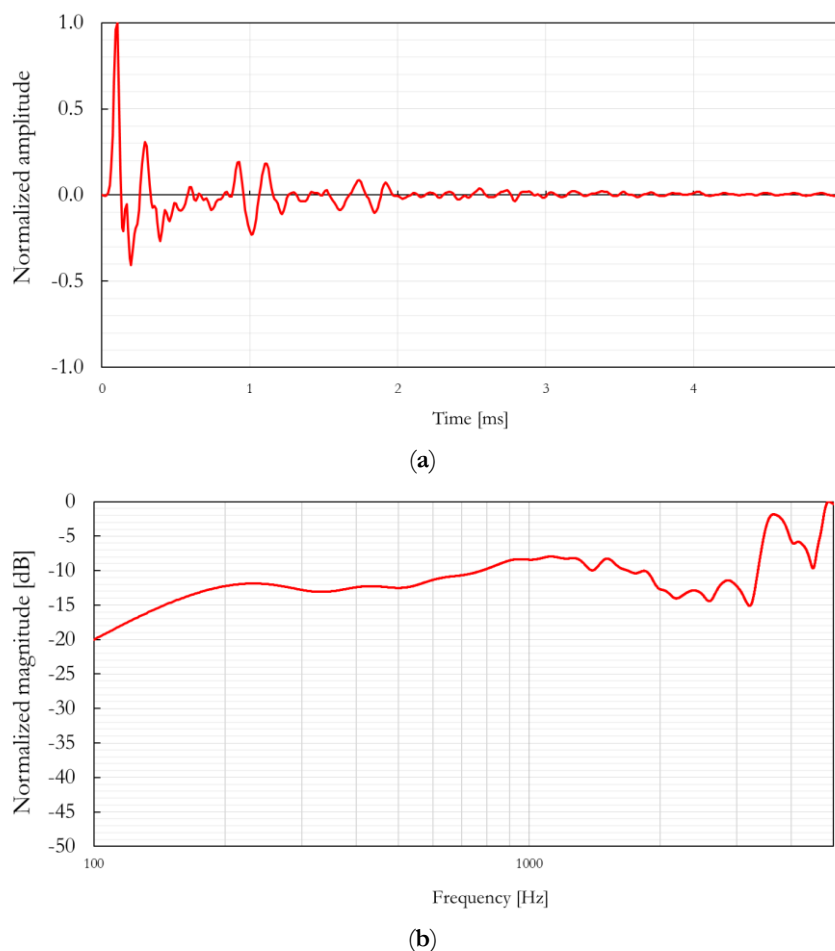


**Figure 41.** Characteristics of sound source measured under free-field conditions: (a) impulse response; (b) magnitude of frequency response in the measurement frequency range (100 Hz – 5000 Hz).

### 5.3.1 Conventional Noise Barrier

#### 5.3.1.1 Outdoor installation

A barrier system which consisted of two different sections, one made of an absorptive (only the side towards the railway is sound absorbing) and the other one of a reflective transparent polyacrylic panel, was installed in 2014 along the railway near Knivsta station in Knivsta, Sweden. The barrier was 720 m long. The focus in this dissertation was just on the absorptive section of the barrier, while detailed description and results of the characterisation of the transparent polyacrylic panel is presented in [107].

The absorptive barrier panel was made in aluminium, coated with polyester-powder and filled with mineral wool, see the cross section of the panel in Figure 42. A 40 mm thick mineral wool layer was inserted in the 1.3 mm thick aluminium frame, with 15 mm air gap at the front and 65 mm air gap at the back. Therefore, the total thickness of the panel was 122.6 mm. Front side of the panel was perforated enabling noise to interact with the mineral wool, while the back side was non perforated. A barrier element was made by assembling eight panels with height of 0.5 m and width of 3.96 m on top of each other. Hence, the total size of the barrier element was approx. 4 × 4 m. However, due to uneven ground on-site, measured height was 3.75 m, making the total size of the barrier element slightly lower. The elements were separated from each other by steel posts.

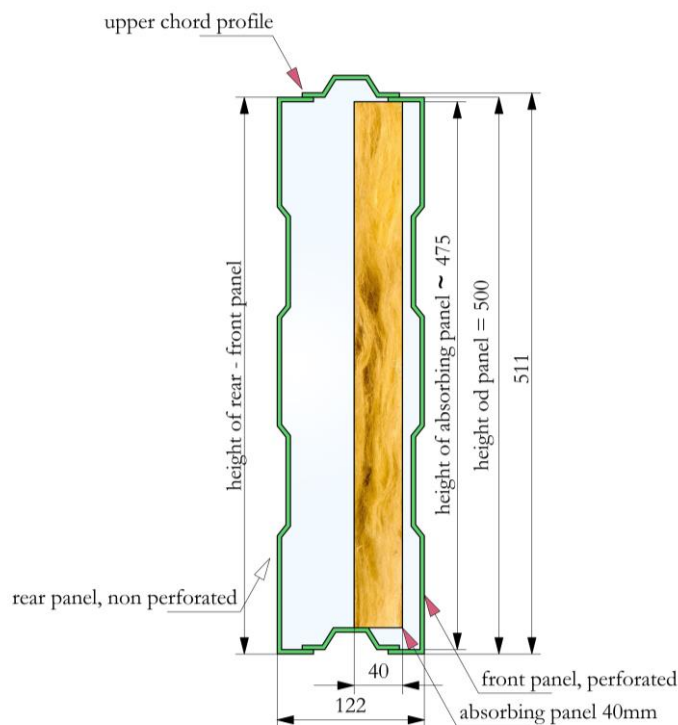


Figure 42. Section and perforation type of the absorptive panel installed in Knivsta, Sweden.

As described in Section 5.2.1, EN 1793-6 [29] and EN 1793-5 [28] measurement methods were used in order to determine *in situ* sound insulation and sound reflection properties of the barrier element. For the given size of the barrier element, calculated low-frequency limits were  $f_{\text{MIN,SI}} = 191$  Hz and  $f_{\text{MIN,RI}} = 180$  Hz. Hence, the results of the standardised *in situ* characterisation were investigated in one-third octave bands, starting from the one with central frequency of 250 Hz, for both sound insulation and sound reflection measurements. The values in lower one-third octave bands were retained for presentation purposes, as recommended by the *in situ* measurement methods.

The results for airborne sound insulation measurement were investigated for two configurations, in front of the panel and in front of the post, as shown in Figure 43. In the former, the middle column



(a)

(b)

**Figure 43.** Measurement setup in case of the absorptive barrier for two different configurations: (a) In front of panel; (b) In front of post.

of microphone grid faced the centre of the panel, whereas in the latter, it faced a centre of the post. The results of sound reflection measurements were investigated just in front of the panel. Both loudspeaker and central microphone (M5) were placed at height of approx. 1.88 m.

### 5.3.1.2 Laboratory Installation

Acoustic properties of the barrier element consisting of identical panels, as described in the previous section, was also measured and evaluated under the laboratory conditions. Sound insulation and sound absorption measurements were implemented according to ISO 140–3 [83] and ISO 354 [84], as described in Section 5.2.2. The measurements were performed on a test element consisting of twelve panels, with a total size of  $3.94 \times 2.99$  m. A post, arranged asymmetrically, was used to separate two sections of the test sample. Dimensions of the sections were  $1.545 \times 0.5$  m and  $2.46 \times 0.5$  m, with respective masses 11.6 kg and 19.0 kg. The test assembly in the wall test stand is shown in Figure 44. The cross section of the panel was same as shown in Figure 42.

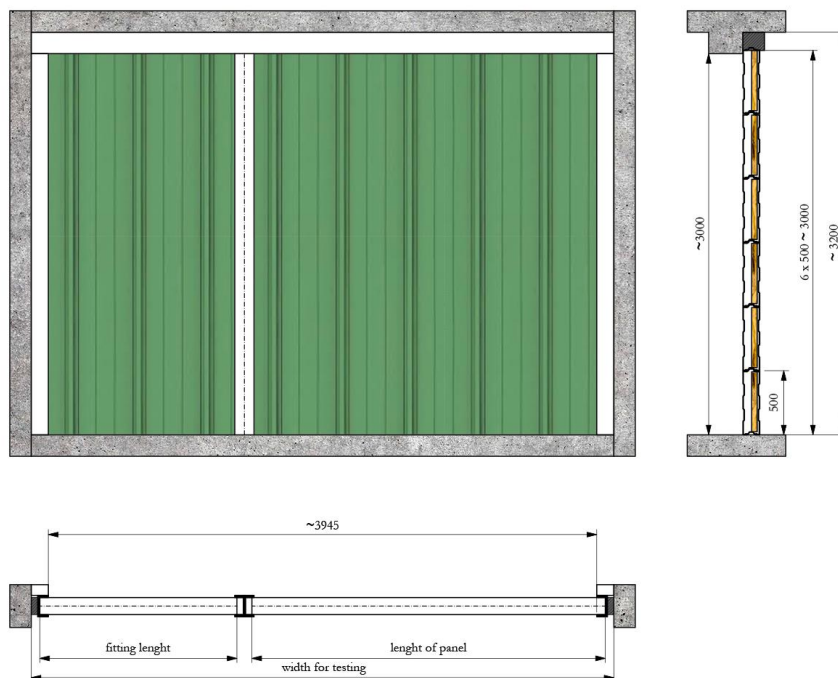


**Figure 44.** Laboratory test element of the absorptive barrier in the wall test stand.

### 5.3.2 Sonic Crystal

The SC barrier, which is shown in Figure 45a, was made of a total of three rows, each having 30 cylindrical units with a height of 3 m and an external radius of 8 cm. The lattice period was 0.22 m and the corresponding filling fraction of the scatterers was 41.5%. The actual size of the barrier sample was  $6.54 \times 0.6 \times 3$  m. The cylinders were placed on a metal base, which was located at about 0.17 m from the ground. Given the value of the lattice period, the *Bragg band gap* was expected to be centred at approx. 780 Hz, where the lattice period equals one-half wavelength. Keeping in mind that results of characterisation were shown in one-third octave bands, Bragg band gap were expected in one-third octave band with a central frequency of 800 Hz.

Figure 45b shows the internal cross-section of the upgraded cylindrical building units comprised of rubber crumb as the porous core and an MP aluminium shell as the outer layer. The porous core consisted of rubber crumb inserted into a perforated steel cylinder with a radius of 4 cm and a thickness of 1 mm. The diameter of the perforations on the steel cylinder was 3 mm and the cylinder perforation ratio was 32.6%, making the cylinder acoustically transparent [76]. Thus, it allowed sound to interact with the rubber crumb. The purpose of the inner core was to dissipate high-frequency components of the acoustic energy penetrating the micro-perforations of the external aluminium shell.

The outer MP layer was made of an aluminium plate with a thickness of 1 mm and a perforation ratio of 3.3%. Since the micro-perforations were punched, the resulting pore geometry was complex. However, according to research with similar plates [108], the perforations of the MP layer can be modelled as rectangular apertures with an effective length of 1.11 mm and effective width of 95  $\mu\text{m}$ . Characterisation of this type of MP plates in an impedance tube revealed broadband reflection and absorption spectra [72].

For the given size of the SC barrier, the calculated low-frequency limit was  $f_{\text{MIN}} = 259$  Hz. Hence, the results of the standardised characterisation were presented in one-third octave bands, starting from a central frequency of 315 Hz. The values in the lower one-third octave bands were retained for presentation purposes, as recommended by the EN 1793-6 [29] and EN 1793-5 [28] standards. The results for both reflection and airborne sound insulation measurements have been investigated for the two configurations represented in Figure 46. In configuration A, the middle column of microphone grid faced the centre of a cylinder, whereas in configuration B, it faced a space between two adjacent cylinders. Considering the distance of 0.4 m between microphones in the microphone grid and the lattice parameter of 0.22 m, the spacing between the microphones was not a multiple of the lattice constant.



**Figure 45.** Sonic crystal (SC) barrier sample implemented on the campus of Universitat Politècnica de València: (a) Appearance of SC barrier sample made of three rows of absorbing cylindrical units, along with experimental setup; (b) internal cross-section of a cylindrical unit, consisting of a porous core made of rubber crumb and outer micro-perforated aluminium shell [34].

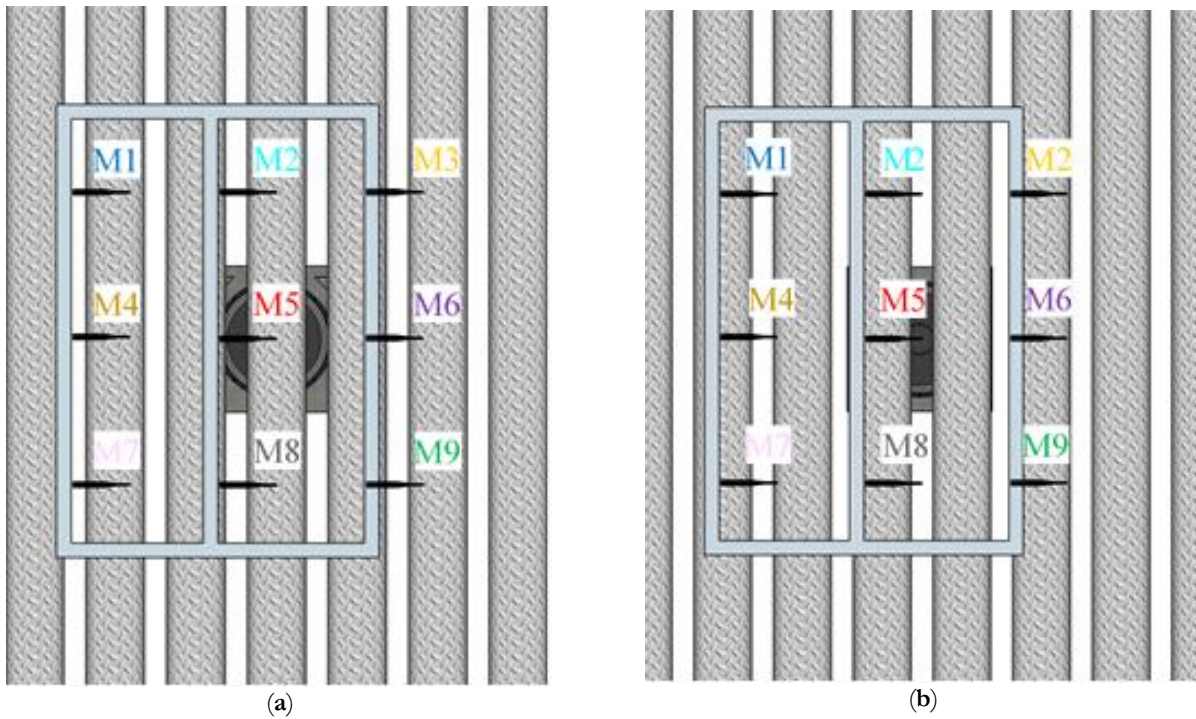


**Figure 46.** Positions of the microphone grid in two different configurations: (a) Configuration A, the middle column of microphones faces the centre of the cylinders; (b) configuration B, the middle column of microphone grid faces the centre of the space between two adjacent cylinders [34].

## 5.4 Experimental Results and Discussions

In this section, results of implementation of the *in situ* measurement methods explained in Section 5.2.1 have been presented. First, the *in situ* measurements have been applied to conventional noise barrier explained in Section 5.3.1.1. The results of the *in situ* measurements have been compared to results of application of the laboratory measurements (Section 5.2.2) to identical barrier element (Section 5.3.1.2). The results from the laboratory measurements have been obtained from the manufacturer. Second, the *in situ* measurements have been applied to *sonic crystal* (SC) barrier explained in Section 5.3.2. These results have been compared to results from SCs investigated by another author [33].

### 5.4.1 Conventional Noise Barrier

As explained in Section 5.1, a correlation between laboratory and *in situ* measurements exists, although sound fields are different. For comparison purposes, results from laboratory measurements were compared with those obtained *in situ*. Since *in situ* and laboratory measurements were calculated for different frequency ranges, 250–5000 Hz and 100–5000 Hz respectively, frequency range used in laboratory measurements was reduced in order to match that in the *in situ* measurement, and single-number ratings were recalculated.

#### 5.4.1.1 Sound Insulation

The results of the standardised EN 1793–6 [29] measurement of sound insulation indices  $SI$  for the absorptive barrier element described in the Section 5.3.1.1, computed according to (22), are shown in Figure 47. Results are presented for two configurations, in front of the post and in front of the barrier element, as shown in Figure 43. Additionally, results of corresponding laboratory measurement of the identical barrier sample (see Section 5.3.1.2) are added for comparison purposes. It should be kept in mind that sound insulation indices  $SI$  shown in Figure 47 were result of averaging over nine microphones. In order to investigate possible areas on the barrier where leakage has occurred, more detailed investigation is presented later in this section.

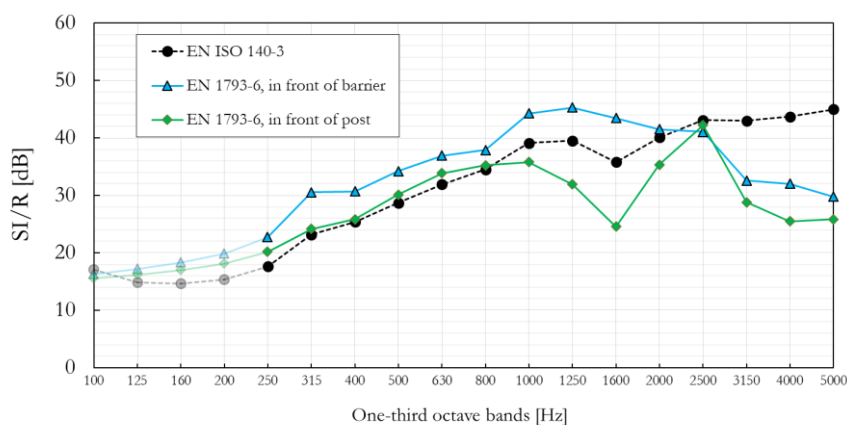
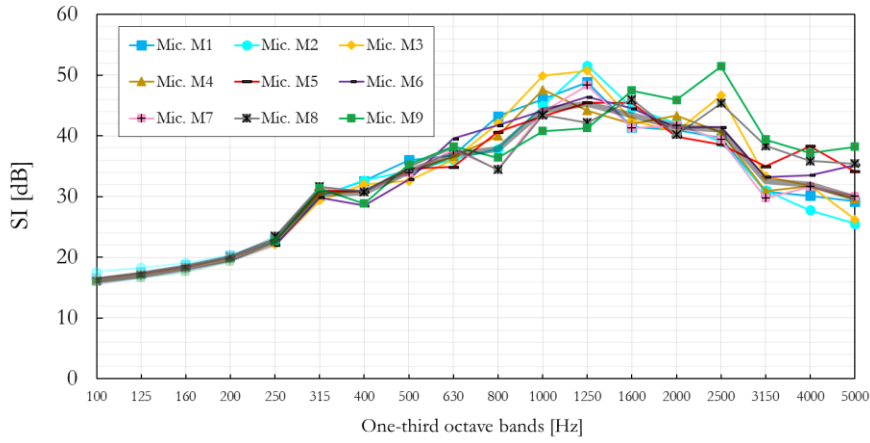


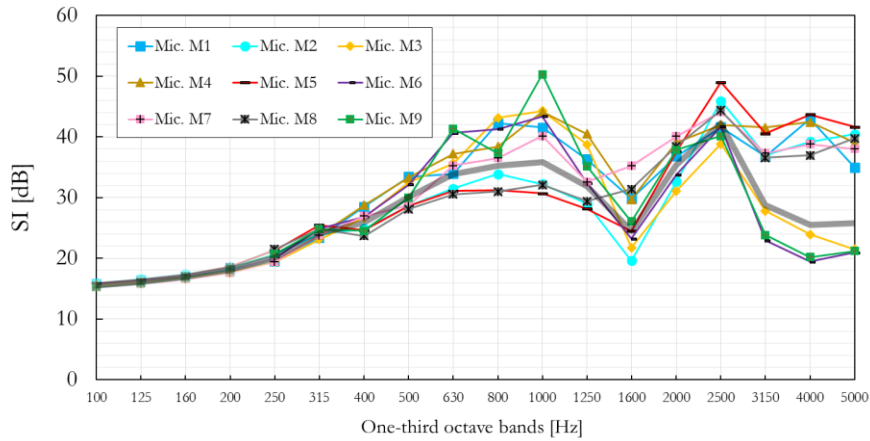
**Figure 47.** Sound insulation index ( $SI$ ) of the absorptive noise barrier measured in two different configurations. Results are compared with laboratory measurement of the identical barrier sample. Sound insulation indices  $SI$  are result of averaging over nine microphones.

The maximum  $SI$  value measured in front of the barrier element was 45.3 dB at 1250 Hz, while the maximum  $SI$  value measured in front of the post was 42.2 dB at 2500 Hz. Values of sound insulation indices  $SI$  measured in front of the post were lower than values measured in front of the barrier element in almost whole measurement frequency range. The only exception was one-third octave band centred at 2500 Hz, where  $SI$  index of the post had a slightly higher value. According to results obtained from a range of noise barriers investigated in [30], a tendency for lower  $SI$  values in front of posts was observed in many cases, especially at high frequencies. Although the difference at high frequencies between two configurations in Figure 47 existed, it was not significant compared to differences at other frequencies. The reason was that the barrier elements themselves were made of joint panels and allowed for leakage at high frequencies due to imperfect connections between them. In general, those imperfections are mostly characteristic of connections between barrier elements and posts. In the same research [30], authors emphasized the importance of workmanship, design of connections and efficient sealing in order to avoid a potential leakage. They also stated that laboratory measurements are more similar to *in situ* measurements in front of posts, which was also the case with the absorptive barrier element presented in this dissertation. Namely, two curves had identical values except in two frequency ranges, 1000–2000 Hz and 3150–5000 Hz. This is believed to be due to a leakage, where the former refers to a leakage caused by the presence of the post and the latter to a leakage in connections between different panels. It was also noticeable that drop in the  $SI$  curve at 1600 Hz was more pronounced in *in situ* measurements but prevailed in both laboratory and *in situ* measurements. This was somehow expected since laboratory test samples are usually assembled with more attention than those *in situ*. A drop in the  $SI$  curve in frequency range 3150–5000 Hz supported the last statement.

In order to further investigate leakage between different panels of the barrier element and in element/post connection, Figure 48 shows values of sound insulation indices  $SI$  measured at individual microphone positions for both configurations. Values of sound insulation indices  $SI$  measured in front of the barrier element (Figure 48a) did not differ significantly between different microphones. However, expected increment of  $SI$  values with frequency was not visible at high frequencies, which indicated a potential leakage between panels forming the barrier element. Strong position-dependent characteristics of the EN 1793–6 [29] *in situ* measurement method was more obvious in front of the post (Figure 48b). This was especially pronounced at high frequencies, where three microphones (M3, M6 and M9) showed a significant drop in sound insulation properties of the barrier element compared to other microphones. Although problems in element/post connections were not discovered by visual inspection, asymmetrical drop in sound insulation properties indicated a leakage at one side of the post. This undesirable effect was somehow expected since posts are often marked as weak positions for most noise barriers. Impulse responses at individual microphone positions M1–M9 for configuration A and B are presented in Figure A.5 and Figure A.6 (see Appendix C), respectively. Maximum values of the free-field impulse responses are normalised to 1.



(a)



(b)

**Figure 48.** Sound reflection index ( $RI$ ) of the absorptive noise barrier measured at individual microphone positions M1–M9. Thick black curve shows the averaged  $SI$  values over all nine microphones. (a) Sound insulation index  $SI$  in front of barrier element; (b) Sound insulation index  $SI$  in front of post.

Single-number rating of EN 1793–2 [27] laboratory measurement of airborne sound insulation properties was  $DL_{R,100-5000 \text{ Hz}} = 25 \text{ dB}$ . To compare this result with the result of *in situ* measurement, the single-number rating was recalculated for the frequency range 250–5000 Hz. The new single-number rating was  $DL_{R,250-5000 \text{ Hz}} = 27.3 \text{ dB}$ . Finally, single-number ratings of EN 1793–6 [29] *in situ* measurements for two configurations, in front of a post and in front of a barrier element, were  $DL_{SI,250-5000 \text{ Hz}} = 27.5 \text{ dB}$  and  $DL_{SI,250-5000 \text{ Hz}} = 31.9 \text{ dB}$ , respectively.

#### 5.4.1.2 Sound Reflection

The results of the standardised EN 1793–5 [28] measurements of sound reflection indices  $RI$  for the absorptive barrier element described in the Section 5.3.1.1, calculated according to (26), are shown in Figure 49. Unlike results of sound insulation measurements presented in the previous section, results of sound reflection measurements are presented only for configuration in front of a barrier element, see Figure 43a. In general, sound reflection properties for configurations in front of posts are not of interest. As in case of sound insulation measurements, sound reflection indices  $RI$  presented in Figure 49 were results of averaging over nine microphones. Additionally, results were averaged over six microphones in order to be presented in extended frequency range. In order to investigate reflection properties for different incident angles, investigation of  $RI$  at individual microphone positions is presented later in this section.

The measurements of  $RI$  evaluated by averaging over six and nine microphones were identical. Therefore, discussions have been made only for the latter case, while results for the former case were

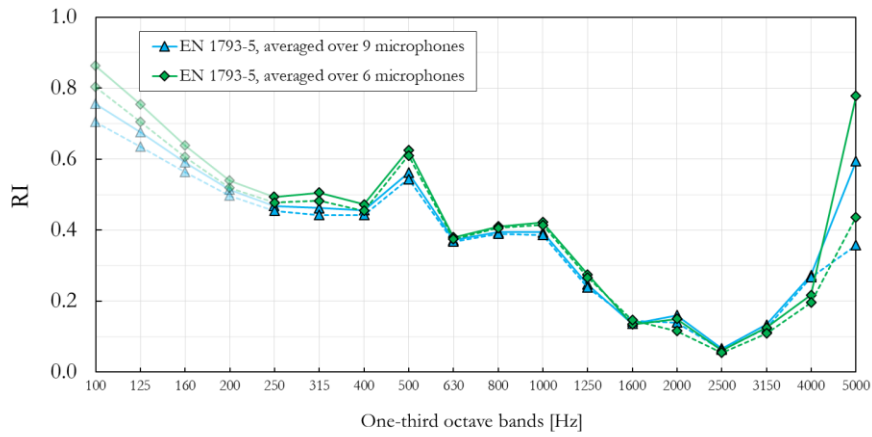


Figure 49. Sound reflection index ( $RI$ ) of the absorptive noise barrier measured in front of barrier element.

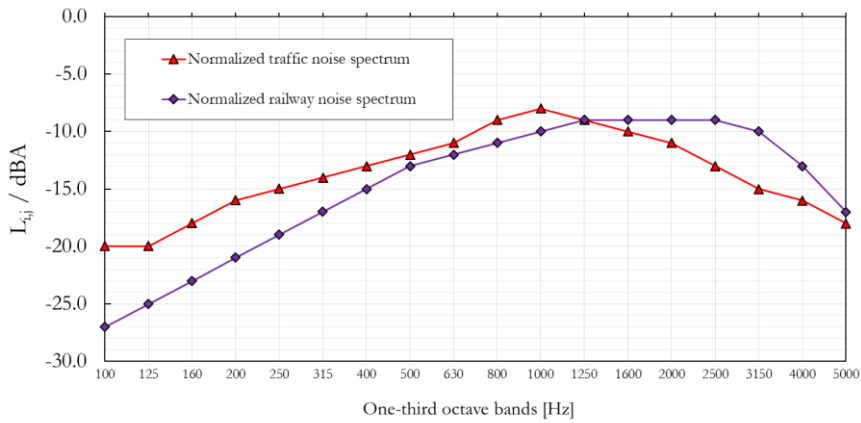
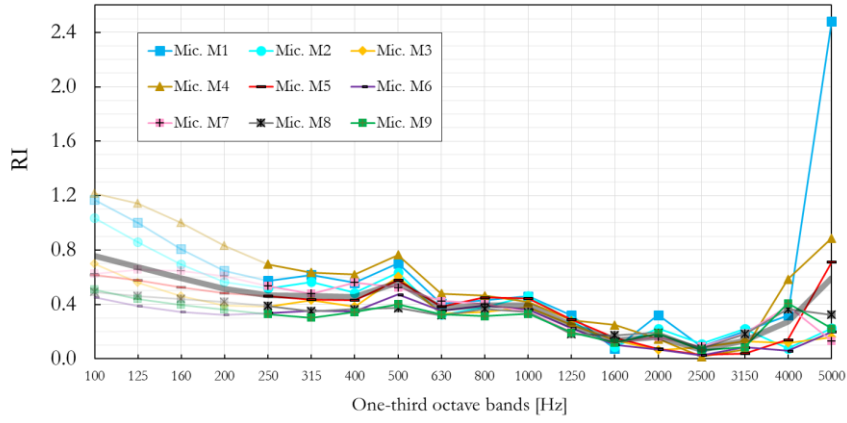


Figure 50. Normalized traffic and railway noise spectrum according to EN 1793-3 [105] and EN 16272-3-2 [109], respectively. Spectra are A-weighted and normalized to 0 dB.

kept for presentation purposes. The minimum measured  $RI$  value was 0.07 at 2500 Hz. This was exactly at the frequency where normalized railway noise spectrum shows a maximum value, see Figure 50. The result justified efficiency of the barrier, which had been designed to be efficient against a railway noise. Normalized traffic spectrum in Figure 50 is presented just for comparison purposes.

In order to investigate sound reflection for different incident angles, Figure 51 shows values of  $RI$  measured at individual microphone positions. Values of  $RI$  measured in front of the barrier element varied between different microphones, but curves showed a similar trend. This trend was observed in almost all one-third octaves band, except in those with central frequencies of 4000 Hz and 5000 Hz. However, deviations at high frequencies were not unusual having in mind different incident angles. Value of sound reflection index  $RI$  in one-third octave band centred at 5000 Hz at microphone position M1 was unusually high, probably due to wrong data acquisition. Therefore, results in Figure 49 were recalculated without microphone M1 and presented with intersected curves. Impulse responses at individual microphone positions M1–M9 for configuration A and B are presented in Figure A.7 (see Appendix C). Maximum values of the free-field impulse responses are normalised to 1.

Results of comparison between *in situ* and laboratory measurements of identical barrier samples (see Section 5.3.1.1 and Section 5.3.1.2) are shown in Figure 52. While EN 1793-5 [28] *in situ* measurements give information about sound reflection index  $RI$ , traditional ISO 354 [84] laboratory measurements give information about conventional sound absorption coefficient  $\alpha_s$ . In order to compare them, sound reflection indices were converted to conventional sound absorption coefficients by taking the complement to one. Absorption coefficients obtained under laboratory conditions were higher than those from *in situ* measurement in the whole frequency range, except at 2500 Hz where curves approached



**Figure 51.** Sound reflection index ( $RI$ ) of the absorptive noise barrier measured at individual microphone positions M1–M9 in front of the barrier element. Thick black curve shows averaged  $RI$  values over all nine microphones.

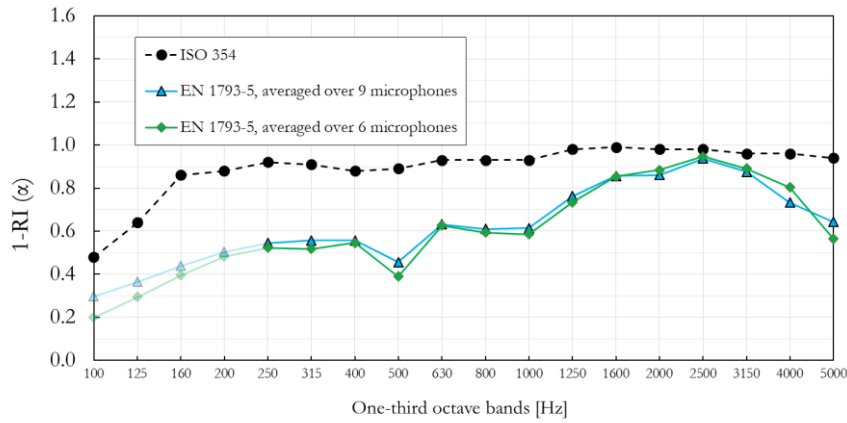


**Figure 52.** Sound absorption of the absorptive noise barrier. Results are compared with laboratory measurement of the identical barrier sample.

each other. The differences between laboratory and *in situ* measurements occurred due to three reasons. First, diffuse sound field in case of the laboratory measurement differs significantly from directional sound field in case of the *in situ* measurement. Second, sampling and averaging of the sound field for two measurements are different. Finally, the steady state excitation signal in case of laboratory measurement differs from the excitation signal used in case of the *in situ* measurement.

Single-number rating of the ISO 354 [84] laboratory measurement of sound absorption properties was  $DL_{\alpha,100-5000 \text{ Hz}} = 12 \text{ dB}$ . To match the frequency range of *in situ* measurement, the single-number rating was recalculated for the frequency range 250–5000 Hz. The new single-number rating was  $DL_{\alpha,250-5000 \text{ Hz}} = 13 \text{ dB}$ . Single-number ratings of the EN 1793-5 [28] *in situ* measurement averaged over nine and six microphones were  $DL_{RI,250-5000 \text{ Hz}} = 5.1 \text{ dB}$  and  $DL_{RI,250-5000 \text{ Hz}} = 4.9 \text{ dB}$ , respectively. However, in order to compare it with the result of laboratory measurements, single-number ratings were recalculated for sound absorption values shown in Figure 52. The recalculated single-number rating of sound absorption  $DL_{\alpha,250-5000 \text{ Hz}} = 5 \text{ dB}$  was same when averaged over nine and six microphones.

#### 5.4.1.3 Signal-To-Noise Ratio

The results of the effective  $SNR$  for  $SI$  measurements, calculated according to (28), are presented in Figure 53. The calculations were done for individual microphone positions. The effective  $SNR$  calculation method presented in [101] was employed. This calculation method takes an advantage over the calculation method presented in [100], because of the extended frequency range in which the results are investigated (see Section 5.2.1.3).

The results in Figure 53 are presented for  $SI$  measurements in the presence of the barrier. Although the sound transmission through the barrier was attenuated by the barrier itself,  $SNR$  values were still high. This stems from the fact that measurements were performed between train passages i.e., when the background noise was low.

The results of the effective  $SNR$  for  $RI$  measurement are presented in Figure 54. As in case for  $SI$  measurement,  $SNR$  values were high and even more consistent between different microphone positions. As explained in Section 5.2.1.3, the effective  $SNR$  was calculated for reflected sound components. This case was more critical compared to  $SNR$  calculated for direct sound component, since reflection from the barrier was significantly attenuated.

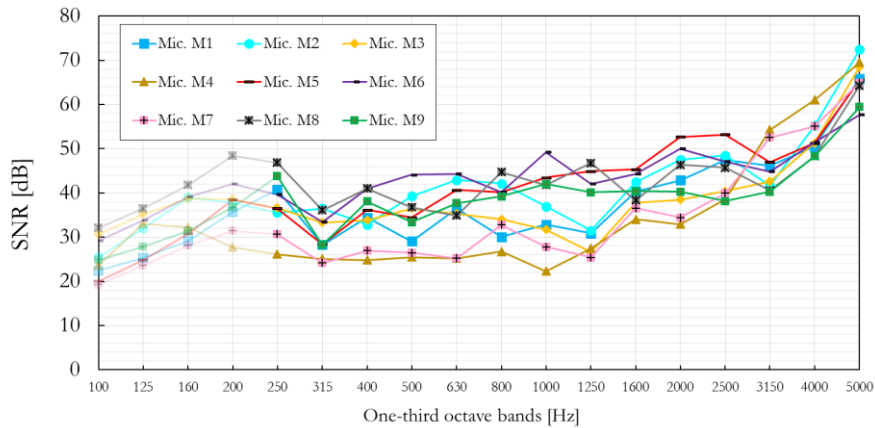


Figure 53. Frequency-dependant signal-to-noise ratio ( $SNR$ ) of the absorptive noise barrier measured at individual microphone positions M1–M9 for  $SI$  measurement.

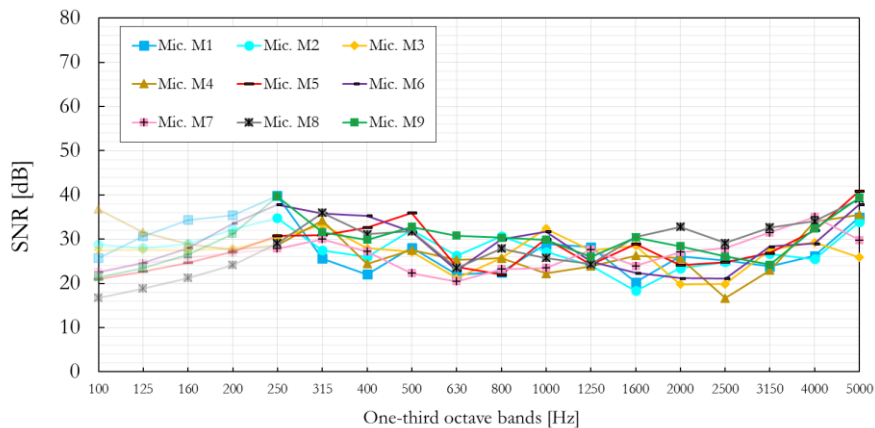


Figure 54. Frequency-dependant signal-to-noise ratio ( $SNR$ ) of the absorptive noise barrier measured at individual microphone positions M1–M9 for  $RI$  measurement.

### 5.4.2 Sonic Crystal

A *sonic crystal* (SC) noise barrier consisting of a square distribution of empty micro-perforated (MP) cylindrical shells was constructed and characterised by researchers of Universitat Politècnica de València (UPV) in 2011 [72]. The building units of the barrier investigated in this dissertation are slightly different to those employed in [72], but their space arrangement remained the same (see Section 5.3.2). Namely, the barrier presented in [72] consisted of empty MP cylindrical shells, while the barrier presented in this dissertation consisted of MP cylindrical shells and additional inner core filled with rubber crumb. To better quantify the effects of micro-perforations on the barrier performance, measured data were compared with those resulting from the standardised characterisation of the SC barrier made of three rows of rigid polyvinyl chloride (PVC) cylinders [33]. The results presented in this section are published in [34].

### 5.4.2.1 Acoustic Bands

In order to better understand phenomena behind SC barriers, a single unit cell was modelled in *COMSOL Multiphysics* (The COMSOL Group, Stockholm, Sweden) and band diagram of a square lattice of rigid cylinders was computed (see Figure 55). This cell comprises a single cylinder in a squared domain of air whose dimension was defined by the lattice constant. *Floquet conditions* were configured on the four external boundaries of the unit cell and an eigenfrequency analysis was performed at wave vectors contained along the principal directions in the lattice.

The dark and light grey stripes in Figure 55 define complete and partial band gaps, respectively. The first complete band gap covers the frequency region of 850–970 Hz while the second covers the interval from 2890 Hz to 2965 Hz. In addition to the complete band gaps, four partial band gaps or pseudo gaps appear along the direction  $\Gamma X$ . This is the preferred direction for efficient acoustic barrier design, as implemented in [71–77].

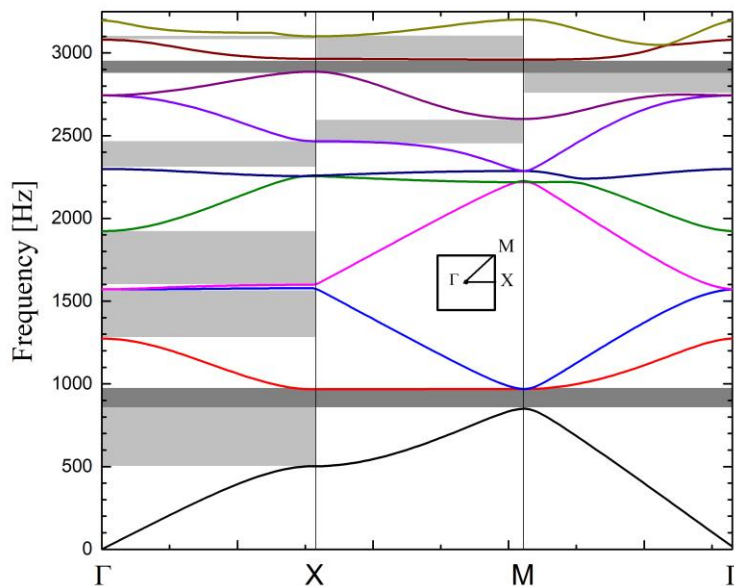


**Figure 55.** Acoustic bands of a square lattice of rigid cylinders embedded in air [34]. Dark stripes indicate complete band gaps and light grey stripes define the partial gaps. The inset plots the reciprocal lattice together with high symmetry positions that define the irreducible region.

### 5.4.2.2 Sound Insulation

The results of the standardised EN 1793–6 [29] measurements of sound insulation indices  $SI$  for the SC barrier with absorptive MP cylinders described in Section 5.3.2, computed according to (22), are shown in Figure 56. Results are presented for both configuration A and configuration B, as explained in Figure 46. The  $SI$  peak values in both configurations corresponded to a complete band gap, as predicted from the lattice constant (see Figure 55). Those values were determined to be 18.6 dB and 16.9 dB for configuration A and B, respectively. In general, a good match between two configurations was obtained, with a larger deviation in one-third octave band centred at 1000 Hz. Keeping in mind that  $SI$  values shown in Figure 56 were result of averaging over nine microphones and a strong position-dependant behaviour of SCs [33,34], detailed investigation is presented below.

In order to emphasize the contribution of MP and inner core filled with rubber crumb, Figure 57 shows the comparison of results corresponding to the standardised characterisation of the SC barrier with absorptive MP cylinders and SC barrier with rigid PVC cylinders provided in [33], calculated in the same manner. Even though the lattice constants were slightly different, 0.22 m in the case of SC with absorptive MP cylinders and 0.2 m in the case of SC with rigid PVC cylinders, Bragg gaps were expected to be within the same one-third octave band centred at 800 Hz. Indeed,  $SI$  values in the complete band gap were similar to those of SC with rigid PVC cylinders, just slightly lower. This is believed to be due to

the absorptive nature of the building units, which slightly dampens the effect of the Bragg scattering. However,  $SI$  curves around the complete band gap were wider in case of SC with absorptive MP cylinders because of the absorption mechanism introduced by the MP layer, showing a significant difference at low frequencies. Additionally, the  $SI$  peak in configuration B was ‘smeared out’ towards the 1000 Hz region, making the difference in the complete band gap between the two SC barriers even more obvious.

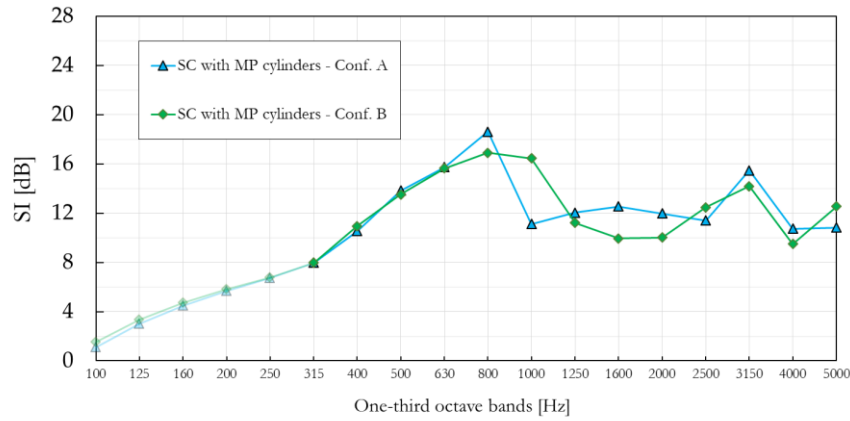
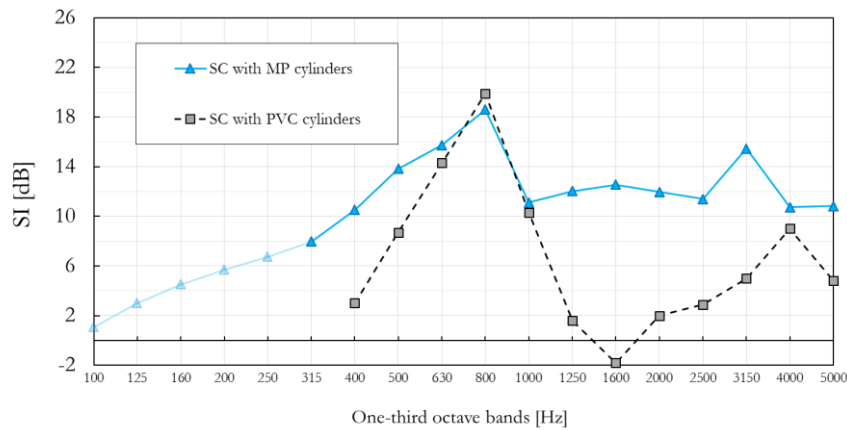
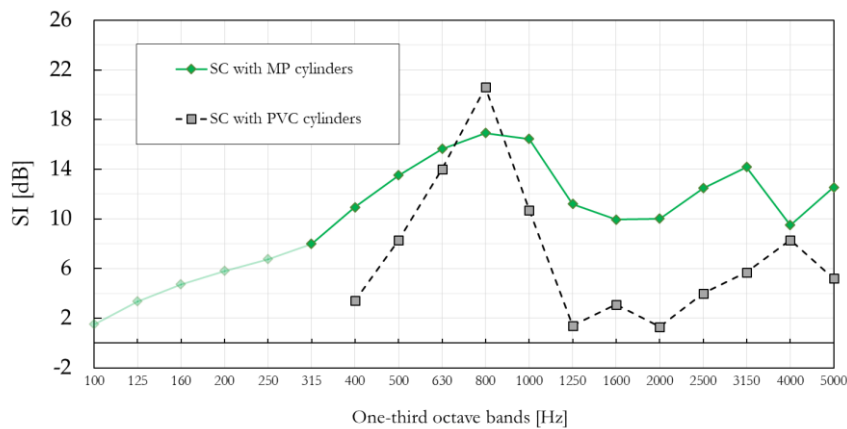


**Figure 56.** Sound insulation index ( $SI$ ) of SC barrier with micro-perforated (MP) cylinders [34] measured in two different configurations. Curves are result of averaging over nine microphones.



(a)



(b)

**Figure 57.** Sound insulation index ( $SI$ ) of SC barrier with micro-perforated (MP) cylinders [34] measured in two different configurations. Results are compared with those of standardised characterisation of SC barrier with PVC cylinders presented in [33, Fig. 6]. (a) Sound insulation index  $SI$ , configuration A; (b) sound insulation index  $SI$ , configuration B. Curves are result of averaging over nine microphones.

The presence of the absorbing MP layer was even more noticeable in the frequency region 1250–5000 Hz, showing a maximum difference of 14.4 dB in the one-third octave band centred at 1600 Hz, in the case of configuration A. Low  $SI$  values at twice the Bragg frequency measured for the SC barrier with rigid PVC cylinders, negative in configuration A and around zero in configuration B, significantly differed from those measured for the SC barrier with MP cylinders. Around this frequency, the first diffracted mode became propagative, according to the band diagram in Figure 55. However, this was barely visible only in configuration A. The reason was that the  $SI$  curve was the result of averaging over nine microphones. This was most evident when  $SI$  values were investigated at individual microphone positions, as shown in Figure 58. Although high  $SI$  values were measured at as many as six microphones at 1600 Hz in configuration A, the contribution of low  $SI$  values at the same frequency to the overall  $SI$  values was disregarded after averaging. A similar effect was noticeable at 3150 Hz in configuration B where a new diffracted mode started propagating, but this time it was more apparent in the averaged  $SI$  curve. Impulse responses at individual microphone positions M1–M9 for configuration A and B are presented in Figure A.8 and Figure A.9 (see Appendix C), respectively. Maximum values of the free-field impulse responses are normalised to 1.

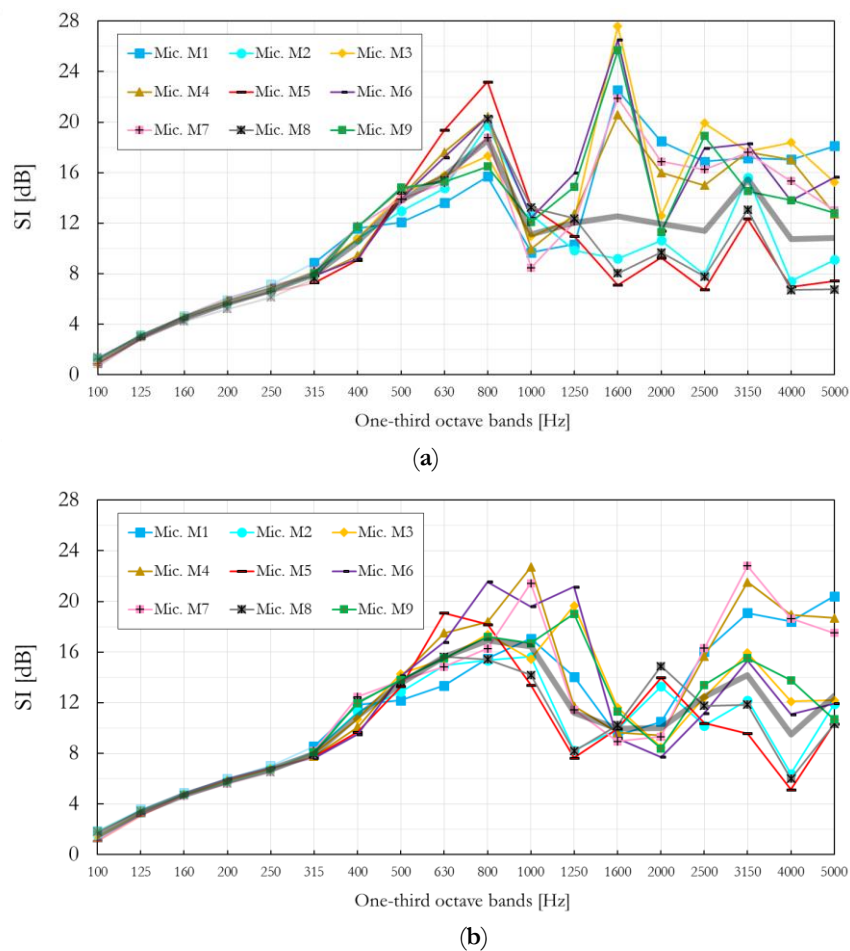


**Figure 58.**  $SI$  values measured at individual microphone positions M1–M9 [34]. Thick black curve shows the averaged  $SI$  values over all nine microphones. (a) Sound insulation index  $SI$ , configuration A; (b) Sound insulation index  $SI$ , configuration B.

The maximum  $SI$  value of 23.2 dB at the Bragg frequency in configuration A was measured for microphone position M5. In configuration B, the maximum  $SI$  value of 21.5 dB at the Bragg frequency was measured for microphone position M6. However, these values were not the maximum values for all microphone positions and frequencies. The maximum  $SI$  value of 27.6 dB in configuration A was measured for microphone position M3 at 1600 Hz. In configuration B, the maximum  $SI$  value of 22.8 dB was measured for microphone position M7 at 3150 Hz, which was also near the cut-off frequency of

the diffracted mode. The diverse  $SI$  curves between individual microphone positions in both configurations were a consequence of the occurrence of different modes above the diffraction limit. Asymmetry of absorption properties of different cylinders, but also inherently imperfect positioning of the microphone grid, might have been additional reasons. Despite the differences in the  $SI$  values between different microphone positions, characteristic frequency phenomena like the Bragg gap and diffracted modes were still easily noticeable. The method itself will average out all large deviations between the  $SI$  values in the same frequency range, providing overall information about the effectiveness of the SC barrier. It is still very important to be aware of the strong position–dependent insulation behaviour of SCs.

As explained in Section 5.2.1.1, a single–number rating,  $DL_{SI}$ , has been introduced by the EN 1793–6 [29] standard in order to categorise the airborne sound insulation performance of noise barriers. Since there were no posts in the case of SCs, only one single–number rating was calculated, without any global rating. Single–number rating values were calculated for different low frequency limits,  $f_{MIN} = 315$  Hz in the case of SC with absorbing MP and  $f_{MIN} = 400$  Hz in the case of SC with rigid PVC cylinders. Low–frequency limits influenced the calculated single–number values, since they were obtained for different frequency ranges. The calculated single–number values of SC with absorbing MP cylinders were  $DL_{SI, Conf-A} = 12.3$  dB and  $DL_{SI, Conf-B} = 12.2$  dB, while the values of SC with rigid PVC cylinders were  $DL_{SI, Conf-A} = 3.7$  dB and  $DL_{SI, Conf-B} = 5$  dB.

Requirements for sound attenuation and frequency span of the SC barrier needed in practice are a matter of type of noise as well as sound levels for which the barrier is used for. According to categorisation of airborne sound insulation presented in EN 1793–6 [29], there are five possible categories (see Table 13). For given single–number values of SC with absorbing MP cylinders,  $DL_{SI, Conf-A} = 12.3$  dB and  $DL_{SI, Conf-B} = 12.2$  dB, the SC barrier is categorised as D1 against the traffic noise. To rate the SC barrier against other types of noise, appropriate spectrum should be used for calculation of single–number values.

### 5.4.2.3 Sound Reflection

The results of the standardised EN 1793–5 [28] measurements of reflection index  $RI$  for the SC barrier described in Section 5.3.2, computed according to (26), are shown in Figure 59. Results are presented for both configuration A and configuration B, as shown in Figure 46. A good match between two configurations was obtained, except in the one–third octave band with a central frequency of 4000 Hz. In this one–third octave band, configuration B exhibits significantly greater  $RI$  value compared to configuration A, which is further investigated below.

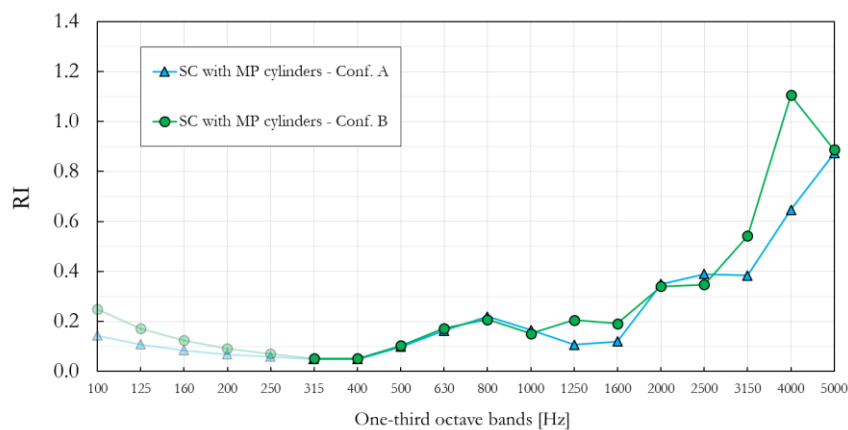
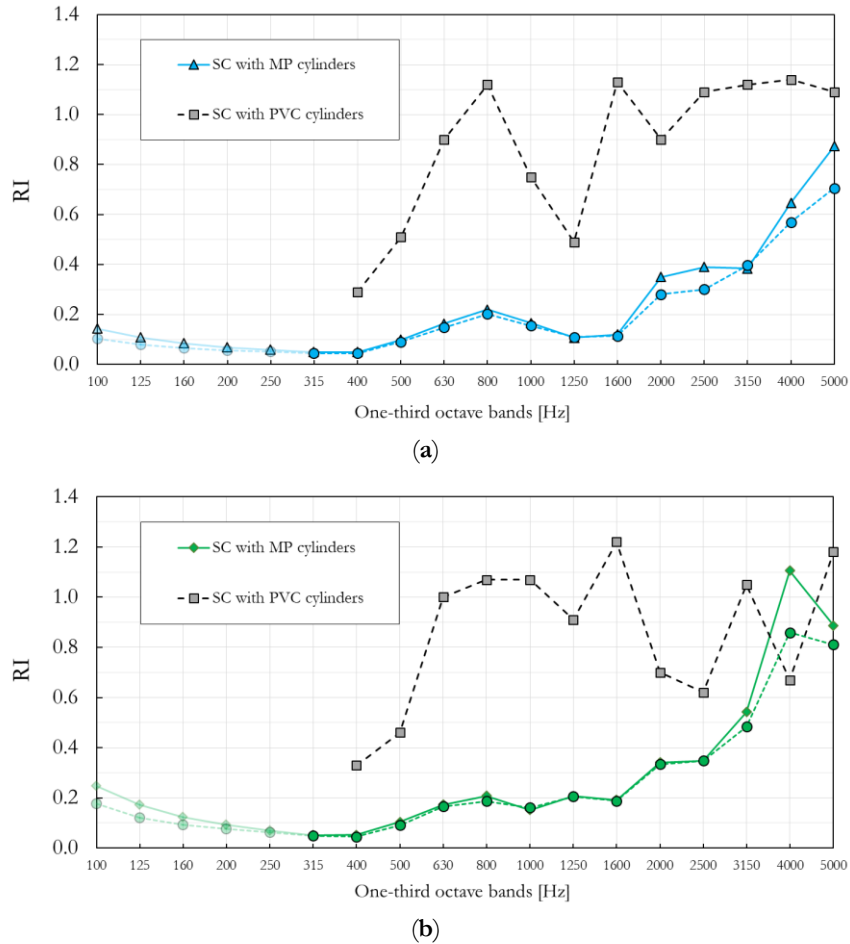


Figure 59. Sound reflection index ( $RI$ ) of SC barrier with micro–perforated (MP) cylinders [34] measured in two different configurations. Curves are result of averaging over nine microphones.

For the sake of comparison, the results of characterisation of the SC barrier with absorptive MP cylinders were also compared with those of the SC barrier with rigid PVC cylinders [33], see Figure 60. The maximum  $RI$  values in the Bragg gap were well defined in both configurations of SC with rigid PVC cylinders, with values approx. 0.9 higher than of SC with absorptive MP cylinders. The reason was that absorptive units played a significant role in damping the effect of Bragg scattering. Compared to rigid PVC cylinders, which provided only reflection mechanism, absorptive cylinders highlighted the absorption mechanism combined with Bragg scattering, leading to a pronounced reduction of the barrier reflective properties.



**Figure 60.** Sound reflection index ( $RI$ ) of the SC barrier with MP cylinders [34] measured in two different configurations. The results are compared with results of the standardised characterisation of SC barrier with PVC cylinders presented in [33, Fig. 7] (a) Reflection index  $RI$ , configuration A; (b) Reflection index  $RI$ , configuration B. Curves are result of averaging over nine microphones.

While SC barrier with rigid PVC cylinders showed a remarkable difference between  $RI$  values evaluated in two configurations, SC barrier with MP cylinders showed a similar trend. Namely, both configurations displayed a local maximum in the one-third octave band centred at 800 Hz and increased at higher frequencies. Small differences were visible in two frequency ranges: (i) In the one-third octave bands with the central frequency of 1250 Hz and 1600 Hz, and (ii) in the one-third octave bands, higher than the one centred at 2500 Hz. In both cases, the values were higher in configuration B. Compared to the barrier based on rigid PVC cylinders,  $RI$  values in the case of SC made of absorptive MP cylinders were significantly lower in nearly all one-third octave bands. The only exception was the one-third octave band centred at 4000 Hz in configuration B, where a higher  $RI$  was obtained for the barrier with absorptive cylinders. To investigate possible differences between different microphones,  $RI$  values were calculated at individual microphone positions, as shown in Figure 61. It was observed that microphone M7 exhibits an extraordinarily high value in the one-third octave band centred at 4000 Hz in

configuration B, probably due to a wrong data acquisition. For that reason, results in Figure 60 were recalculated without microphone M7 and presented with blue and green intersected curves for configurations A and B, respectively. The higher  $RI$  value found in SCs with MP cylinders at 4 kHz still prevailed, although after removing the effect of microphone M7, the difference was lower. The slightly higher reflectance was due to the reflectance of the barrier with rigid PVC cylinders, which abruptly decreased at this specific third–octave band as a consequence of an interference phenomenon. An additional factor behind this behaviour might be given by the fact that the temporal window in the case of SC with PVC cylinders was centred on the arrival of the direct sound, not on the arrival of the first reflection as it is suggested by [33]. In that way, multiple scattering components coming from the surrounding cylinders were most likely windowed out. Also, two barriers were completely different, one being absorptive and the other one being completely reflective. This means that multiple scattering components did not contribute to the overall energy of reflections in the same way for two barriers. While authors in [33] highlighted the importance of the first reflection in  $RI$  measurements, it was the scattered energy that made a significant contribution to the overall energy of the reflections in case of the SC with MP cylinders. Impulse responses at individual microphone positions M1–M9 for configuration A and B are presented in Figure A.10 and Figure A.11 (see Appendix C), respectively. Maximum values of the free–field impulse responses are normalised to 1.

As explained in Section 5.2.1.2, a single–number rating,  $DL_{RI}$ , has been introduced by the EN 1793–5 [28] standard in order to indicate the performance of the product. The calculated values in the case of SC with absorptive MP cylinders were  $DL_{RI} = 6.9$  dB and  $DL_{RI} = 6.3$  dB for configuration A and B, respectively. The corresponding values in the case of SC with rigid PVC cylinders were  $DL_{RI} = 0.8$  dB and  $DL_{RI} = 0.5$  dB for configuration A and B, respectively.

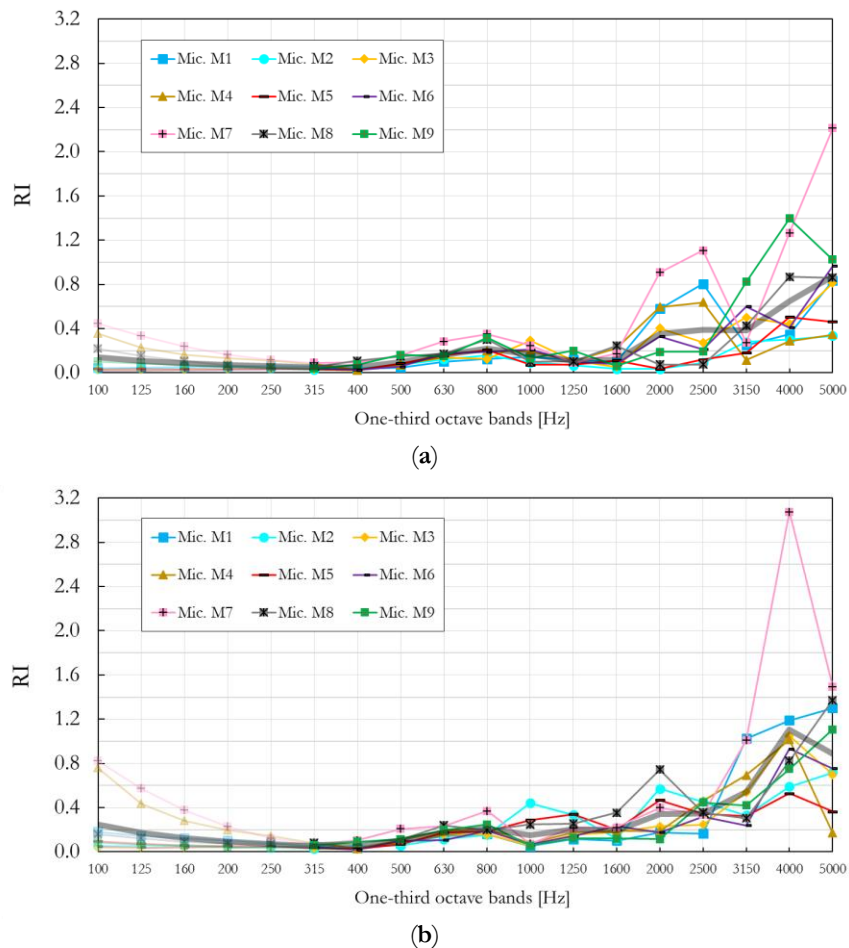


**Figure 61.**  $RI$  values measured at individual microphone positions M1–M9 [34]. Thick black curve shows the averaged  $RI$  values over all nine microphones. (a) Reflection index  $RI$ , configuration A; (b) Reflection index  $RI$ , configuration B.

#### 5.4.2.4 Signal–To–Noise Ratio

The results of calculations of the effective  $SNR$  for  $SI$  measurement, calculated according to (28), are presented in Figure 62. As in case for the conventional noise barrier, the calculations of the effective  $SNR$  were calculated for individual microphone positions according to calculation method presented in [101]. More detailed explanation of the calculation method is presented in Section 5.2.1.3.

The results in Figure 62 are presented for  $SI$  measurements in the presence of the SC barrier. Although the sound transmitting through the barrier was attenuated by the barrier itself,  $SNR$  values were still high. This stems from the fact that the barrier was located in the university campus, far away from any possible noise source. Additionally, high levels of the excitation signal were used in order to achieve the high  $SNR$  values.

The results of calculations of the effective  $SNR$  for  $RI$  measurement are presented in Figure 63. The effective  $SNR$  was calculated for reflected sound components, as explained in Section 5.2.1.3. Although the reflected sound components were significantly attenuated by the SC barrier itself,  $SNR$  values were still above defined threshold of 10 dB in the whole measurement frequency range.

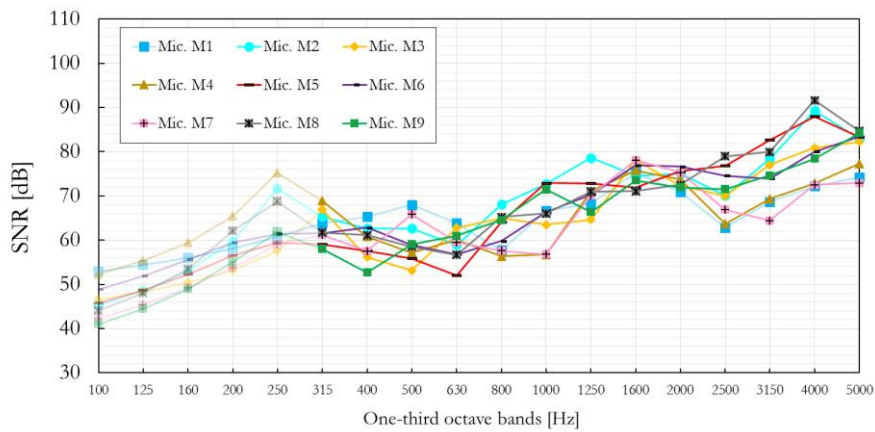


Figure 62. Signal–to–noise ratio ( $SNR$ ) of sonic crystal noise barrier measured at individual microphone positions M1–M9 for sound insulation measurement performed in presence of the barrier.

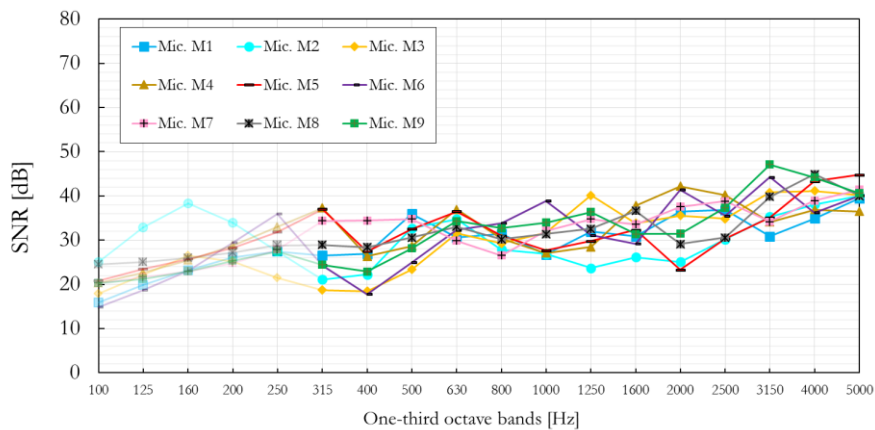


Figure 63. Frequency–dependant signal–to–noise ratio ( $SNR$ ) of the SC barrier with MP cylinders measured at individual microphone positions M1–M9 for  $RI$  measurement.

# Chapter 6

## Conclusions

In this dissertation, two of three elements that can be recognised in noise annoyance analysis have been investigated: the sound source and the transmission path. First, characterisation methods of specific noise sources in urban environments, such as entertainment premises and vessels, have been investigated. Noise from entertainment premises has been investigated from the aspect of floating river clubs which present culturally-specific floating structures typical for the Balkan region. Noise from vessels has been investigated from the aspect of moored ships, primarily due to increased traffic of cruise and cargo vessels and their stay in ports in the vicinity of residential areas. These noise sources have rarely been the subject of research and mostly subjected to control performed as a result of noise complaints. Second, noise barriers have been investigated from the aspect of their possible application as protection methods against these types of noise sources.

As the first goal of this dissertation, characterisation of outdoor noise emitted by two low-frequency noise sources on the water, floating river clubs and moored ships, have been investigated. These two noise sources are considered as specific in this dissertation, due to their low-frequency spectral content, directional characteristics, and limited accessibility. After the evaluation of the standardised ISO measurement methods, a simplified measurement method used in Nordic countries, the Nordtest method, has been introduced. More precisely, two different Nordtest measurement methods, Nordtest Sphere and Nordtest Box, have been applied together with the most common standardised measurement method, ISO 3744, in two cases. In the former case, the methods have been applied to a 1:10 scale model of a typical floating river club in different scenarios. In the latter case, the methods have been applied to a cottage made of lightweight partitions, which present a simplified case of floating river clubs due to its location on a hard ground. In both cases, the results have shown that differences in obtained values of sound power levels between Nordtest Sphere and ISO 3744 lie mostly within standard deviations defined by ISO 3744. Moreover, the results have shown that the Nordtest Box method overestimates sound power levels compared to the ISO 3744 measurement method. Therefore, the Nordtest Sphere method has been suggested in this dissertation as optimal measurement method in case of floating river clubs, which was the main goal of this dissertation.

In the next step, the Nordtest Sphere measurement method has been applied to two floating river clubs in Belgrade, Serbia. Moreover, the results of measured sound power levels have been further used to calculate sound pressure levels in a far-field, at distances 80–215 m from the floating river clubs. The sound pressure levels have been calculated under assumption that floating river clubs can be considered a point noise source, as defined by the Nordtest method. The calculated sound pressure levels have been then compared to those obtained from measurements at the same measurement positions. It has been shown that application of the Nordtest Sphere method underestimates sound power levels by approximately 5–15 dB in the frequency range 31.5–100 Hz. Additionally, a good agreement between the calculated and measured sound pressure levels has been observed in the frequency range 125–3150 Hz.

In addition to characterisation of the outdoor entertainment noise, indoor entertainment noise has been also investigated in this dissertation. The reason for this is the fact that noise annoyance in outdoor environments is often caused by indoor entertainment noise transmitted through building partitions. Hence, indoor sound level spectra for different types of entertainment premises, including floating river clubs, has been investigated. The indoor sound spectra can be also used to improve rating of sound insulation of building elements against this type of noise. As a result of the investigation, a new sound spectrum for discotheques i.e., entertainment premises with complex audio systems with several independent subwoofers, has been proposed. The proposed spectrum has not been investigated in the literature, and therefore, represents contribution of this research. Spectrum adaptation term calculated from the proposed sound level spectrum has been named  $C_{SUB}$ . Additionally, a classification of sound spectra based on a type of audio systems has been proposed. As an illustration, the application of the

proposed sound spectrum to rating of sound insulation has been tested by using four common building elements. Differences of up to 11 dB have been obtained between spectrum adaptation terms calculated by using the spectrum for disco music suggested by the ISO 717-1 international standard ( $C_{tr}$ ) and the one for discotheques proposed in this dissertation ( $C_{SUB}$ ), with higher values in the former case. The proposed sound level spectrum for discotheques presents a more realistic assessment of the sound insulation against a pronounced low-frequency entertainment noise.

Finally, sound power levels of funnel outlets, as the most dominant low-frequency noise sources on moored ships, have been investigated by implementation of both near-field and far-field measurements. The far-field measurements, performed at distances 65–380 m from the ships, have been used to validate near-field sound power levels and to introduce necessary corrections. Corrections of approx. 4–14 dB in the limited frequency range 25–50 Hz have been obtained from the far-field measurements. The obtained corrections refer to cases of single funnel outlets, where sound power levels have been calculated from measurements of sound pressure levels at distances 1–2 m. In one case, sound power levels of a cluster of funnel outlets have been determined from measurements of sound pressure levels at distance of approx. 20 m from the cluster. In this case, a good agreement between near-field and far-field sound power levels has been obtained in the whole frequency range.

As the second goal of this dissertation, application of the EN 1793-5 and EN 1793-6 standardised *in situ* method to determine acoustic properties of noise barriers to two different barrier types has been investigated. First, the *in situ* methods have been applied to an absorbing screen-type i.e., conventional noise barrier. The results have been compared to those obtained by application of laboratory measurements to an identical barrier sample. On the one hand, the results have shown generally higher values of sound insulation indices in case of application of the *in situ* measurement methods in front of a barrier element than in front of a barrier post, which is in line with results found in the literature. On the other hand, a good agreement has been obtained below 1000 Hz in case of the laboratory and *in situ* measurements in front of a barrier post, with lower values of sound insulation indices at higher frequencies in the latter case. Both *in situ* measurements, in front of a barrier element and in front of a post, have expressed deterioration of sound insulation at frequencies 3150–5000 Hz, indicating bad workmanship. This phenomenon has not been observed in case of the laboratory measurements. The results have indicated underestimation of sound insulation properties of the noise barrier when measured in the laboratory environment, which is the common way to rate acoustic properties of noise barriers. Second, the *in situ* methods have been applied to a noise barrier based on sonic crystals. Application of *in situ* methods to noise barriers based on sonic crystals has not been sufficiently investigated in the literature, since there are very few such practical implementations outside laboratory environments. The results have shown a strong dependency of sound insulation indices on microphone positions, which have not been obtained in case of the conventional noise barrier. The diverse sound insulation values at individual microphone positions have been mainly a consequence of complex pressure patterns above diffraction limit. Because of this strong position-dependable behaviour, but also keeping in mind the fixed distance between adjacent microphones defined by the *in situ* measurement methods, a need for adjustment of their applicability to barriers based on sonic crystals has been indicated.

The use of noise barriers as protection methods against low-frequency noise from floating river clubs is questionable for two reasons. First, there is no efficient way to rate their acoustic properties in the low-frequency range of interest. On the one hand, the low-frequency range limitation in case of *in situ* measurement methods, investigated in this dissertation, occurs due to the size of the barrier i.e., to obtain values of sound insulation and sound reflection indices below 100 Hz a barrier sample larger than  $6 \times 6$  m is needed. On the other hand, the low-frequency range limitation in case of conventional laboratory measurements occurs due to the size of the laboratory facility. Namely, large measurement facilities are needed to avoid the influence of strong room modes below 100 Hz. Because of the room modes, deviations of measurement results in the low-frequency range are large, making the measurement results uncertain. Second, because of the distance between floating river clubs and residential areas, which are usually a few hundred meters, noise barriers should be placed very close to floating river clubs. Placing

them at larger distances from floating river clubs would make them inefficient. Residential buildings are usually located on the opposite side of the river to floating river clubs, which means that noise barriers should be placed on the same floating foundation as the floating river clubs. This could compromise the stability of floating river clubs, since thick and heavy noise barriers are required in order to attenuate the low-frequency entertainment noise.

Due to the above-mentioned reasons and fact that most floating river clubs in Belgrade operate in the existing environment, the most reasonable protection methods in case of floating river clubs are those at the noise source. They include limitations of sound levels indoors and use of building elements with high values of sound insulation indices. As explained earlier, the sound level spectrum proposed in this dissertation is a step forward towards more accurate rating of sound insulation in case of the pronounced low-frequency entertainment noise. Additionally, the proposed spectrum could be used to calculate the noise from floating river clubs and more generally, for entertainment premises with complex audio systems with several independent subwoofers, outwards and thus improve the accuracy of noise predictions in their vicinity. The spectrum proposed in this dissertation has been accepted by SoundPLAN, widely used software for the prediction of environmental noise, and incorporated in the internal library as suggested noise spectrum for entertainment premises such as clubs.

## 6.1 Scientific contributions

Based on the results presented in this dissertation, the initial hypotheses have been confirmed and following scientific contributions have been made:

- Application of simplified measurement methods in case of floating river clubs has been investigated and validated as alternative to complex measurement methods defined by international ISO standards.

In order to determine sound power level of floating river clubs, a simplified measurement method used in Nordic countries, Nordtest Sphere, has been suggested as an alternative to the commonly employed standardised measurement method ISO 3744. The results presented in the dissertation have shown that differences between the Nordtest Sphere method and the ISO 3744 method are found within or around standard deviations suggested by ISO 3744. By utilising the Nordtest Sphere method, it is possible to facilitate a characterisation of floating river clubs and at the same time, preserve a sufficient accuracy.

- The relevant scientific contribution refers to suggested corrections to sound power levels at low frequencies obtained from measurements at distances closer to the noise sources, which were obtained by measuring sound pressure levels at larger distances from floating river clubs and moored ships.

The results presented in the dissertation have shown that measurements of sound pressure levels at distances closer to noise sources underestimate values of sound power levels at low frequencies. In case of floating river clubs and moored ships, those differences varied mostly between 5–15 dB and 4–14 dB at frequencies below 100 Hz and 50 Hz, respectively. Sound pressure levels at control measurement positions have been measured at distances 80–215 m and 65–380 m from floating river clubs and moored ships, respectively. The presented corrections allow for more accurate predictions of the low-frequency noise at larger distances from the noise sources.

- A new sound level spectrum for entertainment premises with audio systems configured for recorded music with pronounced low-frequency content has been proposed.

The results presented in the dissertation have indicated overestimation of sound insulation of building elements against pronounced low-frequency entertainment noise if spectra suggested by current version of the ISO 717–1 are used. A new sound level spectrum to rate building elements against the low-frequency entertainment noise has been proposed. The proposed spectrum allows for more realistic rating of sound insulation by single-number ratings and spectrum-adaptation terms. Such spectrum has

not existed in the literature. Additionally, a classification of sound level spectra regarding types of audio systems has been indicated.

- A need for adjustment of application of the standardised *in situ* methods to determine acoustic properties of noise barriers, EN 1793–5 and EN 1793–6, to barriers based on *sonic crystals*, has been indicated.

When applied to sonic crystals, *in situ* sound insulation measurements exhibit a strong dependency on microphone positions. The diverse sound insulation values at individual microphone positions are mainly a consequence of complex sound pressure patterns above diffraction limit. The deviations of sound insulation at individual microphone positions in case of screen-type noise barriers have another meaning i.e., indicate a bad workmanship. Because of the strong position-dependable behaviour, but also keeping in mind the fixed distance between adjacent microphones suggested by the *in situ* methods, adjustment of their applicability to barriers based on sonic crystals requires further investigation.

## 6.2 Future work

The research presented in this dissertation can be extended in several different directions. Measurement methods described in this dissertation have been applied to a limited number of objects. A prospective source of future research may be directed towards better defining of deviations between the methods, and investigation of uncertainty and variance could be performed accordingly. This could include more objects with different geometries, but also repeated measurements at same measurement positions. Also, different measurement methods define different distribution of measurement positions on the same imaginary measurement surface. Investigation of choice of measurement positions and differences in sound power levels between different choices could account for sound power levels at a specific angle.

As another possible direction, investigations regarding noise simulations and noise predictions from floating river clubs and funnel outlets could be performed. Since in the dissertation, a simple calculation model has been utilised, it would imply that representation of low-frequency noise sources, floating river clubs and funnel outlets, should be carried out by a point source i.e., acoustic monopole. However, generally speaking, more complex representations could lead to potentially more accurate noise predictions. As an example, it would be interesting to see comparison between representations of the low-frequency noise sources by area and point noise sources. Directivity patterns for different geometries of floating river clubs as well as different audio setups indoors would be interesting to know. Furthermore, an analysis of noise from a cluster of floating river clubs could be investigated. It would be reasonable to assume that such clusters radiate noise closely to line sound sources. Different distribution of low-frequency noise sources in the cluster could be analysed as well.

Measurements of indoor entertainment noise have been performed by using a single microphone position. Hence, a measurement method which employs several measurement positions could be developed and implemented. Also, the proposed sound level spectrum for discotheques has been obtained from limited number of measured spectra, and it is due to this finding that, a more comprehensive study including more venues and a greater variety of geographical locations ought to be undertaken if the standardisation should occur. Moreover, further classification regarding e.g., music types, different geometries, etc. could be developed.

Finally, when applying *in situ* methods to determine acoustic properties of noise barriers, size of a barrier sample limits the frequency range in which values of sound insulation ( $SI$ ) indices are presented. This could be improved e.g., in case of noise barriers based on sonic crystals, by making a scale model of the barrier. In that case, it is possible to make a model of a barrier sample large enough to allow representation of  $SI$  in a wider frequency range and rate the barrier against a low-frequency noise. Additionally, a new methodology to apply *in situ* measurement to noise barriers based on sonic crystals could be developed. At the end, the majority of sonic crystals have been optimised against the traffic noise. Hence, an optimization against a low-frequency noise could also be made.

# References

- [1] E. Murphy and E. A. King, “Strategic Noise Mapping,” in *Environmental Noise Pollution*, 1st ed. Burlington, MA, USA: Elsevier, 2014, ch. 4, sec. 3, pp. 85.
- [2] “Environmental Noise Guidelines for the European Region,” WHO Regional Office for Europe, Copenhagen, Denmark, Jun. 27, 2018. Accessed: Jul. 28, 2021. [Online]. Available: <https://www.euro.who.int/en/health-topics/environment-and-health/noise/publications/2018/environmental-noise-guidelines-for-the-european-region-2018>
- [3] “Environmental noise in Europe – 2020,” European Environment Agency, Copenhagen, Denmark, EEA Report No 22/2019, Mar. 05, 2020. Accessed: Jul. 28, 2021. [Online]. Available: <https://www.eea.europa.eu/publications/environmental-noise-in-europe>
- [4] L. Fritschi, A. L. Brown, R. Kim, D. Schwela, and S. Kephelopoulos, “Burden of disease from environmental noise: Quantification of healthy life years lost in Europe,” WHO Regional Office for Europe, Copenhagen, Denmark, JRC64428, 2011. Accessed: Jul. 28, 2021. [Online]. Available: <https://www.euro.who.int/en/publications/abstracts/burden-of-disease-from-environmental-noise.-quantification-of-healthy-life-years-lost-in-europe>
- [5] “European Union Directive 2002/49/EC.” Eur-lex.europa.eu. <https://eur-lex.europa.eu/legal-content/EN/TXT/PDF/?uri=CELEX:32002L0049&from=EN> (accessed Jul. 28, 2021)
- [6] SoundPLANnoise. (2020), SoundPLAN GmbH. Accessed: Jul. 28, 2021. [Online]. <https://www.soundplan.eu/en/software/soundplannoise/>
- [7] CadnaA. (2020), DataKustik GmbH. Accessed: Jul. 28, 2021. [Online]. <https://www.datakustik.com/products/cadnaa/cadnaa/>
- [8] Olive Tree Lab Suite. (2019), PEMARD. Accessed: Jul. 28, 2021. [Online]. <https://www.mediterraneanacoustics.com/olive-tree-lab-suite.html>
- [9] *Acoustics – Determination of sound power levels and sound energy levels of noise sources using sound pressure – Engineering methods for an essentially free field over a reflecting plane*, ISO 3744:2010, Oct. 2010.
- [10] *Acoustics – Determination of sound power levels of noise sources using sound intensity – Part 1: Measurement at discrete points*, ISO 9614–1:1993, Jun. 1993.
- [11] Siemens, “A guide to measuring sound power – An overview of international standards,” 2020. Accessed: Jul. 28, 2021. [Online]. Available: <https://community.sw.siemens.com/s/relatedlist/ka64O0000004R09QAE/AttachedContent Documents>
- [12] G. Leventhall, “Low frequency noise. What we know, what we do not know, and what we would like to know,” *Journal of Low Frequency Noise Vibration and Active Control*, vol. 28, no. 2. Multi-Science Publishing Co. Ltd, pp. 79–104, 2009. doi: [10.1260/0263-0923.28.2.79](https://doi.org/10.1260/0263-0923.28.2.79)
- [13] B. Berglund, P. Hassmén, and R. F. S. Job, “Sources and effects of low-frequency noise,” *J. Acoust. Soc. Am.*, vol. 99, no. 5, pp. 2985–3002, May 1996. doi: [10.1121/1.414863](https://doi.org/10.1121/1.414863)

- [14] G. H. Leventhall, “Low frequency noise and annoyance,” *Noise Heal.*, vol. 6, no. 23, pp. 59–72, Apr. 2004.
- [15] *Folkhälsomyndighetens allmänna råd om buller inomhus*, FoHMFS 2014:13, Feb. 2014. [Online]. Available: <https://www.folkhalsomyndigheten.se/publicerat-material/publikationsarkiv/f/fohmfs-201413/>
- [16] M. Mirowska, “Evaluation of low–frequency noise in dwellings. New polish recommendations,” *J. Low Freq. Noise Vib. Act. Control*, vol. 20, no. 2, pp. 67–74, 2001. doi: [10.1260/0263092011493163](https://doi.org/10.1260/0263092011493163)
- [17] A. Cocchi, P. Fausti, and S. Piva, “Experimental Characterisation of the Low Frequency Noise Annoyance Arising from Industrial Plants,” *J. Low Freq. Noise, Vib. Act. Control*, vol. 11, no. 4, pp. 124–132, Dec. 1992. doi: [10.1177/026309239201100404](https://doi.org/10.1177/026309239201100404)
- [18] F.A. Everest and K.C. Pohlman, “Loudness versus Frequency,” in *Master handbook of acoustics*, 5th ed. New York, NY, USA: McGraw–Hill Education, 2009, ch. 4, sec. 3, pp. 46.
- [19] *Acoustics – Rating of sound insulation in buildings and of building elements – Part 1: Airborne sound insulation*, ISO 717–1:2013, Mar. 2013.
- [20] W. E. Scholes and J. W. Sargent, “Designing against noise from road traffic,” *Appl. Acoust.*, vol. 4, no. 3, pp. 203–234, 1971.
- [21] C.G. Gordon, W.J. Galloway, B.A. Kugler, and D.L. Nelson, “Highway noise. A design guide for highway engineers,” *Highw Res Bd, Nat Coop Highw Res Progr. Rep 117*, 1973.
- [22] M. P. Peiró–Torres, M. J. Parrilla Navarro, M. Ferri, J. M. Bravo, J. V. Sánchez–Pérez, and J. Redondo, “Sonic Crystals Acoustic Screens and Diffusers,” *Appl. Acoust.*, vol. 148, pp. 399–408, May 2019. doi: [10.1016/j.apacoust.2019.01.004](https://doi.org/10.1016/j.apacoust.2019.01.004)
- [23] U. J. Kurze, “Noise Reduction by Barriers,” *J. Acoust. Soc. Am.*, vol. 53, no. 1, pp. 339–339, Jan. 1973. doi: [10.1121/1.1982407](https://doi.org/10.1121/1.1982407)
- [24] I. Ekici, H. Boughah, “A review of research on environmental noise barriers,” *Build. Acoust.*, vol. 10, no. 4, pp. 289–323, Sep. 2003. doi: [10.1260/135101003772776712](https://doi.org/10.1260/135101003772776712)
- [25] V. M. García Chocano, “New devices for noise control and acoustic cloaking,” Ph.D. dissertation, Dept. Eng. Elect., Universitat Politècnica de València, Valencia, Spain, 2015. [Online]. Available: <https://riunet.upv.es/handle/10251/53026>
- [26] *Road traffic noise reducing devices – Test method for determining the acoustic performance – Part 1: Intrinsic characteristics of sound absorption under diffuse sound field conditions*, SS–EN 1793–1:2017, Mar. 2017.
- [27] *Road traffic noise reducing devices – Test method for determining the acoustic performance – Part 2: Intrinsic characteristics of airborne sound insulation under diffuse sound field conditions*, SS–EN 1793–2:2018, Apr. 2018.
- [28] *Road traffic noise reducing devices – Test method for determining the acoustic performance – Part 5: Intrinsic characteristics – In situ values of sound reflection under direct sound field conditions*, SS–EN 1793–5:2016, Apr. 2016.

- [29] *Road traffic noise reducing devices – Test method for determining the acoustic performance – Part 6: Intrinsic characteristics – In situ values of airborne sound insulation under direct sound field conditions*, SS-EN 1793–6:2012, Nov. 2012.
- [30] M. Garai and P. Guidorzi, “European methodology for testing the airborne sound insulation characteristics of noise barriers in situ: Experimental verification and comparison with laboratory data,” *J. Acoust. Soc. Am.*, vol. 108, no. 3, p. 1054, 2000. doi: [10.1121/1.1286811](https://doi.org/10.1121/1.1286811)
- [31] NORDTEST, “Industrial plants: Noise emission (NT ACOU 080),” 1991. [Online]. Available: <http://www.nordtest.info/wp/1991/02/15/industrial-plants-noise-emission-nt-acou-080/>
- [32] S. M. Dimitrijević, M. M. Mijić, and D. S. Šumarac Pavlović, “Indoor sound level spectra of public entertainment premises for rating airborne sound insulation,” *J. Acoust. Soc. Am.*, vol. 147, no. 3, pp. EL215–EL220, Mar. 2020. doi: [10.1121/10.0000800](https://doi.org/10.1121/10.0000800)
- [33] F. Morandi, M. Miniaci, A. Marzani, L. Barbaresi, and M. Garai, “Standardised acoustic characterisation of sonic crystals noise barriers: Sound insulation and reflection properties,” *Appl. Acoust.*, vol. 114, pp. 294–306, Dec. 2016. doi: [10.1016/j.apacoust.2016.07.028](https://doi.org/10.1016/j.apacoust.2016.07.028)
- [34] S. M. Dimitrijević, V. M. García-Chocano, F. Cervera, E. Roth, and J. Sánchez-Dehesa, “Sound insulation and reflection properties of sonic crystal barrier based on micro-perforated cylinders,” *Materials (Basel)*, vol. 12, no. 7, Aug. 2019. doi: [10.3390/ma12172806](https://doi.org/10.3390/ma12172806)
- [35] R. J. M. Craik and J. R. Stirling, “Amplified music as a noise nuisance,” *Appl. Acoust.*, vol. 19, no. 5, pp. 335–346, 1986.
- [36] A. Chung, W. M. To, K. K. Iu, and M. Yeung, “Impact and control practices of bar and pub sound in densely populated cities,” *J. Acoust. Soc. Am.*, vol. 142, no. 4, pp. 2484–2484, Oct. 2017. doi: [10.1121/1.5014065](https://doi.org/10.1121/1.5014065)
- [37] K. Vuković. “Belgrade’s floating river clubs.” BBC.com. <https://www.bbc.com/travel/article/20170822-belgrades-floating-river-clubs> (accessed Jul. 28, 2021).
- [38] “The “Splavs” floating river clubs.” Serbia.com. <https://www.serbia.com/visit-serbia/enjoy-serbia/nightlife/the-splavs-floating-river-clubs/> (accessed Jul. 28, 2021).
- [39] G. Hübner, “Final results of a national round robin test determining the sound power level of machines/equipment,” in *INTER-NOISE and NOISE-CON Cong. Conf. Proc., InterNoise97*, Budapest, Hungary, Aug. 1997, pp. 1146–1151.
- [40] R. D. Hellweg Jr, “International round robin test of ISO/DIS 7779,” in *INTER-NOISE and NOISE-CON Cong. Conf. Proc., InterNoise88*, Avignon, France, Aug. 1988, pp. 1105–1108.
- [41] F. Spandöck, “Akustische Modellversuche,” *Ann. Phys.*, vol. 412, no. 4, pp. 345–360, 1934. doi: [10.1002/andp.19344120402](https://doi.org/10.1002/andp.19344120402)
- [42] T. Hidaka, K. Suzuki and Y. Yamada, “A new miniature loudspeaker for room acoustical scale model experiment,” in *Proc. 20th Int. Cong. Acous., ICA 2010*, Sydney, Australia, Aug. 2010, pp. 2351–2354.
- [43] M. Barron, “Acoustic scale models,” in *Auditorium Acoustics and Architectural Design*, 2nd ed. Abingdon, UK: Spon Press, 2010, ch. 3, sec. 9, pp. 62.

- [44] M. Barron, “Auditorium acoustic modelling now,” *Appl. Acoust.*, vol. 16, no. 4, pp. 279–290, 1983. doi: [10.1016/0003-682X\(83\)90020-8](https://doi.org/10.1016/0003-682X(83)90020-8)
- [45] K. A. Mulholland, “The prediction of traffic noise using a scale model,” *Appl. Acoust.*, vol. 12, no. 6, 1979. doi: [10.1016/0003-682X\(79\)90004-5](https://doi.org/10.1016/0003-682X(79)90004-5)
- [46] R. J. Orłowski, “Scale modelling for predicting noise propagation in factories,” *Appl. Acoust.*, vol. 31, no. 1–3, 1990. doi: [10.1016/0003-682X\(90\)90058-3](https://doi.org/10.1016/0003-682X(90)90058-3)
- [47] J. Picaut and L. Simon, “Scale model experiment for the study of sound propagation in urban areas,” *Appl. Acoust.*, vol. 62, no. 3, 2001. doi: [10.1016/S0003-682X\(00\)00028-1](https://doi.org/10.1016/S0003-682X(00)00028-1)
- [48] T. J. Cox, B. M. Fazenda, and S. E. Greaney, “Using scale modelling to assess the prehistoric acoustics of stonehenge,” *J. Archaeol. Sci.*, vol. 122, 2020. doi: [10.1016/j.jas.2020.105218](https://doi.org/10.1016/j.jas.2020.105218)
- [49] “SB26STAC-C000-4 product specifications.” SBAcoustics.com. <https://sbacoustics.com/product/sb26stac-c000-4/> (accessed Jul. 28, 2021).
- [50] “XT25TG30-04 product specifications, Peerless by Tymphany.” Parts-express.com. <https://www.parts-express.com/pedocs/specs/264-1016-tymphany-xt25tg30-04-spec-sheet.pdf> (accessed Jul. 28, 2021).s
- [51] M. Caniato, F. Bettarello, C. Schmid, and P. Fausti, “Assessment criterion for indoor noise disturbance in the presence of low frequency sources,” *Appl. Acoust.*, vol. 113, pp. 22–33, Dec. 2016. doi: [10.1016/j.apacoust.2016.06.001](https://doi.org/10.1016/j.apacoust.2016.06.001)
- [52] H. K. Park and J. S. Bradley, “Evaluating standard airborne sound insulation measures in terms of annoyance, loudness, and audibility ratings,” *J. Acoust. Soc. Am.*, vol. 126, no. 1, pp. 208–219, Jul. 2009. doi: [10.1121/1.3147499](https://doi.org/10.1121/1.3147499)
- [53] D. B. Mašović, D. S. Š. Pavlović, and M. M. Mijić, “On the suitability of ISO 16717-1 reference spectra for rating airborne sound insulation,” *J. Acoust. Soc. Am.*, vol. 134, no. 5, pp. EL420–EL425, Nov. 2013. doi: [10.1121/1.4824629](https://doi.org/10.1121/1.4824629)
- [54] Dolby Laboratories, “Technical Guidelines for Dolby Stereo Theaters,” 1994. Accessed: Jul. 28, 2021. [Online]. Available: <http://www.film-tech.com/warehouse/manuals/DOLBYTG1994.pdf>
- [55] S. Sadhra, C. A. Jackson, T. Ryder, and M. J. Brown, “Noise exposure and hearing loss among student employees working in university entertainment venues,” *Ann. Occup. Hyg.*, vol. 46, no. 5, pp. 455–463, Jul. 2002. doi: [10.1093/annhyg/mef051](https://doi.org/10.1093/annhyg/mef051)
- [56] NEPTUNES, “Noise measurement protocol moored ships,” 2019. [Online]. Available: <https://neptunes.pro/downloads/Noise-Measurement-Protocol-V2-1.pdf>
- [57] *Measurement of airborne noise emitted by machines; enveloping surface method, chimneys*, DIN 45635-47, Jun. 1985.
- [58] R. Witte, “NEPTUNES Measurement protocol and Noise Label,” in *INTER-NOISE and NOISE-CON Cong. Conf. Proc., InterNoise19*, Madrid, Spain, Sep. 2019, pp. 7389–7392.
- [59] *Acoustics – Attenuation of sound during propagation outdoors – Part 2: General method of calculation*, ISO 9613-2:1996, Dec. 1996.

- [60] C. H. Kasess, W. Kreuzer, and H. Waubke, “Deriving correction functions to model the efficiency of noise barriers with complex shapes using boundary element simulations,” *Appl. Acoust.*, vol. 102, pp. 88–99, Jan. 2016. doi: [10.1016/j.apacoust.2015.09.009](https://doi.org/10.1016/j.apacoust.2015.09.009)
- [61] R. K. Pirinchieva, “The influence of barrier size on its sound diffraction,” *J. Sound Vib.*, vol. 148, no. 2, pp. 183–192, Jul. 1991. doi: [10.1016/0022-460X\(91\)90570-A](https://doi.org/10.1016/0022-460X(91)90570-A)
- [62] “Highway Traffic Noise: Analysis and Abatement Guidance,” U.S. Department of Transportation – Federal Highway Administration, Washington, D.C., USA, FHWA–HEP–10–025, Dec. 2011. Accessed: Jul. 28, 2021. [Online]. Available: [https://www.fhwa.dot.gov/environment/noise/regulations\\_and\\_guidance/analysis\\_and\\_abatement\\_guidance/revguidance.pdf](https://www.fhwa.dot.gov/environment/noise/regulations_and_guidance/analysis_and_abatement_guidance/revguidance.pdf)
- [63] J. P. Arenas, “Potential problems with environmental sound barriers when used in mitigating surface transportation noise,” *Sci. Total Environ.*, vol. 405, no. 1–3, pp. 173–179, Nov. 2008. doi: [10.1016/j.scitotenv.2008.06.049](https://doi.org/10.1016/j.scitotenv.2008.06.049)
- [64] F. J. Fahy, D. G. Ramble, J. G. Walker, and M. Sugiura, “Development of a novel modular form of sound absorbent facing for traffic noise barriers,” *Appl. Acoust.*, vol. 44, no. 1, pp. 39–51, 1995. doi: [10.1016/0003-682X\(94\)P4418-6](https://doi.org/10.1016/0003-682X(94)P4418-6)
- [65] R. Martínez–Sala, J. Sancho, J. V. Sánchez, V. Gómez, J. Llinares, and F. Meseguer, “Sound attenuation by sculpture,” *Nature*, vol. 378, no. 6554, p. 241, Nov. 1995. doi: [10.1038/378241a0](https://doi.org/10.1038/378241a0)
- [66] J. V. Sánchez–Pérez *et al.*, “Sound attenuation by a two–dimensional array of rigid cylinders,” *Phys. Rev. Lett.*, vol. 80, no. 24, pp. 5325–5328, 1998. doi: [10.1103/PhysRevLett.80.5325](https://doi.org/10.1103/PhysRevLett.80.5325)
- [67] C. Rubio *et al.*, “Existence of full gaps and deaf bands in two–dimensional sonic crystals,” *J. Light. Technol.*, vol. 17, no. 11, pp. 2202–2207, Nov. 1999. doi: [10.1109/50.803012](https://doi.org/10.1109/50.803012)
- [68] D. Caballero *et al.*, “Large two–dimensional sonic band gaps,” *Phys. Rev. E – Stat. Physics, Plasmas, Fluids, Relat. Interdiscip. Top.*, vol. 60, no. 6, pp. R6316–R6319, 1999. doi: [10.1121/1.423640](https://doi.org/10.1121/1.423640)
- [69] C. Goffaux and J. P. Vigneron, “Theoretical study of a tunable phononic band gap system,” *Phys. Rev. B – Condens. Matter Mater. Phys.*, vol. 64, no. 7, 2001. doi: [10.1103/PhysRevB.64.075118](https://doi.org/10.1103/PhysRevB.64.075118)
- [70] T. Elnady *et al.*, “Quenching of acoustic bandgaps by flow noise,” *Appl. Phys. Lett.*, vol. 94, no. 13, 2009. doi: [10.1063/1.3111797](https://doi.org/10.1063/1.3111797)
- [71] J. V. Sanchez–Perez, C. Rubio, R. Martinez–Sala, R. Sanchez–Grandia, and V. Gomez, “Acoustic barriers based on periodic arrays of scatterers,” *Appl. Phys. Lett.*, vol. 81, no. 27, pp. 5240–5242, Dec. 2002. doi: [10.1063/1.1533112](https://doi.org/10.1063/1.1533112)
- [72] V. M. García–Chocano, S. Cabrera, and J. Sánchez–Dehesa, “Broadband sound absorption by lattices of microperforated cylindrical shells,” *Appl. Phys. Lett.*, vol. 101, no. 18, Oct. 2012. doi: [10.1063/1.4764560](https://doi.org/10.1063/1.4764560)
- [73] L. Sanchis, F. Cervera, J. Sánchez–Dehesa, J. V. Sánchez–Pérez, C. Rubio, and R. Martínez–Sala, “Reflectance properties of two–dimensional sonic band–gap crystals,” *J. Acoust. Soc. Am.*, vol. 109, no. 6, pp. 2598–2605, Jun. 2001. doi: [10.1121/1.1369784](https://doi.org/10.1121/1.1369784)
- [74] C. Goffaux, F. Maseri, J. O. Vasseur, B. Djafari–Rouhani, and P. Lambin, “Measurements and calculations of the sound attenuation by a phononic band gap structure suitable for an insulating

- partition application,” *Appl. Phys. Lett.*, vol. 83, no. 2, pp. 281–283, Jul. 2003. doi: [10.1063/1.1592016](https://doi.org/10.1063/1.1592016)
- [75] V. M. García–Chocano and J. Sánchez–Dehesa, “Optimum control of broadband noise by arrays of cylindrical units made of a recycled material,” *Appl. Acoust.*, vol. 74, no. 1, pp. 58–62, Jan. 2013. doi: [10.1016/j.apacoust.2012.06.008](https://doi.org/10.1016/j.apacoust.2012.06.008)
- [76] J. Sánchez–Dehesa, V. M. García–Chocano, D. Torrent, F. Cervera, S. Cabrera, and F. Simon, “Noise control by sonic crystal barriers made of recycled materials,” *J. Acoust. Soc. Am.*, vol. 129, no. 3, pp. 1173–1183, Mar. 2011. doi: [10.1121/1.3531815](https://doi.org/10.1121/1.3531815)
- [77] O. Umnova, K. Attenborough, C.M. Linton, “Effects of porous covering on sound attenuation by periodic arrays of cylinders,” *J. Acoust. Soc. Am.*, vol. 119, no. 1, pp. 278–284, Jan. 2006. doi: [10.1121/1.2133715](https://doi.org/10.1121/1.2133715)
- [78] V. Romero–García, J. V. Sánchez–Pérez, L. M. García–Raffi, J. M. Herrero, S. García–Nieto, and X. Blasco, “Hole distribution in phononic crystals: Design and optimization,” *J. Acoust. Soc. Am.*, vol. 125, no. 6, pp. 3774–3783, Jun. 2009. doi: [10.1121/1.3126948](https://doi.org/10.1121/1.3126948)
- [79] A. Lardeau, J. P. Groby, and V. Romero–García, “Broadband transmission loss using the overlap of resonances in 3D sonic crystals,” *Crystals*, vol. 6, no. 5, May 2016. doi: [10.3390/cryst6050051](https://doi.org/10.3390/cryst6050051)
- [80] C. Lagarrigue, J. P. Groby, and V. Tournat, “Sustainable sonic crystal made of resonating bamboo rods,” *J. Acoust. Soc. Am.*, vol. 133, no. 1, pp. 247–254, Jan. 2013. doi: [10.1121/1.4769783](https://doi.org/10.1121/1.4769783)
- [81] T. Cavalieri, A. Cebrecos, J. P. Groby, C. Chaufour, and V. Romero–García, “Three–dimensional multiresonant lossy sonic crystal for broadband acoustic attenuation: Application to train noise reduction,” *Appl. Acoust.*, vol. 146, pp. 1–8, Mar. 2019. doi: [10.1016/j.apacoust.2018.10.020](https://doi.org/10.1016/j.apacoust.2018.10.020)
- [82] C. Rubio, S. Castiñeira–Ibáñez, A. Uris, F. Belmar, and P. Candelas, “Numerical simulation and laboratory measurements on an open tunable acoustic barrier,” *Appl. Acoust.*, vol. 141, pp. 144–150, Dec. 2018. doi: [10.1016/j.apacoust.2018.07.002](https://doi.org/10.1016/j.apacoust.2018.07.002)
- [83] *Acoustics – Measurement of sound insulation in buildings and of building elements – Part 3: Laboratory measurements of airborne sound insulation of building elements*, ISO 140–3:1995, May 1995.
- [84] *Acoustics – Measurement of sound absorption in a reverberation room*, ISO 354:2003, May 2003.
- [85] *Road traffic noise reducing devices – Test method for determining the acoustic performance – Part 2: Intrinsic characteristics of airborne sound insulation under diffuse sound field conditions*, EN 1793–2:2012, Nov. 2012.
- [86] *Road traffic noise reducing devices – Test method for determining the acoustic performance – Part 1: Intrinsic characteristics of sound absorption under diffuse sound field conditions*, SS–EN 1793–1:2017, Apr. 2017.
- [87] J. Rubacha, A. Pilch, and M. Zastawnik, “Measurements of the sound absorption coefficient of auditorium seats for various geometries of the samples,” *Arch. Acoust.*, vol. 37, no. 4, pp. 483–488, Dec. 2012. doi: [10.2478/v10168-012-0060-1](https://doi.org/10.2478/v10168-012-0060-1)
- [88] W. O. Hughes, A. M. Mcnelis, C. Nottoli, and E. Wolfram, “Examination of the Measurement of Absorption Using the Reverberant Room Method for Highly Absorptive Acoustic Foam,” *29th Aerosp. Test. Semin.*, no. October 2015, 2015.

- [89] M. S. Bischel, K. P. Roy, and J. V. Greenslade, “Comparison of ASTM and ISO sound absorption test methods,” in *Proceedings – European Conference on Noise Control*, 2008, pp. 1669–1674. doi: [10.1121/1.2933311](https://doi.org/10.1121/1.2933311)
- [90] “Noise barriers – Adrienne research project (1995–1997).” [Austica.ing.unibo.it. http://acustica.ing.unibo.it/Researches/barriers/adrienne.html](http://acustica.ing.unibo.it/Researches/barriers/adrienne.html) (accessed Jul. 28, 2021).
- [91] G. Watts and P. Morgan, “Measurement of airborne sound insulation of timber noise barriers: Comparison of in situ method CEN/TS 1793–5 with laboratory method EN 1793–2,” *Appl. Acoust.*, vol. 68, no. 4, pp. 421–436, Apr. 2007. doi: [10.1016/j.apacoust.2006.03.001](https://doi.org/10.1016/j.apacoust.2006.03.001)
- [92] *Road traffic noise reducing devices – Test method for determining the acoustic performance – Part 5: Intrinsic characteristics – In situ values of sound reflection and airborne sound insulation*, CEN/TS 1793–5:2003, Mar. 2003.
- [93] “QUIESST Guidebook to Noise Reducing Devices optimisation.” [Austica.ing.unibo.it. http://acustica.ing.unibo.it/Researches/barriers/QUIESST\\_final\\_Guidebook.pdf](http://acustica.ing.unibo.it/Researches/barriers/QUIESST_final_Guidebook.pdf) (accessed Jul. 28, 2021).
- [94] Q. Li, D. Duhamel, Y. Luo, and H. Yin, “Analysing the acoustic performance of a nearly–enclosed noise barrier using scale model experiments and a 2.5–D BEM approach,” *Appl. Acoust.*, vol. 158, Jan. 2020. doi: [10.1016/j.apacoust.2019.107079](https://doi.org/10.1016/j.apacoust.2019.107079)
- [95] M. Garai *et al.*, “Repeatability and reproducibility of in situ measurements of sound reflection and airborne sound insulation index of noise barriers,” *Acta Acust. united with Acust.*, vol. 100, no. 6, pp. 1186–1201, Nov. 2014. doi: [10.3813/AAA.918797](https://doi.org/10.3813/AAA.918797)
- [96] M. Garai, “Experimental verification of the European methodology for testing noise barriers in situ: Sound reflection,” in *INTER–NOISE and NOISE–CON Cong. Conf. Proc., InterNoise00*, Nice, France, Aug. 2000, pp. 4629–4636.
- [97] F. Asdrubali, G. Pispola and F. D’Alessandro, “Acoustic intrinsic performances of noise barriers: Accuracy of in situ measurement techniques,” in *12<sup>th</sup> Int. Cong. Sound Vib., ICSV 12*, Lisbon, Portugal, Jul. 2005, pp. 2832–2839.
- [98] M. Garai and P. Guidorzi, “In situ measurements of the intrinsic characteristics of the acoustic barriers installed along a new high speed railway line,” *Noise Control Eng. J.*, vol. 56, no. 5, pp. 342–355, Sep. 2008. [10.3397/1.2969244](https://doi.org/10.3397/1.2969244)
- [99] P. Guidorzi and M. Garai, “Advancements in Sound Reflection and Airborne Sound Insulation Measurement on Noise Barriers,” *Open J. Acoust.*, vol. 03, no. 02, pp. 25–38, 2013. doi: [10.4236/oja.2013.32A004](https://doi.org/10.4236/oja.2013.32A004)
- [100] M. Garai and P. Guidorzi, “In–situ measurements of sound reflection and sound insulation of noise barriers: Validation by means of signal–to–noise ratio calculations,” *J. Acoust. Soc. Am.*, vol. 133, no. 5, pp. 3451–3451, May 2013. doi: [10.1121/1.4806114](https://doi.org/10.1121/1.4806114)
- [101] J. Bull, G. Watts, and J. Pearse, “The use of in–situ test method EN 1793–6 for measuring the airborne sound insulation of noise barriers,” *Appl. Acoust.*, vol. 116, pp. 82–86, Jan. 2017. doi: [10.1016/j.apacoust.2016.09.006](https://doi.org/10.1016/j.apacoust.2016.09.006)
- [102] J. Radosz, “Acoustic performance of noise barrier based on sonic crystals with resonant elements,” *Appl. Acoust.*, vol. 155, pp. 492–499, Dec. 2019. doi: [10.1016/j.apacoust.2019.06.003](https://doi.org/10.1016/j.apacoust.2019.06.003)

- [103] E. Roth, “Evaluation of a new method for determining the sound absorption of noise barriers in situ,” M.S. thesis, Department of Earth Sciences, Uppsala university, Uppsala, Sweden, 2018. [Online]. Available: <http://www.diva-portal.org/smash/get/diva2:1223919/FULLTEXT01.pdf>
- [104] P. Houtave, J. P. Clairbois and C. Glorieux, “In-situ measurements according to EN 1793-5 and EN 1793-6 – When sample size matters,” in *INTER-NOISE and NOISE-CON Cong. Conf. Proc., InterNoise17*, Hong Kong, China, Dec. 2017, pp. 2958–2966.
- [105] *Road traffic noise reducing devices. Test method for determining the acoustic performance. Normalized traffic noise spectrum*, BS EN 1793-3:1998, Feb. 1998.
- [106] *Acoustics – Attenuation of sound during propagation outdoors – Part 1: Calculation of the absorption of sound by the atmosphere*, ISO 9613-1:1993, Jun. 1993.
- [107] A. Sjöberg, “Evaluation of standard EN 1793-6:2012 to examine noise barriers efficiency in situ,” M.S. thesis, Department of Earth Sciences, Uppsala university, Uppsala, Sweden, 2018. [Online]. Available: <http://www.diva-portal.org/smash/get/diva2:1193634/FULLTEXT01.pdf>
- [108] S. Allam and M. Åbom, “A new type of muffler based on microperforated tubes,” *J. Vib. Acoust. Trans. ASME*, vol. 133, no. 3, pp. 31005-1–31005-8, 2011. doi: [10.1115/1.4002956](https://doi.org/10.1115/1.4002956)
- [109] *Railway applications – Track – Noise barriers and related devices acting on airborne sound propagation – Test method for determining the acoustic performance – Part 3-2: Normalized railway noise spectrum and single number ratings for direct field applications*, EN 16272-3-2:2014, Jul. 2014.

## Appendix A – Scale Model Experiment, Signal-to-Noise Ratio

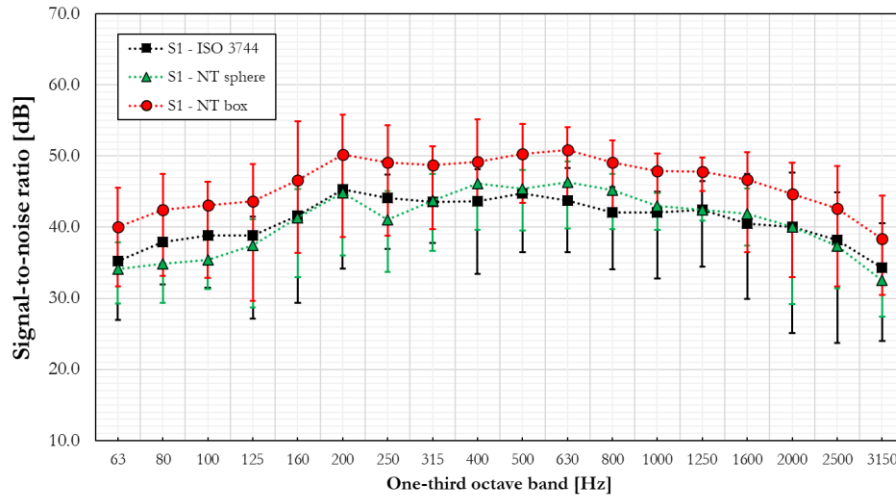


Figure A.1. Signal-to-noise ratio (SNR) for scenario S1.

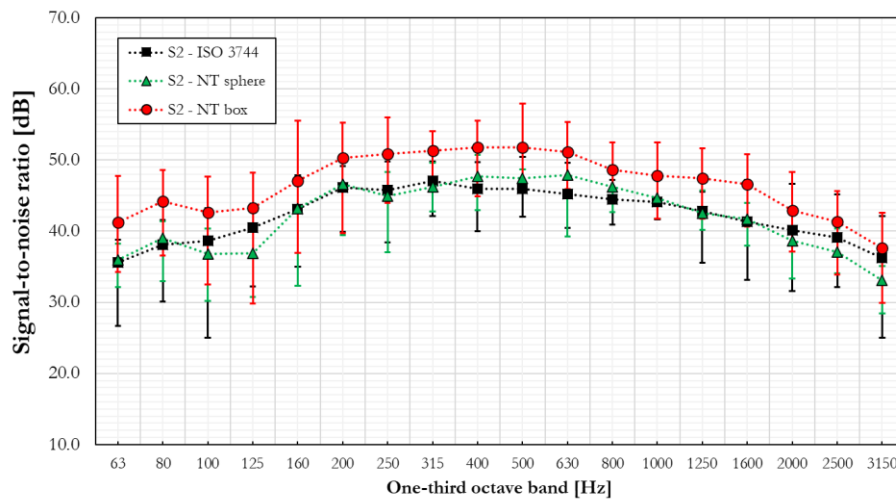


Figure A.2. Signal-to-noise ratio (SNR) for scenario S2.

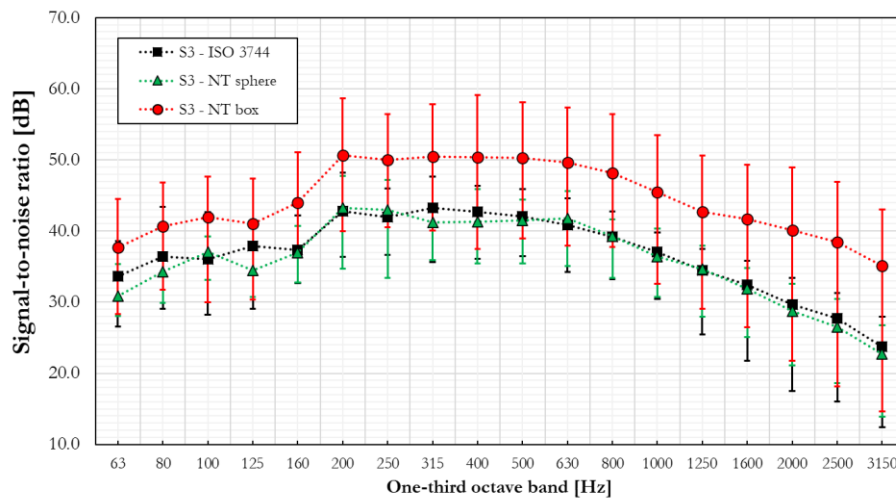
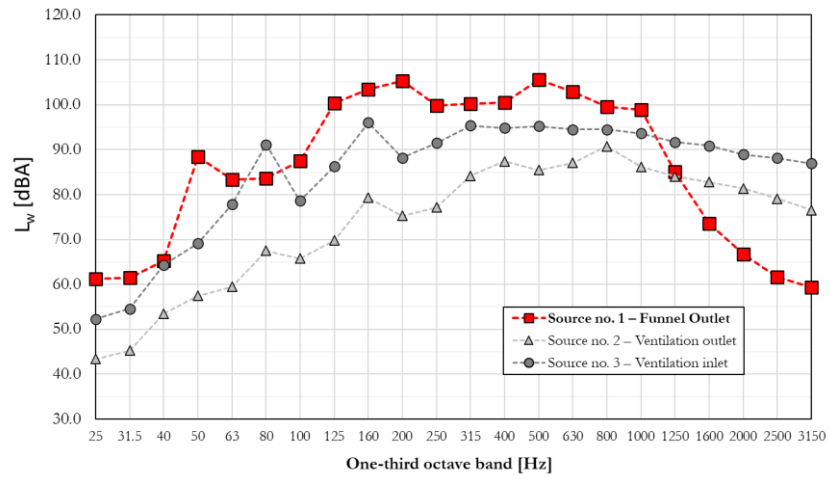
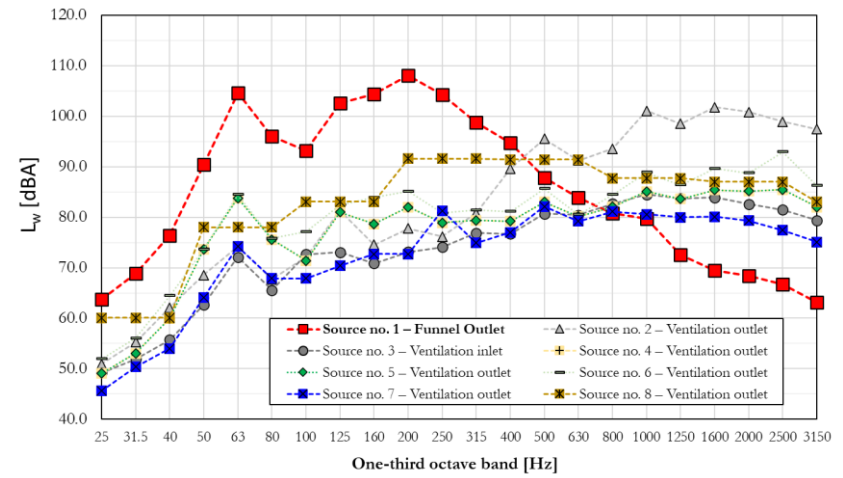


Figure A.3. Signal-to-noise ratio (SNR) for scenario S3.

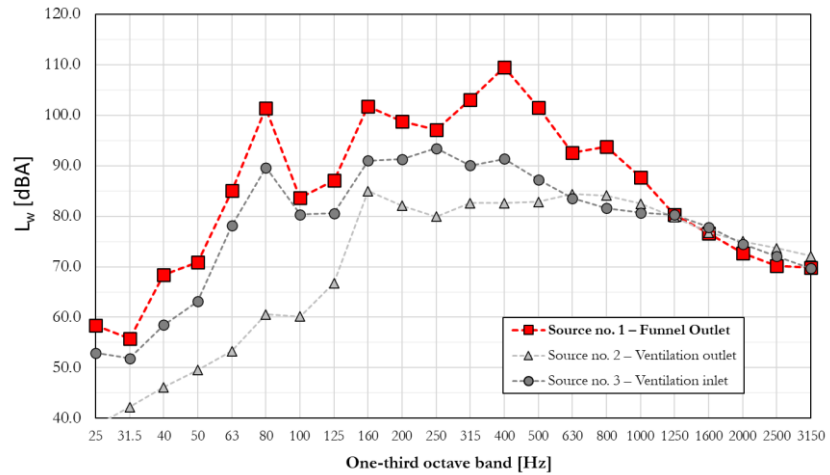
## Appendix B – Moored Ships, Sound Power Levels of Individual Noise Sources



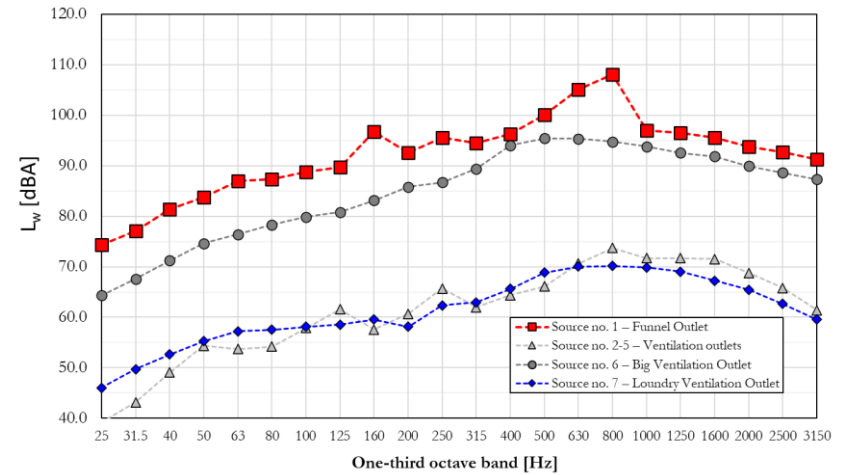
(a)



(b)



(c)



(d)

**Figure A.4.** Sound power levels of all noise sources for individual ships: (a) Ship 1, (b) Ship 2, (c) Ship 3, and (d) Ship 4.

## Appendix C – Noise Barriers, Impulse Responses at Individual Microphones

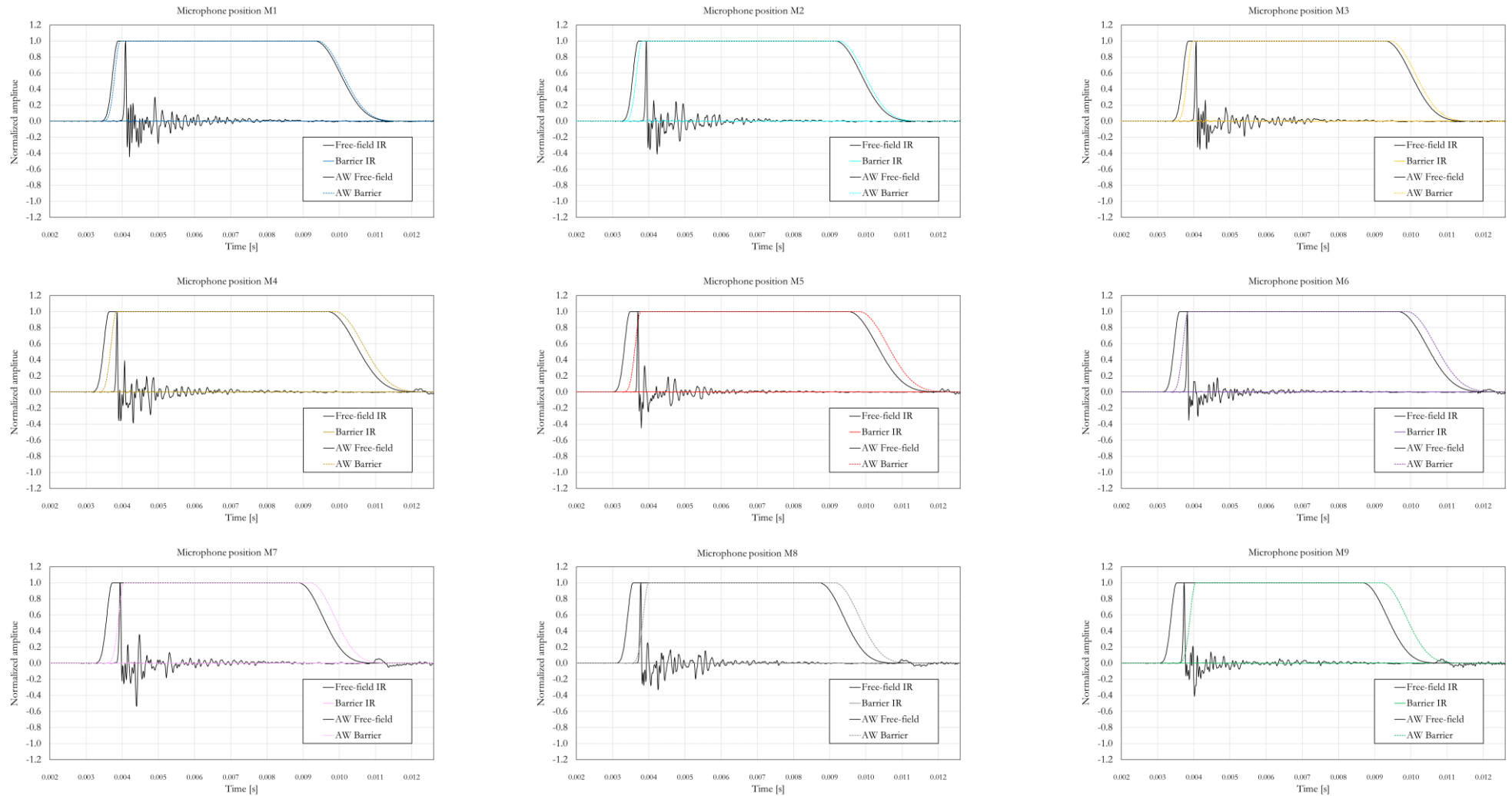


Figure A.5. Impulse responses at individual microphone positions M1 – M9 for conventional barrier characterised according to EN 1793–6, configuration A.

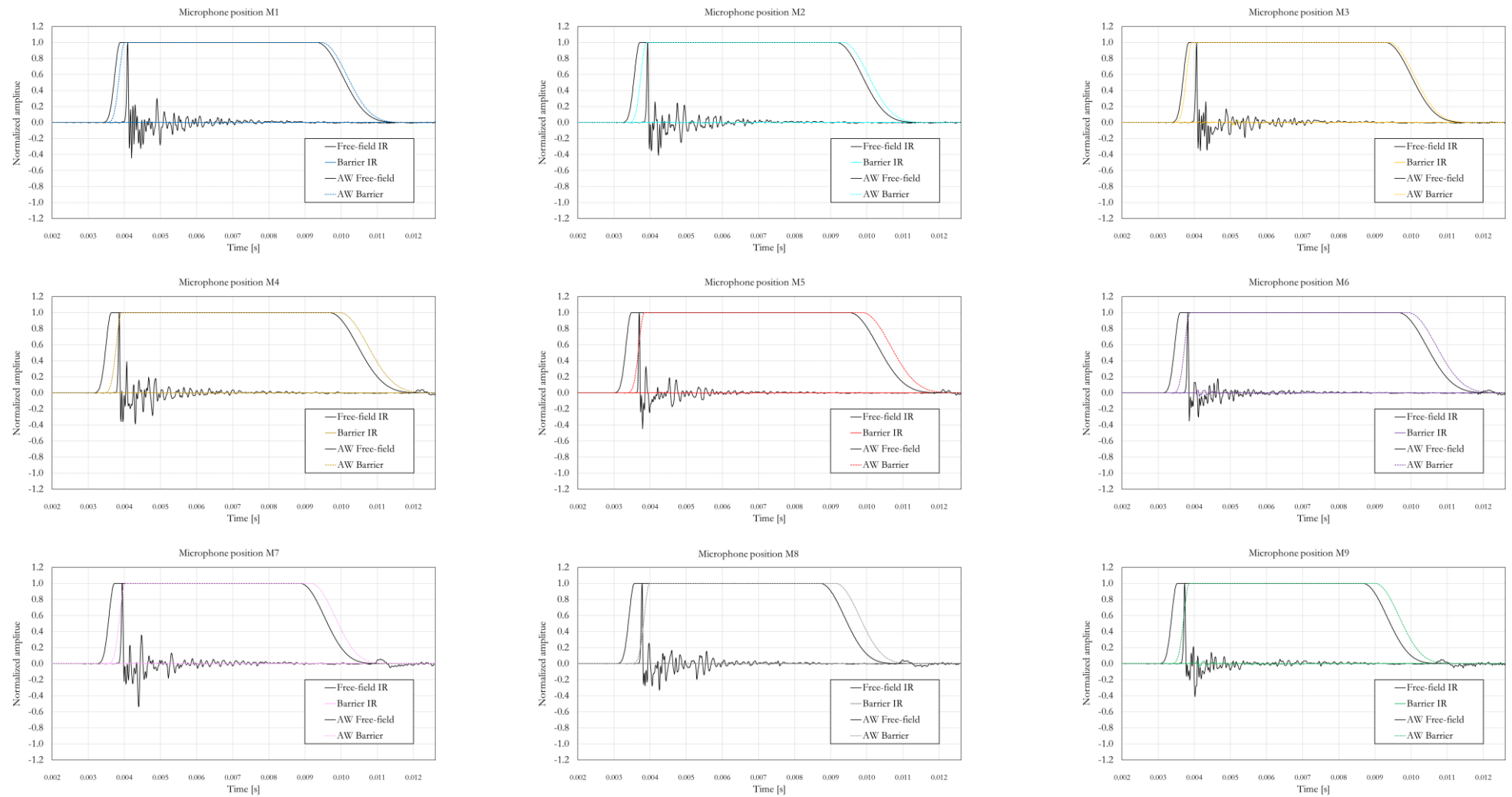


Figure A.6. Impulse responses at individual microphone positions M1 – M9 for conventional barrier characterised according to EN 1793–6, configuration B.

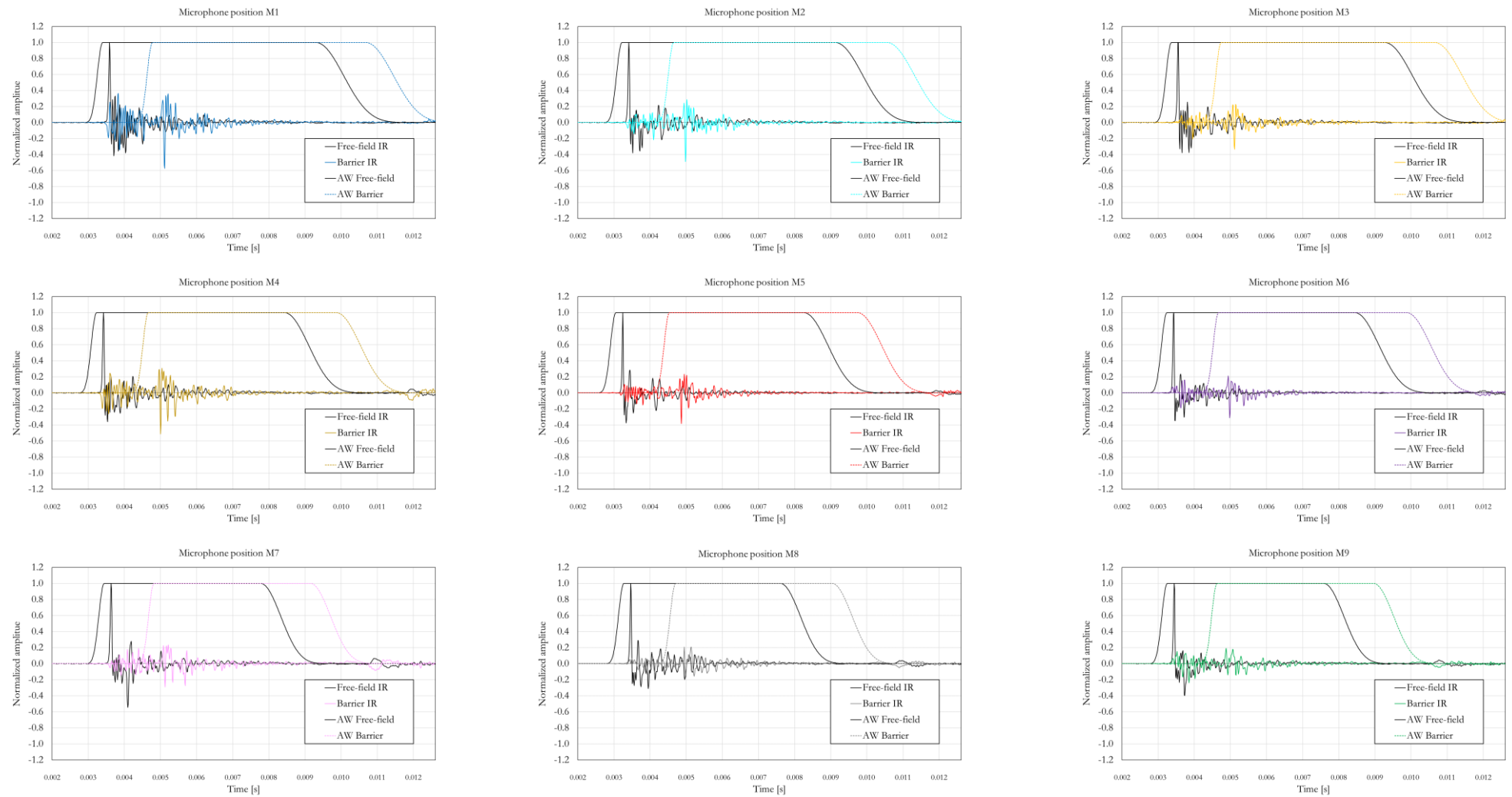
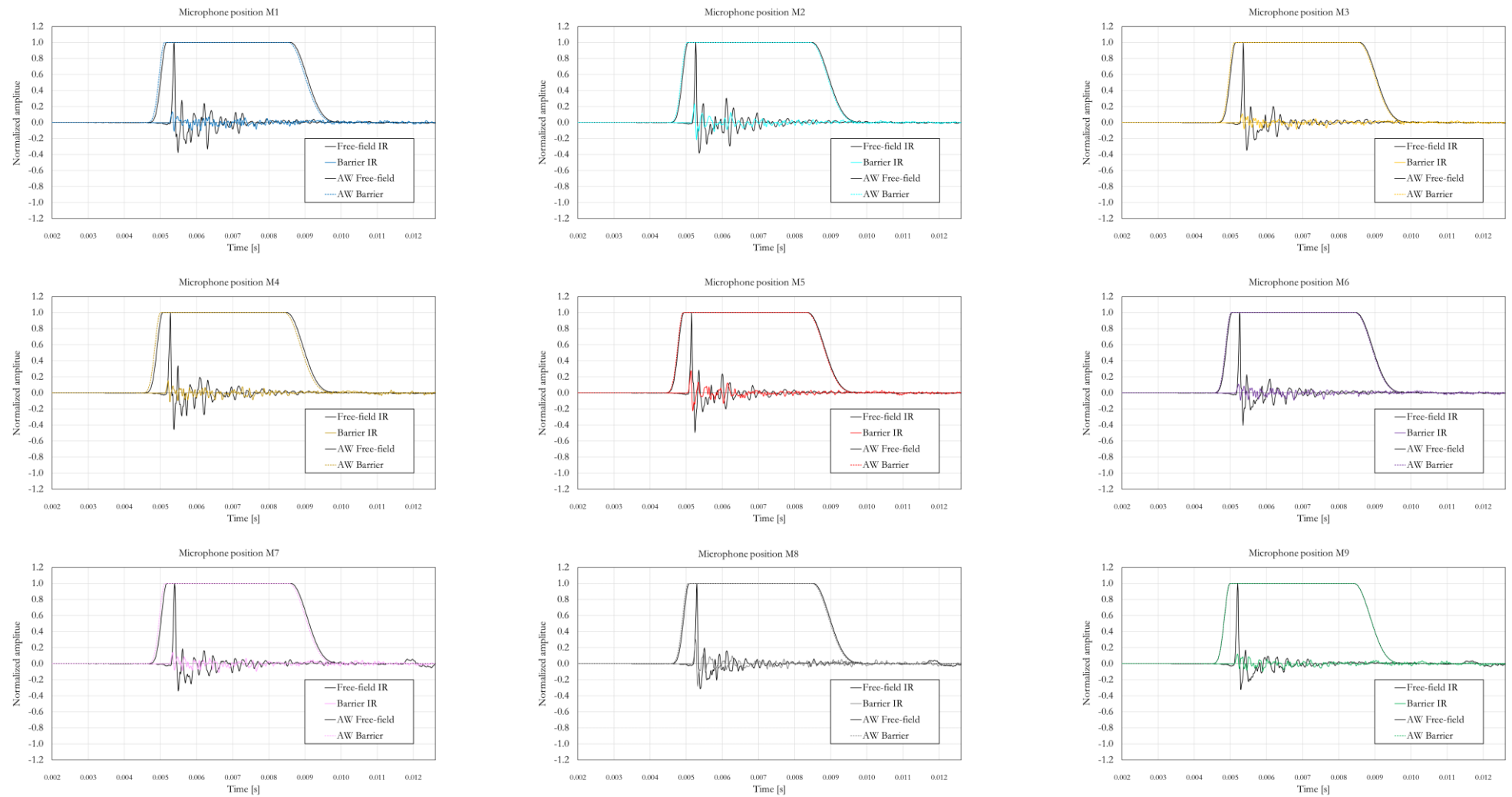


Figure A.7. Impulse responses at individual microphone positions M1 – M9 for conventional barrier characterised according to EN 1793–5.



**Figure A.8.** Impulse responses at individual microphone positions M1 – M9 for sonic crystal barrier characterised according to EN 1793–6, configuration A.

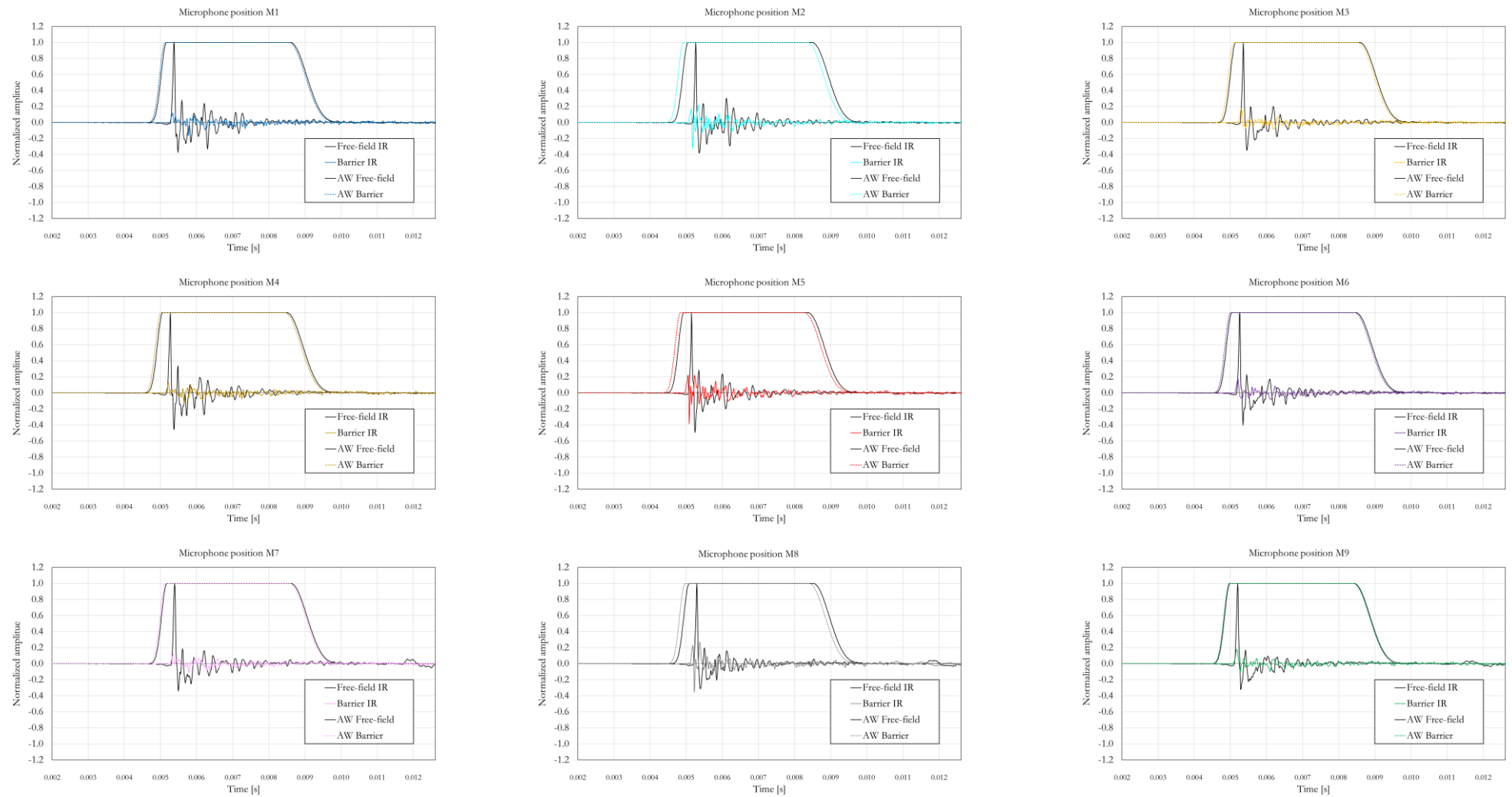
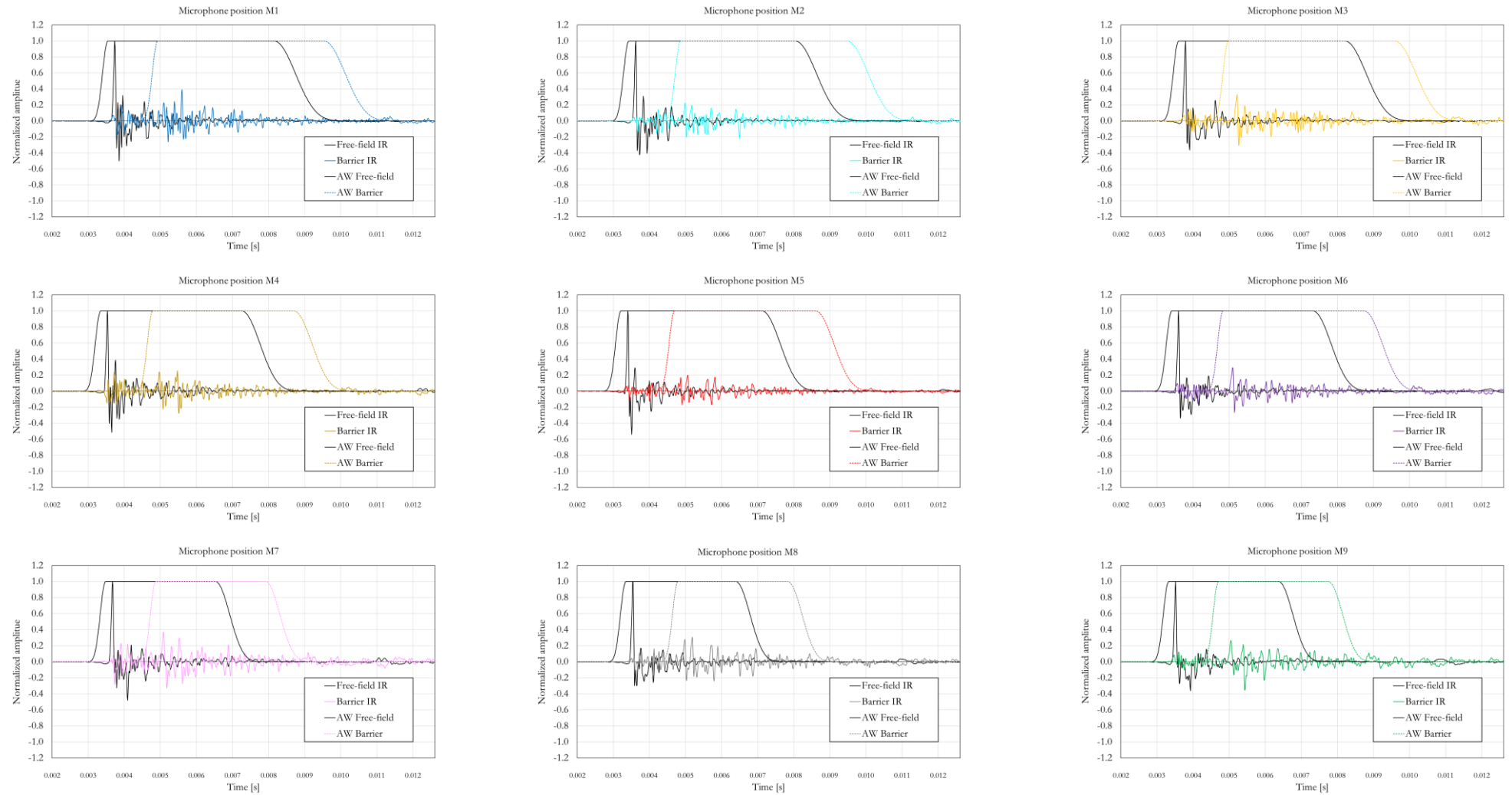
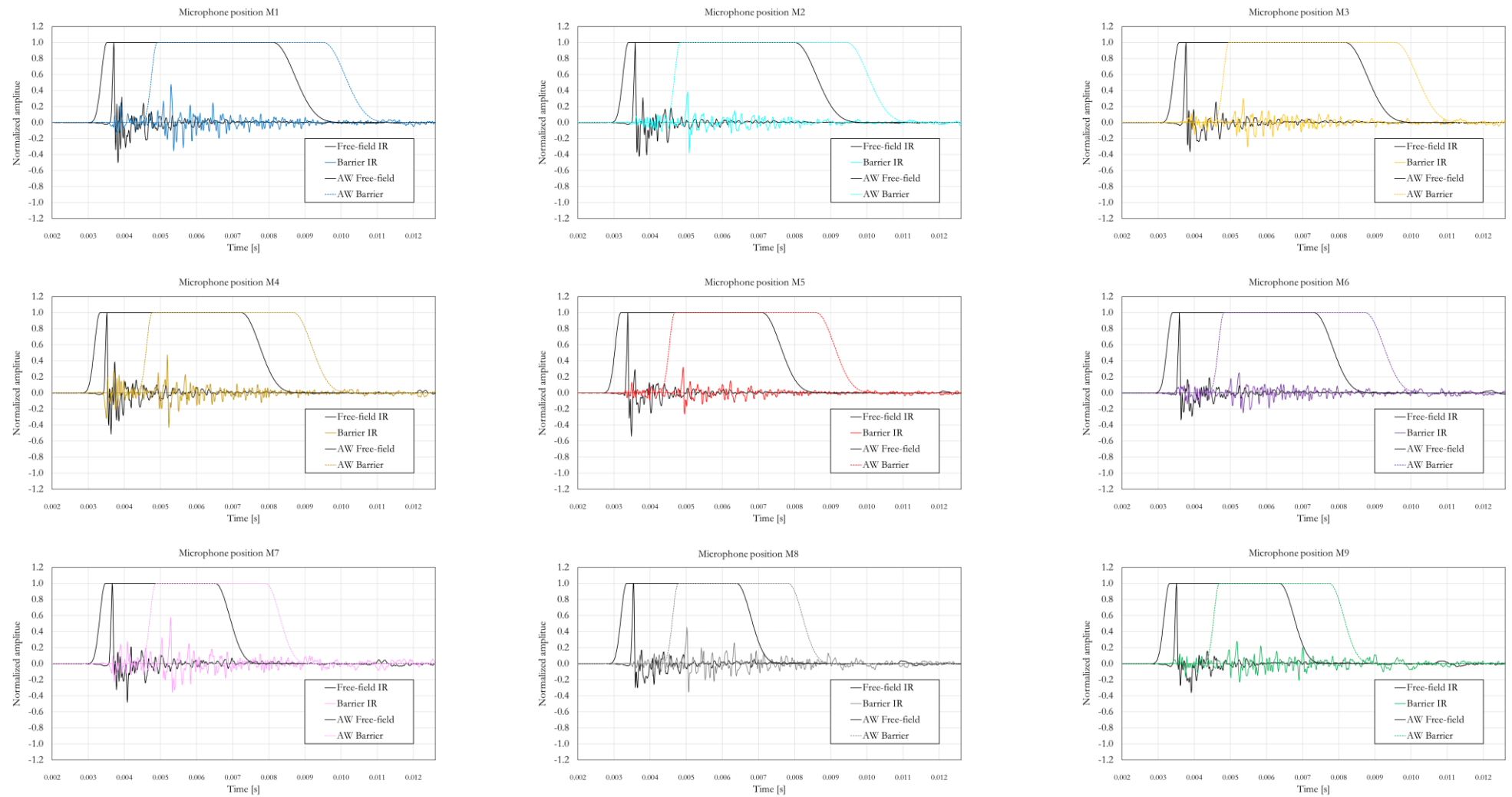


Figure A.9. Impulse responses at individual microphone positions M1 – M9 for sonic crystal barrier characterised according to EN 1793–6, configuration B.



**Figure A.10.** Impulse responses at individual microphone positions M1 – M9 for sonic crystal barrier characterised according to EN 1793–5, configuration A.



**Figure A.11.** Impulse responses at individual microphone positions M1 – M9 for sonic crystal barrier characterised according to EN 1793–5, configuration B.

## Author's Biography

Stefan Dimitrijević was born on 15.01.1987. in Leskovac, Serbia. Stefan completed his elementary and high school education in Vršac, Serbia, and graduated at the Department of Telecommunications, module Audio and Visual Technologies, [School of Electrical Engineering](#), University of Belgrade in 2011. The title of his master thesis was “Investigation of Communal Noise in Belgrade”, supervised by Prof. Miomir Mijić. During the last year of undergraduate studies, Stefan was awarded scholarship of Foundation for Young Talents for best students in Serbia.

In 2011, Stefan started to work at the [School of Electrical and Computer Engineering](#) in Belgrade as a teaching assistant. He was teaching Acoustics, Room Acoustics, Sound Reinforcement, Audioelectronics, etc. In the period 2013–2016, Stefan participated in the TEMPUS project “[StudAVP](#)”.

In 2016, Stefan moved to Stockholm, Sweden, and started to work at [Structor Austik](#) as an acoustic engineer. In 2017, Stefan joined the [COST Action “DENORMS”](#), as a member of the “Landscape Sound Insulation by Sonic Crystals” group. In 2018, Stefan’s research “Analysis of In Situ Acoustic Performance of Sonic Crystal Barrier” was funded by DENORMS and took place at the Universitat Politècnica de València in Valencia, Spain. As an outcome from the research, a [scientific paper](#) was published and the research was awarded and presented at the [DENORMS Action Final event](#) in Coimbra, Portugal.

## SCI Publications

1. S. M. Dimitrijević, M. M. Mijić, and D. S. Šumarac Pavlović, “Indoor sound level spectra of public entertainment premises for rating airborne sound insulation,” *J. Acoust. Soc. Am.*, vol. 147, no. 3, pp. EL215–EL220, Mar. 2020.  
<https://doi.org/10.1121/10.0000800>
2. S. M. Dimitrijević, V. M. García–Chocano, F. Cervera, E. Roth, and J. Sánchez–Dehesa, “Sound insulation and reflection properties of sonic crystal barrier based on micro–perforated cylinders,” *Materials (Basel)*, vol. 12, no. 7, 2019.  
<https://doi.org/10.3390/ma12172806>

## Изјава о ауторству

Име и презиме аутора СТЕФАН ДИМИТРИЈЕВИЋ

Број индекса 2011 / 5050

### Изјављујем

да је докторска дисертација под насловом

CHARACTERISATION OF SPECIFIC NOISE SOURCES IN AN URBAN ENVIRONMENT AND PROTECTION METHODS

---

- резултат сопственог истраживачког рада;
- да дисертација у целини ни у деловима није била предложена за стицање друге дипломе према студијским програмима других високошколских установа;
- да су резултати коректно наведени и
- да нисам кршио/ла ауторска права и користио/ла интелектуалну својину других лица.

Потпис аутора

У Београду, 30.08.2021.

Stefan Dimitrijević

## Изјава о истоветности штампане и електронске верзије докторског рада

Име и презиме аутора СТЕФАН ДИМИТРИЈЕВИЋ

Број индекса 2011/5050

Студијски програм ТЕЛЕКОМУНИКАЦИЈЕ

Наслов рада CHARACTERISATION OF SPECIFIC NOISE SOURCES IN AN URBAN ENVIRONMENT AND PROTECTION METHODS

Ментор Проф. др Миомир Мишић

Изјављујем да је штампана верзија мог докторског рада истоветна електронској верзији коју сам предао/ла ради похрањивања у **Дигиталном репозиторијуму Универзитета у Београду**.

Дозвољавам да се објаве моји лични подаци везани за добијање академског назива доктора наука, као што су име и презиме, година и место рођења и датум одбране рада.

Ови лични подаци могу се објавити на мрежним страницама дигиталне библиотеке, у електронском каталогу и у публикацијама Универзитета у Београду.

Потпис аутора

У Београду, 30.08.2021.

Stefan Dimitrijević

## Изјава о коришћењу

Овлашћујем Универзитетску библиотеку „Светозар Марковић“ да у Дигитални репозиторијум Универзитета у Београду унесе моју докторску дисертацију под насловом:

*CHARACTERISATION OF SPECIFIC NOISE SOURCES IN AN URBAN ENVIRONMENT AND PROTECTION METHODS*

---

која је моје ауторско дело.

Дисертацију са свим прилозима предао/ла сам у електронском формату погодном за трајно архивирање.

Моју докторску дисертацију похрањену у Дигиталном репозиторијуму Универзитета у Београду и доступну у отвореном приступу могу да користе сви који поштују одредбе садржане у одабраном типу лиценце Креативне заједнице (Creative Commons) за коју сам се одлучио/ла.

1. Ауторство (CC BY)
2. Ауторство – некомерцијално (CC BY-NC)
3. Ауторство – некомерцијално – без прерада (CC BY-NC-ND)
4. Ауторство – некомерцијално – делити под истим условима (CC BY-NC-SA)
5. Ауторство – без прерада (CC BY-ND)
6. Ауторство – делити под истим условима (CC BY-SA)

(Молимо да заокружите само једну од шест понуђених лиценци.  
Кратак опис лиценци је саставни део ове изјаве).

Потпис аутора

У Београду, 30.08.2021.

*Stefan Dimitrijević*

1. **Ауторство.** Дозвољаваате умножавање, дистрибуцију и јавно саопштавање дела, и прераде, ако се наведе име аутора на начин одређен од стране аутора или даваоца лиценце, чак и у комерцијалне сврхе. Ово је најслободнија од свих лиценци.
2. **Ауторство – некомерцијално.** Дозвољаваате умножавање, дистрибуцију и јавно саопштавање дела, и прераде, ако се наведе име аутора на начин одређен од стране аутора или даваоца лиценце. Ова лиценца не дозвољава комерцијалну употребу дела.
3. **Ауторство – некомерцијално – без прерада.** Дозвољаваате умножавање, дистрибуцију и јавно саопштавање дела, без промена, преобликовања или употребе дела у свом делу, ако се наведе име аутора на начин одређен од стране аутора или даваоца лиценце. Ова лиценца не дозвољава комерцијалну употребу дела. У односу на све остале лиценце, овом лиценцом се ограничава највећи обим права коришћења дела.
4. **Ауторство – некомерцијално – делити под истим условима.** Дозвољаваате умножавање, дистрибуцију и јавно саопштавање дела, и прераде, ако се наведе име аутора на начин одређен од стране аутора или даваоца лиценце и ако се прерада дистрибуира под истом или сличном лиценцом. Ова лиценца не дозвољава комерцијалну употребу дела и прерада.
5. **Ауторство – без прерада.** Дозвољаваате умножавање, дистрибуцију и јавно саопштавање дела, без промена, преобликовања или употребе дела у свом делу, ако се наведе име аутора на начин одређен од стране аутора или даваоца лиценце. Ова лиценца дозвољава комерцијалну употребу дела.
6. **Ауторство – делити под истим условима.** Дозвољаваате умножавање, дистрибуцију и јавно саопштавање дела, и прераде, ако се наведе име аутора на начин одређен од стране аутора или даваоца лиценце и ако се прерада дистрибуира под истом или сличном лиценцом. Ова лиценца дозвољава комерцијалну употребу дела и прерада. Слична је софтверским лиценцама, односно лиценцама отвореног кода.